Graphene Oxide Nanohybrids as Platforms for Carboplatin Loading and Delivery

Dissertation

zur Erlangung des akademischen Grades
Doctor of Philosophy (Ph. D.)

vorgelegt der
Fakultät Mathematik und Naturwissenschaften
der Technischen Universität Dresden

von
Sami A Makharza (M.Sc)
geboren am 07. Oktober 1978 in AlThahria (Palästina)

eingereicht am 08.08.2014

Gutachter:

Prof. Dr. Bernd Büchner
     TU Dresden, Fachrichtung Physik, Dresden, Deutschland
     IFW Dresden, Deutschland

Prof. Dr. Michael Mertig
     TU Dresden, Physikalische Chemie, Dresden, Deutschland
     Kurt Schwabe Institut für Sensortechnik, 04736 Waldheim, Deutschland

     Datum der Verteidigung: 13.02.2015

List of Contributions

I **Sami Makharza**, Orazio Vittorio, Giuseppe Cirillo, Steffen Oswald, Maria Kavallaris, Bernd Büchner, Michael Mertig and Silke Hampel. *Graphene Oxide – Gelatin Nanohybrids as Functional Tools for Enhanced Carboplatin Activity in Neuroblastoma Cells.* Pharm. Res. December (**2014**).

II **Sami Makharza**, Giuseppe Cirillo, Alicja Bachmatiuk, Orazio Vittorio, Rafael Gregorio Mendes, Steffen Oswald, Silke Hampel and Mark H. Rümmeli. *Size-Dependent Nanographene Oxide as a Platform for Efficient Carboplatin Release.* J. Mater. Chem. B (**2013**), 1, 6107.

III **Sami Makharza**, Giuseppe Cirillo, Alicja Bachmatiuk, Imad Ibrahim, Nicholas Ioannides, Barbara Trzebicka, Silke Hampel and Mark H. Rümmeli. *Graphene Oxide-Based Drug Delivery Vehicles: Functionalization, Characterization and Cytotoxicity Evaluation.* J. Nanopart. Res. (**2013**), 15, 2099.

IV Imad Ibrahim, Alicja Bachmatiuk, Daniel Grimm, Alexey Popov, **Sami Makharza**, Martin Knupfer, Bernd Büchner, Gianaurelio Cuniberti and Mark H. Rümmeli. *Understanding High-Yield Catalyst-Free Growth of Horizontally Aligned Single-Walled Carbon Nanotubes Nucleated by Activated C60 Species.* ACS Nano. (**2012**), 6(12), 10825.

V Book chapter: C. G. Rocha, M. H. Rümmeli, I. Ibrahim, H. Sevincli, F. Börrnert, J. Kunstmann, A. Bachmatiuk, M. Pötschke, W. Li, **S. A. M. Makharza**, S. Roche, B. Büchner, G. Cuniberti. *Tailoring the Physical Properties of Graphene.* in *Graphene: Synthesis and Applications.* W. Choi, J-W. Lee (editors), CRC Press (2011). ISBN: 978-1439861875.

VI Oral presentation at Graphene 2014 International Conference and Exhibition. Toulouse, France, May 06 - 09, (**2014**).

Contribution report

Papers I, II and III are mainly the work of the author. Paper IV is the main work of I. Ibrahim where the author contributed with data analysis and discussion of FTIR and XPS results. (V) is contribution in a book chapter. (VI) is a conference contribution.

Papers Prior PhD

I **Sami Makharza**, Jihan Auisa, Sawsan Abu Sharkh, Jamal Ghabboun, Maryam Faroun, Hasan Dweik, Wadie Sultan and Mukhles Sowwan. *Structural and Thermal Analysis of Copper-Doped Poly(Nisopropylacrylamide) Films.* Int. J. Polym. Anal. Charact. (**2010**), 15, 1-12.

II Saqer M Darwish, Sawsan E Abusharkh, Musa M Abuteir, **Sami A Makharza**, Mahmoud M Abu-hadid. *Spectroscopic Investigations of Pentobabital Interaction with Human Serum Albumin.* J. Mol. Struct. (**2010**), 963, 122-129.

III Monzer Fanun, **Sami Makharza**, Mukhles Sowwan. *Fluorescence Spectroscopy Study of Polyoxyethylene Surfactant Micellar Systems.* J. Dispersion Sci. Technol. (**2010**), 31, 1561-1567.

IV Monzer Fanun, **Sami Makharza**, Mukhles Sowwan. *Transition from Micelles to Microemulsions in Sugar Based Surfactant Systems Probed by Fluorescence Spectroscopy and AFM.* J. Dispersion Sci. Technol. (**2010**), 31, 1212-1219.

V Monzer Fanun, **Sami Makharza**, Mukhles Sowwan. *UV-Visible and AFM Studies of Nonionic Microemulsions.* J. Dispersion Sci. Technol. (**2010**), 31, 501-511.

VI Mukhles Sowwan, Maryam Faroun, Ishaq Musa, Imad Ibrahim, **Sami Makharza**, Wadie Sultan and Hasan Dweik. *Study on the Morphology of Polyacrylamide – Silica Fumed Nanocomposite Thin Films.* Int. J. Phys. Sci. (**2008**), 3, 144-147.

VII Mukhles Sowwan, Mayy Magalseh, Imad Ibrahim, **Sami Makharza**, Wadie Sultan and Hasan Dweik. *Effect of Cu^{+2} Doping on the Nano-Scale Surface Roughness of Polyacrylamide Thin Replicas.* Int. J. Polymer. Mater. (**2008**), 57, 396-403.

VIII H. Dweik, W. Sultan, M. Sowwan and **S. Makharza.** *Analysis, Characterization and Some Properties of Polyacrylamide Copper Complexes.* Int. J. Polymer. Mater. (**2008**), 57, 228-244.

List of Collaborators:

TECHNISCHE
UNIVERSITÄT
DRESDEN

Leibniz Institute
for Solid State and
Materials Research
Dresden

IFW

UNIVERSITÀ
DELLA CALABRIA

CHILDREN'S CANCER
INSTITUTE AUSTRALIA

DAAD
Deutscher Akademischer Austauschdienst
German Academic Exchange Service

AL-QUDS UNIVERSITY

Contents

LIST OF FIGURES

LIST OF TABLES

ACRONYMS

NGO	Nanographene oxide
PAMAM	Polyamidoamide
XPS	X-ray photoelectron spectroscopy
FTIR	Fourier transform infrared
SEM	Scanning electron microscopy
AFM	Atomic force microscopy
CP	Carboplatin
hMSC	Human mesenchymal stem cells
GO	Graphene oxide
CNT	Carbon nanotube
CVD	Chemical vapor deposition
CNM	Carbon nanomaterials
PEG	Polyethylene glycol
SN-38	7-ethyl-10-hydroxycamptothecin
L-929	Murine fibroblast cells
PC-12	Neuroendocrine cells
OLC	Oligodendroglia cells
OBS	Osteoblast cells
hESC	Human embryonic stem cells
hFBC	Human fibroblast cells
ROS	Relative oxygen species
RES	Reticuloendothelial system
DOX	Doxorubcin
IMR-32	Human Neuroblastoma cells

ABSTRACT

Nanographene oxide particles (NGO) were produced via oxidative exfoliation of graphite. Three different sizes of NGO (300 nm, 200 nm and 100 nm) have been separated by using probe sonication and sucrose density gradient centrifugation. There is great interest in functionalized NGO as a nanocarrier for in vitro and in vivo drug delivery, in order to improve dispersibility and stability of the nanocarrier platforms in physiological media.

In this study, the NGO particles were covalently functionalized with zero generation polyamidoamide (PAMAM-G0) and with gelatin via noncovalent interaction. Spectroscopic techniques have been used to discriminate the chemical states of NGO prior and after functionalization. The X-ray photoelectron spectroscopy (XPS) revealed a clear change in the chemical state of NGO after functionalization, for both covalent and noncovalent approaches. Raman spectroscopy gave obvious insight after oxidation of graphite and functionalization of NGO particles depending on the variation of intensity ratios between D, G and 2D bands. The Fourier transform infrared spectroscopy (FTIR) exhibited the presence of oxygen containing functional groups distributed onto graphene sheets after oxidation of graphite. Furthermore, the FTIR is complementary with the XPS which performed a strong reduction in the oxygen contents after functionalization. UV visible spectroscopy was used to understand the binding capacity of gelatin coated NGO particles.

The Microscopy tools, scanning electron microscopy (SEM) and atomic force microscopy (AFM) are used to estimate the dimensions of NGO particles (thickness and lateral width). The nanohybrid systems (NGO-PAMAM and Gelatin-NGO) loaded with carboplatin (CP) were sought for anticancer activity

investigation in HeLa and neuroblastoma cancer cells respectively. Mesenchymal stem cells (hMSCs) were used as a model of normal cells. On HeLa cells, the pristine NGO particles with average widths of 200 nm and 300 nm showed a cytotoxic effect at low (50 μg.ml^{-1}) and high (100 μg.ml^{-1}) concentrations. While the pristine NGO sample with an average width of 100 nm revealed no significant cytotoxicity at 50 μg.ml^{-1}, and only recorded a 10% level at 100 μg.ml^{-1}.

The mesenchymal stem cells showed less than 35% viability for all size distributions. After functionalization with PAMAM, the carrier was found to be able to deliver carboplatin to the cancer cells, by enhancing the drug anticancer efficiency. Moreover, the carboplatin loaded NGO carrier shows no significant effect on the viability of hMSCs even at high concentration (100 μg.ml^{-1}). On neuroblastoma cells, the cell viability assay validated gelatin-NGO nanohybrids as a useful nanocarrier for CP release and delivery, without obvious signs of toxicity. The nano-sized NGO (200 nm and 300 nm) did not enable CP to kill the cancer cells efficiently, whilst the CP loaded gelatin-NGO 100 nm resulted in a synergistic activity through increasing the local concentration of CP inside the cancer cells.

Zusammenfassung

Nanographit-Oxid-Partikel (NGO) wurden durch oxidative Abblätterung (Exfoliation) von Graphit hergestellt. Drei unterschiedliche Größen von NGO (300 nm, 200 nm und 100 nm) wurden durch Ultraschallabscheidung und Zuckergradienten-Zentrifugation getrennt. Generell besteht ein großes Interesse an funktionalisiertem NGO als künstlichem Medikamenten-Transportmedium auf Nanobasis, mit erhöhter Dispergierbarkeit und Stabilität in physiologischen Medien, wie dem menschlichen Körper. In der vorliegenden Arbeit wurden die NGO Partikel zum einen durch Polyamidoamid (PAMAM) der nullten Generation kovalent und zum anderen durch Gelatine nicht-kovalent funktionalisiert.

Spektroskopische Methoden wurden herangezogen um die chemischen Zustände von NGO vor und nach der Funktionalisierung zu unterscheiden. Röntgenphotoelektronenspektroskopiemessungen (XPS) zeigten eine deutliche Änderung der chemischen Zustände nach der Funktionalisierung, sowohl für den kovalenten, als auch für den nicht-kovalenten Ansatz.

Ramanspektroskopiemessungen waren sehr aufschlussreich nach der Oxidation von Graphit und der Funktionalisierung von NGO, in Abhängigkeit von den Änderungen der Intensitätsverhältnisse der D, G und 2D Bänder zueinander. Mit Hilfe von Fourier-Transformations-Infrarotspektrometrie-Messungen (FTIR) konnte das Vorhandensein von funktionellen Gruppen, welche Sauerstoff beinhalten, auf Graphen-Lagen nach der Oxidation von Graphit nachgewiesen werden. Die FTIR-Studien sind hierbei komplementär zur den XPS-Studien in denen ein deutlicher Rückgang des Sauerstoffanteils nach der Funktionalisierung beobachtet wurde. Ultraviolett-Spektroskopie wurde genutzt um den Ursprung der Bindungskapazität der mit Gelatine überzogenen NGO Partikel

zu untersuchen. Zusätzlich wurden die Rasterelektronenmikroskopie (SEM) und Rasterkraftmikroskopie (AFM) herangezogen, um die Maße (Dicke und Breite) der NGO Partikel zu bestimmen.

Das Nanohybrid-System (NGO-PAMAM und Gelatine NGO) wurden mit Carboplatin (CP) beladen. Das System ist vielversprechend im Hinblick auf Krebsbekämpfung von HeLa und Neuroblastoma Krebszellen.

Mesenchymal-Zellen wurden als Modell-Zellen verwendet. An HeLa-Zellen wurden zytotoxische Effekte für NGO Partikel (Breite 200 nm und 300 nm) für niedrige und hohe Konzentrationen beobachtet. Die NGO Ausgangsproben mit einer Durchschnittsbreite von 100 nm zeigen keine signifikante Zytotoxizität bei 50 µg.ml^{-1} und ein Niveau von 10% bei 100 µg.ml^{-1}. Die mesenchymalen Stammzellen zeigten eine Überlebensrate von weniger als 35% für jegliche Größen. Nach der Funktionalisierung mit PAMAM was Trägersystem in der Lage Carboplatin zu den Krebszellen zu liefern. Weiterhin zeigte der mit Carboplatin beladene NGO-Träger keine signifikanten Effekte auf die Lebensdauer der Mesenchymal-Zellen (hMSCs), selbst nicht bei hohen Konzentrationen 100 µg.ml^{-1}.

An Neuroblastomazellen wurden Gel_NGO Nanohybride als nützliche, nicht toxische Nanoträger für CP bestätigt. Das Nano-NGO (200 nm und 300 nm) konnte CP nicht in die Lage versetzen Krebszellen effizient zu vernichten, während mit Gel_NGO (100 nm) eine synergetische Aktivität durch Erhöhung der Konzentration von CP in den Krebszellen resultierte.

MOTIVATION

In the past decade, the rapid development of graphene oxide nanohybrids has brought many interesting insights and prospects to cancer cells diagnosis and treatment. The first exploration of nanographene oxide in drug delivery and cancer therapy was commenced at Stanford University in 2008, motivated by the progress achieved by using carbon nanotubes for biological applications. Since then, graphene and its derivatives were used extensively and exhibited more exciting results compared to other nanostructured materials.

Graphene oxide (GO) particles possess many advantages for biological purposes over other related sp^2 carbon nanomaterials like carbon nanotubes (CNTs). First, high solubility and stability in physiological media, CNTs for instance require cutting and de-bundling process for better stability. Second, no metallic catalysts required for producing graphene oxide particles, while the remaining catalysts (impurities) during CNTs preparation induced cytotoxic effect in cell culture investigation. Third, GO does not require surfactants for dispersibility compering with CNTs, the surfactants being a cause of toxicity. Fourth, extremely large surface area (2630 m^2.g^{-1}) and sp^2 hybridized carbon atoms, GO provides high effectively loading of aromatic drugs on both sides of a single layer through π - π stacking, van der Waal forces, H – bonding, etc. Five, remarkable biocompatibility of GO and facile functionalization thanks to enrich oxygen groups have received increasing attention towards biomedical applications. Many potential aspects have to be taken into account before integrating GO in vitro or in vivo. For example, the size, shape, oxidation methods, degree of oxidation and thickness of graphene oxide particles affect the quality of functionalization, as well as the efficiency of drug molecules on

treated cells.

In summary, graphene oxide nanohybrids emerge as a functional tool for drug loading and delivery, currently many challenges need to be elucidated by effective collaborations crossing multiple disciplines including chemistry, physics, biology and medicine.

ACKNOWLEDGMENT

To my mom, brothers, sisters

and beloved family, Sawsan and Rouand.

1

Introduction to Graphene

In this chapter, a brief introduction on carbon allotropes, graphene, graphene oxide and functionalized graphene oxide materials are elucidated. The toxicity of carbon based nanomaterials, as well as the functionalized nanostructures are extensively evaluated in this chapter. A short background about the drug (Carboplatin) and the cell models used in this study are presented. Most sections in this chapter are published as a review article in Journal of Nanoparticle Research [1].

Citation::

1.1   Allotropes of carbon

Carbon, an element has four valence electrons in its outer shell, two are localized in 2s and two are in the 2p shells, the mixing of 2s and 2p orbitals is generally possible resulting in varied hybridization (sp, sp^2 and sp^3). The promotion of an electron from 2s to 2p orbitals will generate four equivalent hybrid orbitals, sp^3 occurs when a carbon atom bonds to four groups and form four sigma (σ) bonds, while sp^2 has three attached groups formed three sigma bonds and the remaining p orbital comes to form one pi (π) bond. Due to hybridization, pure carbon is available in a large variety of allotropes, for instance diamond and graphite represented as the only carbon allotropes known for a long period of time.[1]

In 1985, Krotto et al. succeeded in synthesis of a spherical network of equivalent sp^2 hybridized carbon atoms in a shape of football called 0-dimensional fullerene,[2] it was reported as the first prepared allotrope of carbon in a macroscopic scale. Afterward the family of synthesized carbon allotropes dilated to include one-dimentional carbon nanotubes (CNT) in 1991,[3] and lately two-dimensional graphene (fig. 1.1). In graphite gallery, a multilayer and planar sheets coalesce via van der Waals forces with a distance 0.34 nm, the layers can be easily exfoliated by using simple technique called "scotch tape" to reach incredibly one atom thick layer known as graphene, the experiment was initially organized by Geim and Novoselov in 2004. As a result, graphene donates an exciting physical and chemical properties in different applications.[4]

1.2   Graphene: history and properties

In 1930s, Landau and Peierls argued that the two dimensional crystals are not exist due to thermodynamic instability, the theory suggested that the thermal fluctuations in 2D crystal lattices lead to such displacement of atoms that

equivalent the interatomic distances at any finite temperature, this suggestion supported by experimental observations. Indeed, as the thickness of thin film (number of layers) decreases the melting temperature drastically decreased and they become unstable and start to decompose or segregate into islands at a thickness typically tens of atomic layers.[5] This theory was dominated until 2004 when the experiment realized 2D graphene crystal, it is consequently defined as one atom thick of ordinary carbon atoms tightly packed into two dimensional honeycomb crystal lattice. Noteworthy, the fascinating physical and chemical properties of graphene enabled its used in many applications, such as, nanoelectronics, sensors, nanomedicine, drug delivery, etc., have been intensively pursued.
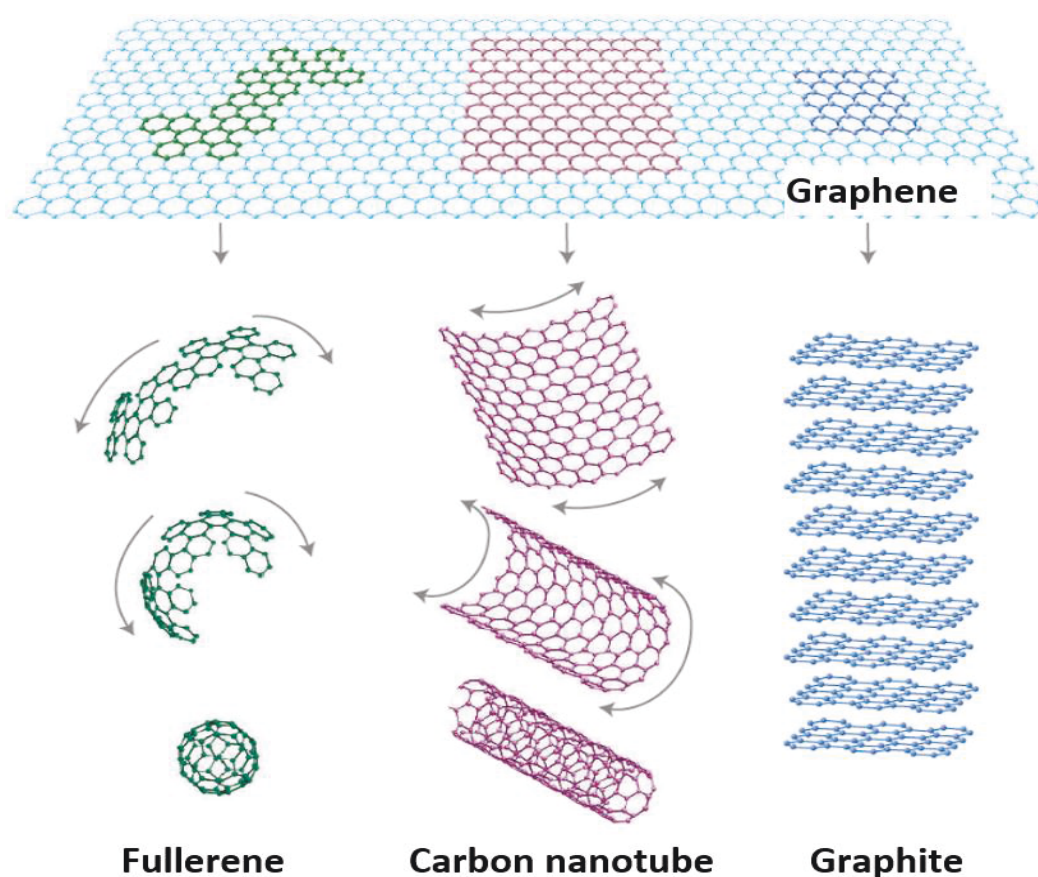
Figure 1.1: Synthetic allotropes of carbon. Reprinted with permission from ref.[6]

In this thesis, the interesting property of graphene resides in its ability to coordinate with other molecules via physisorption, van der Waals forces, H - bonding, π - π stacking, etc. Water soluble derivative of graphene (graphene oxide) motivates toward biological applications, owing to high surface area and low side effects after modifications.

1.3   Methods for graphene production

There are four main methods for obtaining graphene: 1) mechanical exfoliation or scotch tape of bulk graphite, 2) chemical vapor deposition (CVD), 3) epitaxial growth of graphene films on silicon carbide (SiC) and 4) reduction of graphene oxide.[7–11] In the first method, the peeling-off monolayer graphene sheet has been achieved by a simple method known as scotch tape method, and consequently led to the Nobel-Prize-winning in physics for an exceptional breakthrough in high quality graphene production.

In CVD method, the graphene monolayer deposited onto different substrates, such as, Ni, Cu, Co or alloys. The carbon precursors (methylene, ethylene, acetylene, etc.) and other gases such as nitrogen, argon and hydrogen are gathered at elevated temperature up to 1000 °C in a proper chamber.

The reaction time, initial concentrations of gases and carbon precursors, type of substrate and cooling rate should be controlled and optimized in order to obtain few layers or even one layer of graphene.

1.4   Graphene oxide

The superiority of GO resides effectively in its chemical structure, which confers an astonishing chemical versatility, high aspect ratio and extraordinary physical properties. GO can be produced based on oxidation of graphite powder using

of oxidizing agents in strong acidic medium, Brodie, 1859 and Hummers, 1958 are known as the major protocols for obtaining GO.

The presence of oxygen groups on pristine graphene basal plane and edges makes it as an amenable for chemical functionalization, with organic compounds or biological molecules in covalent and or non-covalent approaches under suitable conditions.

1.4.1 Structure and properties

Fig. 1.2 shows the chemical structure of graphene and GO. Over the years, considerable effort went toward understanding the structure of GO.

In GO, the carbon atoms covalently bonded to oxygen containing groups are sp^3 hybrids and can disrupt the sp^2 conjugated system of graphene lattice structure. sp^3 hybridized regions are randomly distributed either in or out of the basal plane of graphene sheets or at the edges.[12–14] The properties of GO are unreliable and depend on its synthesis methods, processing and experimental conditions.[15]

Electrically, GO is considered an insulating material due to its widespread saturated sp^3 bonds, vacancies (missing carbon atoms) and negatively charged density species bound to carbon. For these reasons, the energy gap increases and makes GO nonconducting.[16,17] Nevertheless, the structural and electronic properties of GO can be modified via chemical and thermal treatments.[18] The optical properties also depend on the oxidation level of GO,[19] the multiple layers of GO change considerably the corresponding optical properties, for instance, the refractive index of thermally reduced GO is higher than that in stacked GO.

GO is highly soluble and disperses well in water and physiological media, making it attractive for medical purposes after numerous modifications.
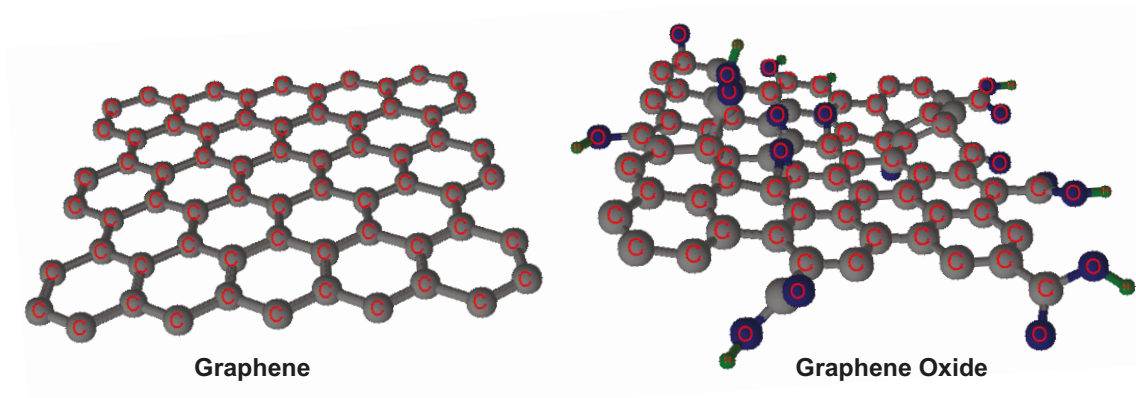
Figure 1.2: Chemical structure of graphene and graphene oxide.

1.4.2 | Methods for obtaining graphene oxide

The most common chemical routes for GO preparation arise from expandable graphite by chemical exfoliation using various oxidizing agents, such as potassium permanganate $KMnO_4$ and potassium chlorate $KClO_3$. These routs were comprehensively covered in previous reviews[13, 20] and summarized in table 1.1.

The first procedures for GO were developed by Brodie (1859),[21] Staudenmaier (1898)[22] and Hummers and Offeman (1958).[23] Brodie treated graphite with $KClO_3$ and fuming nitric acid (HNO_3). Staudenmaier improved Brodie's approach by slowly adding $KClO_3$ over one week to a solution containing concentrated sulfuric acid (H_2SO_4), concentrated HNO_3 (63%) and graphite. The mass ratio of graphite to $KClO_3$ was 1:10, the possibility of explosion and length of time required are the main drawback of this approach. Hummers and Offeman reported an alternative method, which is safer and also not time consuming. In this protocol, a water-free mixture of concentrated H_2SO_4, sodium nitrate ($NaNO_3$) and $KMnO_4$ are involved, the reaction was performed at 45 °C and continued for approximately 2 h.

Minor modifications to the Hummers method were developed and still remain in use.[24]

Table 1.1: Methods for the oxidation of graphite to graphite oxide.

	Brodie	Staudenmaier	Hummers	Modified Hummers	
year	1859	1898	1958	1999	2004
Oxidants	$KClO_3$, HNO_3	$KClO_3$ (or $NaClO_3$), HNO_3,H_2SO_4	$NaNO_3$, $KMnO_4$, H_2SO_4	pre-ox: $K_2S_2O_8$, P_2O_5,H_2SO_4 ox: $KMnO_4$,H_2SO_4	$NaNO_3$, $KMnO_4$, H_2SO_4
C:O ratio	2.16[21] 2.28[26]	N/A[22] 1.85[26]	2.25[23] 2.17[26]	1.3[25]	1.8[24]
Reaction time	3-4 days[21] 10 hours[26]	1-2 days[22] 10 days[26]	2 hours[23] 9 - 10 hours[26]	6h pre-ox+2h ox[25]	5 days[24]
Intersheet spacing (A°)	5.95[26]	6.23[26]	6.67[26]	6.9[25]	8.3[24]

1.4.3 Functionalization of carbon: covalent and noncovalent

It is well known that carbon nanomaterials aggregate in cell culture media (buffers) caused by the charge screen effect, therefore, surface modification is the key to render the solubility and the biocompatibility of carbon nanomaterials for biological systems. Depending on application purposes, two surface coating regimes are developed, including covalent and noncovalent approaches, allowing GO to be used in biological systems. Before surface functionalization, the size distribution and individual separation of GO are essential for in vitro and in vivo drug delivery.

Covalent functionalization, the covalent functionalization of Nanoscaled carbon materials (CNMs) is preceded by an oxidation of the graphite in acidic media with strong oxidizing agents, resulting in oxygen-rich groups. As described above, the GO is highly oxidized by oxygen groups with C/O ratio of 2:1. The presence of these functional groups allows various chemical routes already known in chemistry to functionalize GO, for instance, covalent functionalization of GO by sodium azide, reduction of azide functionalized GO with $LiAlH_4$ producing amino-functionalized GO and functionalization of GO

with acylation, esterification and nucleophilic ring opening reaction.[27] Fig. 1.3(a and b) represents the covalent interaction of polyethylene glycol (PEG) and PAMAM for 7-ethyl-10-hydroxycamptothecin (SN-38) and carboplatin drug leading and delivery respectively.[28]
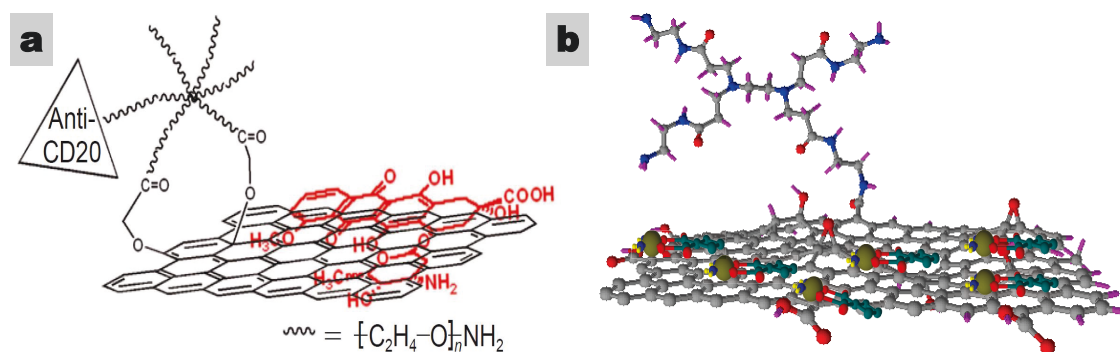
Figure 1.3: Covalent functionalization of NGO. a, PEG functionalized NGO for SN-38 loading, reprinted with permission from ref.[29] **b,** PAMAM functionalized NGO for carboplatin loading.

Noncovalent functionalization, the non-covalent functionalization with different chemical substances is essential and considered to have less impact on the structure and properties of graphene. The attachment of functional groups to GO mostly occurs via $\pi - \pi$ interaction, electrostatic binding, van der Waals and H-bonding.[30–32] For the first time, via non-covalent functionalization, PEG-NGO was employed as a nanocarrier to load therapeutic anticancer drugs and its cellular uptake was studied.[29,33] Owing to their high conjugation system, pristine graphene and GO possess the ability to bind with aromatic compounds including cancer drugs, fluorescence molecule (fluorescein), catalytic hybrid and combinations of molecules.

1.5 Carboplatin

Carboplatin, cisplatin and oxaliplatin are the three members of platinum based therapeutic anticancer drug agents. These compounds have the ability to bind the DNA molecules, forming a variety of structural adducts and induce

apoptosis in cancer cells. The carboplatin or paraplatin-AQ (trade name) is a chemotherapy drug used for killing some forms of cancer cells, such as ovarian, neck, bladder, breast, etc., which shows less side effects compared to its analog form cisplatin, in which the two chloride atoms are replaced by bidentate dicarboxylate ligand (fig. 1.4). The use of any therapeutic agent against cancer cells - in vitro or in vivo - is limited by its uptake promotion and cytotoxicity. In the same context, carboplatin is superior to cisplatin,[34] it was indicated that larger dose of carboplatin is being clinically used to produce equivalent toxicity to that of cisplatin, the presence of a stable bidentate dicarboxylate chelate ring structure in carboplatin is responsible for reducing the reactivity and cross-linking towards DNA, and producing less cytotoxicity when compared to cisplatin. Thereby, it can be hydrolyzed in much slower rate compared to reactive chloride ligand designated in cisplatin structure.[35] Despite differences in solubility in cell culture media (cisplatin less soluble), this property has no effects at physiological concentrations.
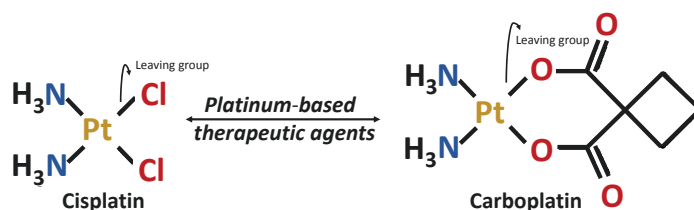
Figure 1.4: Chemical structure of cisplatin and carboplatin as platinum-based chemotherapy agents.

1.5.1 Mechanism of action

Carboplatin and cisplatin have the same mechanism of action toward DNA and RNA cross-linking formation as seen in fig. 1.5. The carboplatin forms longer cross-linking with DNA strands, nevertheless the cross-linking of cisplatin formed faster (6 - 8 hours after administration) than those of carboplatin (18 hours) due in part to the hydrolysis kinetics. Once inside the cancer cell, the carboplatin ring structure is hydroxylated to form the active side, which

efficiently bonds to DNA and RNA strands in order to functionally disrupt these nucleic acids.[34,35]
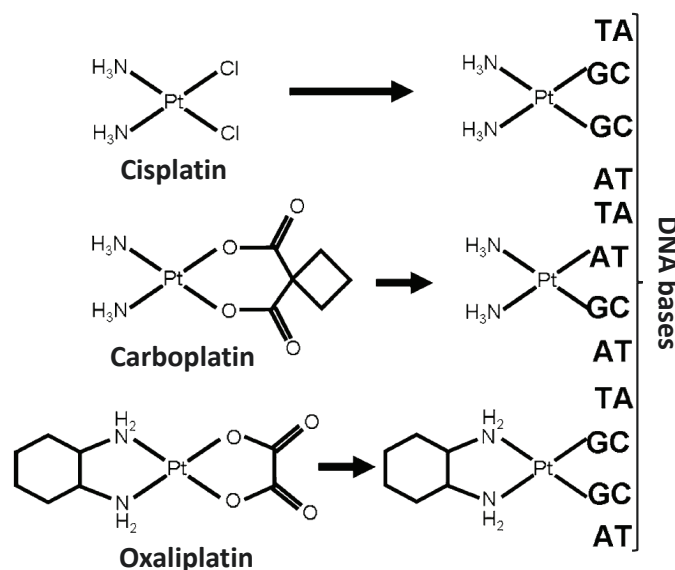
Figure 1.5: Mechanism of DNA platinum based compounds interaction. Reprinted with permission from ref.[36]

1.6   Toxicity assessment of graphene derivatives

Graphene, it has been developed to be a biocompatible platform for adhesion and proliferation of murine fibroblast cells (L-929),[37] neuroendocrine cells (PC-12), oligodendroglia cells (OLC), osteoblasts (OBS)[38] and mesenchymal stem cells.[28] Various cytotoxicity investigations have been evaluated on graphene, GO and functionalized GO in different cell lines.[39–41]

Graphene oxide, a highly biocompatible material, thus, it inspirits the proliferation and adhesion of kidney cells, OBS and human embryonic stem cells (hESc).[38,42] On the contrary, other studies showed GO nanosheets mixed to cell culture media at 20 µg.ml^{-1} can produce 20% reduction in cell viability, whereas 50 µg.ml^{-1} GO induce 50% loss in cell viability, this result was attributed to inhibitory effect due to the GO suspension.[43] Wang et al. examined human fibroblast cells (hFBc) with GO at different concentrations and found that concentration dependent on cytotoxicity when the concentration exceed 50

$\mu g.ml^{-1}$.[39] For the first time, the cyto- and geno-toxic effect of reduced GO nanoparticles were investigated with mesenchymal stem cells,[28] with the study showing that the size and the concentration of GO are effective parameters on the hMSCs cytotoxicity. Recently, in vivo cancer treatment using graphene as nanocarrier has been performed in animal experiments,[44,45] the results performed that the toxicity of graphene oxide to mice depends on different factors, such as, size, concentration, dosage, incubation time, etc.

Functionalized graphene oxide, as previously discussed, GO needs to be functionalized in order to perfectly disperse in culture media, as well as being compatible with tissue organisms. Indeed, GO revealed two types of functionalization (covalent and/or non-covalent) with small molecules or macromolecules, depending on the chemical structure of materials used for GO modification. Functionalized NGO with biocompatible materials such as PEG,[29] dextran,[46] chitosan,[47] pluronic,[48] tween,[42] low generation PAMAM,[28] polyvinylpyrrolidone,[49] gelatin,[50,51] sulfonic acid groups[52] and protein (fetal bovine serum-FBS),[53] etc, revealed high reduction in vitro and in vivo toxicity. In the same context, Zhang et al. measured the cell viability percent of NGO-PEG vehicles as a function of concentration,[54] and the data showed that above 95% of mouse breast cancer cell line (EMT6) remained viable even at high concentration up to 100 $\mu g.ml^{-1}$, which revealed that NGO-PEG has no cytotoxic effect to EMT6 cells after 24 h incubation. In other studies, gelatin-functionalized graphene nanosheets exhibited very low cytotoxic effect against adenocarcinomic human alveolar basal epithelial cells (A549), even at high concentration $300\mu g.ml^{-1}$. Surface modification of GO with appropriate biocompatible materials increases the uptake impact on various cell lines and retorts on the negative performance of pristine graphene and GO via a number of mechanisms such as relative oxygen species (ROS) and cell wall membrane damage.

1.7 Toxicity assessment of other carbon nanomaterials

Several studies emphasized that numerous factors such as chemical composition, size, shape, contaminants, concentration and cell types will influence the cellular uptake and the cytotoxicity of carbon-based materials.[33, 55–59] To the best of our knowledge, there are few experimental reports that compare the cytotoxicity of carbon nanomaterials.[40, 60, 61] Table 1.2 highlights the cytotoxicity evaluation of carbon nanomaterials concerning the size, concentration and biological systems.

Comparsion with CNTs, PEGylated NGO exhibited distinctive in vivo behaviors such as reduced reticuloendothelial systems (RES) accumulation and particularly improved tumor passive targeting effect.[62] The unique 2D structure, small size (10-50 nm) and biocompatibility played an important role to enhance permeability and the retention effect of nanographene sheets (NGS) for high tumor passive uptake. Carbon nanotubes in both forms, single- and multi-wall CNT, are widely considered to be as speculate materials for biomedical applications. The large length-to-diameter aspect ratio (more than 10^6; 1 mm length and 1 nm diameter) with high surface area makes it amenable for high molecular detection and recognition. Pristine CNTs are intrinsically insoluble in water and biological media, i.e., they cannot be explored directly in drug and bimolecular fields, thus, CNTs should be functionalized to render them soluble and compatible in cell culture media. The toxicity of single- and multi-wall CNTs is attributed to numerous factors, for instance, length to diameter ratio, assay methods, functionalization, concentration, time of exposure and nature of cells investigated.

Wörle-Knirsch et al. found that the toxicity of SWCNTs depends on the preparation assay, the results showed that the viability of A549 decreased up to 40 via Methylthiazol Tetrazolium (MTT) assay after addition of SWCNTs, but no changes on viability by using 2-(4-iodophenyl)-3-(4-nitrophenyl)-5-(2,4-

disulfophenyl)-2H-tetrazolium, monosodium salt(WST-1) assay method.[63]

Comparsion with nanoparticles, such as gold nanorods (AuNRs) significantly explored as photothermal agents, the result showed that PEGylated NGS emerged as comparable with PEGylated AuNRs in terms of administration routes (intravenous), injected doses (20 mg.kg^{-1}), NIR laser densities (2 W.cm^{-2}) and irradiation durations (5 min).[64]

Comparsion with fullerene, the first carbon nanomaterial investigated toward biomedical applications due to it being the first to be discovered in 1985,[65] and classified as an inorganic nanoparticle with wide availability due to its small size (ca. 1 nm). Innate fullerene particles have very low dispersibility in water and form negative charge aggregates with an average size of 160 nm. Hence, -OH groups and other organic molecules are induced in fullerene in order to activate its surface for better dispersibility in water and physiological media,[66,67] high dosages of fullerene particles, more than 70 mg.L^{-1} lead to cell death after 24 h incubation, as the fullerene concentration and incubation time increase, the cell mortality increases.[67]

From chemistry point of view, GO has conspicuous advantages in biological applications over other carbon based nanomaterials, such as CNTs. First, high water solubility without the cutting and de-bundling process required for CNTs. Second, it has no or very law oxidative stress commencing from metallic catalyst impurities, which induces CNT toxicity. Third, GO has excellent dispersion in cell culture media which does not entail surfactants, the latter being an influence of CNT - induced toxicity. Fourth, it has high surface area, which tolerates high drug leading capacity via π - π interaction.[68,69]

Table 1.2: Toxicity evaluation of carbon nanomaterials

CNMs	Size	Concentration	Biological system	Comments	Ref
GO	Below 200 nm	50 μg.ml^{-1}	HeLa	No cytotoxic effect even at high concentration	[70]
GO	LD: 350 nm, H: 3.9 nm LD: 2 μm H: 4.05 nm	0 - 20 μg.ml^{-1}	PMØ, J774A.1 LLC, MCF-7 HepG2, HUVEC	No significant difference in cytotoxicity between 350 nm and 2 μm at different concentration.	[71]
GO	1429 $\pm 89 nm$ H: 1.038 nm	20 - 100μg.ml^{-1}	HUVECs	Cell viability is concentration dependent	[72]
rGO	LD = 3.8 $\pm 0.4 \mu$m, LD = 11 $\pm 4 nm$		hMSCs	Cell destruction at 11 $\pm 4 nm$. 3.8 $\pm 0.4 \mu$m has cytotoxic effect only at high concentration of 100 mg.ml^{-1}.	[71]
GO - CS	GO > 1000 nm, 0.8 - 1.2 nm thickness. GO-CS < 500 nm, 4 - 5nm	0.1 - 100 mg.ml^{-1} (GO - CS)	HepG2, HeLa	GO - CS has no obvious cytotoxicity, 80% Cell viability	[73]
GO-PEG	5 - 50 nm	0.1 - 100 mg.ml^{-1}	HCT-116, (72 h)	NGO - PEG exhibited no obvious toxicity	[33]
SWCNTs	1 nm (ϕ) 1000 nm (L)	3.8μg.ml^{-1}	macrophage cells	The macrophages consume high quantity of SWCNT without showing toxic effects.	[74]

Functionalized SWCNTs	1 - 5 nm (ϕ) 0.1 - 1 μm(L)	50 μg.ml^{-1}	HL-60, 3T3, CHO	No toxicity observed for SWCNTs and functionalized SWCNTs by endocytosis.	[75]
SWCNTs, MWCNT, C60,	SWCNT: 1.4 nm (ϕ) 1000 nm (L) MWCNT: 10 - 20 nm (ϕ) 0.5 - 40 μm (L)	0 - 226μg.ml^{-1}	Guinea pig alveolar macrophage	Cytotoxicity of MWCNTs was lower than SWCNTs	[76]
SWCNTs MWCNTS Carbon black Activated C	2 nm (ϕ) 500 nm (L) 50 nm (ϕ) 5000 nm (L) 200 nm (r) 25 nm (r)	0 - 100 μg.ml^{-1}	HDF	Cell survival rate: MWCNTs>CB>AC>SWCNTs	[77]
SWCNTs Carbon black SiO2 ZnO	8 nm (ϕ) L < 5000 nm 10 - 20 nm (ϕ)	5-100μg.ml^{-1}	PMEF	SWCNTs revealed moderately cytotoxic effect than metal oxides, but persuaded more DNA damage.	[61]
SWCNTs MWCNTs	4 nm (ϕ) 0.5 - 100 μm (L) 15 nm (ϕ) 0.5 - 200 μm (L)	200 - 400 μg.ml^{-1}	In vivo	SWCNTs are less toxic than MWCNTs	[78]

List of abbreviations mentioned in table 1.2:

LLC	Lewis lung carcinoma
MCF-7	Breast cancer cells
HepG2	Human liver carcinoma cells
HUVEG	Human umbilical vein endothelial cells
hMSC	Human mesenchymal stem cells
HCT-116	Human colon cancer cells
PMØ	Peritoneal macrophage
J774A.1	Mus musculus, mouse
HL-60	Human promyelocytic leukemia cells
3T3	Mouse embryonic fibroblast cells
CHO	Chinese hamster ovary cells
HDF	Human dermal fibroblast
PMEF	Primary mouse embryonic fibroblast

1.8 Nanoscaled drug delivery vehicles

In vitro tests, various aromatic drugs have been loaded onto functionalized NGO, such as doxorubicin (DOX) and water insoluble 7-ethyl-10-hydroxycamptothecin (SN-38). DOX and SN-38 are the first two drug molecules loaded on PEGylated nanographene oxide (NGO-PEG) as a vehicles for drug delivery. DOX loading onto NGO-PEG achieved by simple mixing with NGO-PEG solution under controlled pH overnight via physisorption π - π stacking. NGO-PEG-Rituxan/DOX with lymphoma cell (Raji-B) investigated in vitro, the result revealed that DOX delivery into Raji B - cells enhanced in NGO-PEG-Rituxan/DOX comparing with free DOX and NGO-PEG/DOX as well. Thiolated Rituxan (marker protein (CD20) + antibody) conjugated to the amine groups onto NGO-PEG is used for selective killing of cancer cells.[29]

Water insoluble molecule SN-38 loaded NGO-PEG via $\pi - \pi$ stacking revealed excellent solubility in the biological environment,[33] NGO-PEG/SN38 exhibited high influence to kill cancer cells in vitro with a human colon cancer cell line (HCT-16). Folic acid loaded NGO with the two anticancer therapeutic drugs (DOX and irinotecan (CPT-11)) showed specific targeting to human breast cancer cells (MCF-7), as well as high cytotoxicity compared to unmodified NGO loaded with DOX or CPT.[52] Methotrexate (MTX) loaded onto gelatin functionalized graphene nanoparticles (GNP) showed better release at low pH than neutral conditions, GNP - gelatin/MTX system exhibited lower cytotoxic effect with adenocarcinomic human alveolar basal epithelial cells (A549) in comparison with free MTX at the same concentration.[51]

In vivo tests, the in vivo therapeutic efficacy of NGO-PEG/DOX was demonstrated through combination of photothermal treatment and chemotherapy, in this study,[54] four mice groups were treated with buffer, DOX, NGO-PEG and NGO-PEG/DOX. The tumor region of NGO-PEG and NGO-PEG/DOX

irradiated by NIR light after 24 h of injection. Free DOX exposed rapid growth of tumor volume as a result of insufficient dosage to reduce it. NGO-PEG group showed reduction in the tumor volume after a few days of injection, and then follows its growth to reach the size of DOX group. NGO-PEG/DOX showed considerable trend with size reduction of tumor volume along a period of 30 days, this group demonstrated as a powerful vehicle for combined chemo-photothermal therapy of cancer in vivo. Furthermore, the result revealed no weight loss was perceived, indicating that the toxicity of materials was not severed.

On the other hand, Yang et al. reported for the first time the behavior of nanographene sheets in vivo by using PEG coating via a fluorescent labeling method, PEG-functionalized GO was labeled with the fluorescent cyanine-7 (Cy7) dye for in vivo investigations, the majority of Cy7 dye molecules are covalently bonded to NGO-PEG via an amide bond formation. Three tumor models (4T1 tumor bearing Balb/c mice, KB and U87MG tumor bearing nude mice) were demonstrated with different time points after intravenously injected by NGO-PEG-Cy7 and subsequently imaged.

The concentration of NGO-PEG-Cy7 versus time was measured and the blood circulation half-life was observed approximately at 1.5 h. NGO-PEG-Cy7 existed in different tumor models over time, NGO-PEG exhibiting an excellent in vivo tumor near-infrared (NIR) photothermal therapy without obvious toxicity to the treated mice. Neither death nor noteworthy body weight drop was observed in the NGO-PEG plus laser-treated materials after 40 days of photothermal therapy, the major organs of treated mice were collected for histology analysis, the results exhibited no noticeable signal of organ distortion, suggesting the assure of using PEGylated NGS for in vivo applications.[56]

Table 1.3 summarizes the cytotoxicity and the cellular uptake in vitro and in vivo for various therapeutic systems.

Table 1.3: In vitro and in vivo toxicity evaluation of therapeutic nanomaterial systems.

Therapeutic systems	Concentration	Biological system	Comments	Ref
		GO based therapeutic systems		
NGO - PEG - Rituxan/DOX	2, 10 mole.L^{-1} In terms of DOX	Raji and CEM cells	High selectivity at [DOX] = 10 mol/L. Rituxan improved doxorubicin delivery into Raji B-cells. Less toxic than free DOX	[29]
NGO - PEG/ SN 38	1 mg.ml^{-1} in terms of SN 38	HCT - 116	High cancer killing potency in comparison with free SN 38 molecules in organic solvents.	[33]
GO - Pluronic (F38)/EA	100 wt% (GO - F38)	MCF-7 and HT-29	High drug loading capacity. EA loaded onto functionalized GO has less cytotoxic effect than free EA.	[79]
GO - Tween 80 (T80)/EA	122 wt% (GO - T80)			
GO - Maltodextrin (MD)/EA	114% (GO - MD)			
GO - CS - CPT CS: Chitosan CPT: Capto- thecin	10 μM	HepG2 HeLa cells	No obvious toxcity measured for GO - CS. GO - CS/CPT possessed higher cytotoxic effect than free CPT	[73]
GO - FA/Ce6 (chlorine e6)	2:1 (wt/wt) 1:1 (wt/wt) (GO-FA):Ce6	MGC-803	GO FA is non-toxic. 2:1 ratio revealed no dark toxicity and more than 80% of cell viability. 1:1 ratio revealed cell viability less than 50%.	[49]

			Toxicity is concentration dependent.	
NGS - PEG/ 125I	20 mg.kg^{-1}	In vivo	PEGylated NGS largely gatheredin the reticuloendothelial system. No toxic effect at 20 mg/kg to the treated mice in a period of 3 months.	[45]
		CNT based therapeutic systems		
CNT - CP CNF - CP	20% 14%	DU145,PC-3, A498, EJ28	No toxic effect observed for unloaded CNTs at 100 μg/ml. No noteworthy toxicity observed for unloaded CNFs at 100 μg/ml. CNT - CP showed low cancer cell growth than free CP.	[80]
DOX - FA - CHI/ALG - SWCNT	300 wt%	HeLa cells	DOX – FA – CHI/ALG – SWCNTs are highly selective system and not cytotoxic.	[81]
DOX - PL - PEG - SWCNT	270 mg.l^{-1} of DOX.	In vivo (SCID mice)	The SWCNT - DOX (5 mg/kg) exposed greater inhibition of tumor growth than free DOX. Mice treated with SWCNT - DOX possessed stable weight and no mortalities compared with free DOX.	[82]
SWCNT-cisplatin	100 μg.ml^{-1}	PC3 DU 145	Free cisplatin and SWCNT - Cisplatin have the same effect on PC3, but less effective DU145.	[83]

Fullerene based therapeutic systems

C60 – PEI – FA/DTX	200 wt%	PC3 In vivo Murine S 180	C60 – PEI – FA has no obvious toxicity to PC3. The system has higher inhibition efficiency than free DTX. C60 – PEI – FA/DTX is more effective than free DTX and C60 - PEI - FA in vivo.	[84]
Nano - C60 (water soluble)	0.24-2 ppb 400 ppb	HepG2, HDF, NHA,	Nano-C60 has cytotoxic effect to tested cell lines after 48 h exposure	[85]
C60(OH)24	100 µg.l^{-1}	HDF HepG2 cells		[86]

List of abbreviations mentioned in table 1.3:

Raji-B	B-lymphoma cells
CEM	Human lymphoblasts
DOX	Doxorubicin
HCT-116	Colorectal carcinoma
SN-38	7-ethyl-10-hydroxycamptothecin
PEG	Polyethylene glycol
MCF-7	Human breast cancer cells
HT-29	Human colorectal adenocarcinoma cells
FA	Folic acid
HepG2	Human liver carcinoma
MGC-803	Human gastric cancer cells
Ce6	Chlorin e6
EA	Ellagic acid
DU145	Human prostate cancer cells
PC-5	Neuronal cells
A498	Homo sapiens carcinoma cells
EJ28	Human bladder cancer cells
PC-3	Human prostate cancer cells
SCID	Severe combined immunodeficiency (mice)
PEI	Polyethylenimine
DTX	Docetaxel
HDF	Normal human fibroblasts
NHA	Normal human astrocytes

1.9 Biological studies

The difference between normal and abnormal cells is profound, not only because of their shape and behavior but also the drastic difference in life expectancy. In culture media, the cancer cells still survive forever, conversely the normal cells such as mesenchymal stem cells die after 50 generations.

In this work, HeLa and neuroblastoma cell lines are used as a model for studying the potency of carboplatin and carboplatin loaded nanohybrids in prohibiting metabolic activity. Mesenchymal stem cells are used for biocompatibility assays.

1.9.1 Mesenchymal stem cells

The human mesenchymal stem cells are usually found in bone marrow and adipose tissue, they considered as adult or somatic cells, as well as a good model of non-malignant multipotent stem cells. They have generated a massive interest in medical purposes because of their ability to self-renew and differentiate readily into variable cell types. Consequently they are rare cells and must be grown to obtain adequate quantity for research and therapeutic applications.[87]

Recently, many reports have been developed to investigate the uptake and cytotoxicity of graphene nanoparticles onto hMSCs, as an important model for biocompatibility assays.[28,55,88–90] The first report,[89] Akhavan et al. has investigated the size dependent cyto- and geno- toxicity of graphene oxide and reduced graphene oxide onto hMSCs, the results showed the effect of nanoparticles concentration and incubation time through monitoring viability.

In conclusion, hMSCs are actively proliferated and repetitively expandable stem cells that could be used in vitro to study the uptake and cytotoxicity of nanographene oxide particles in contrast to other primary stem cells.[91]

1.9.2 | HeLa cancer cells

The most common immortal cancer cell lines model known worldwide in biological research. It was derived from a lady in 1951 called Henrietta Lacks, she died of her cervical cancer eight months later and associated with her name (HeLa). These cells indeed were the first cell lines survive and grow out of human body, and can divide to unlimited times under suitable conditions.[92] HeLa cells were chosen in order to study the effects of NGO samples on cancer cells through anticancer activity measurements.

1.9.3 | Neuroblastoma cancer cells

A tumor of the childhood, represents approximately 9% of all cancers infect children world-wide. It categorized as the most common extracranial solid tumor in infants and existing as diffuse growth of undifferentiated neuroblastic cells. Typically, the tumor starts from adrenal gland and ganglion chain and often displays the ability to affect more than organ or tissue of neural crest cells.

Park et al. studied the effect of graphene on growth of neuroblastoma cells, the fluorescence data demonstrated that the presence of graphene did not influence cell morphology, thereby these findings candidate graphene for biological applications.[93]

The neuroblastoma cell line especially derived from human brain tumor represents a good model to evaluate the cellular uptake and anticancer activity of carboplatin and carboplatin loaded nanohybrids on tumor cells. This study is useful to understand the effect of nanoparticles size, reactive oxygen species and optimum concentrations prior in vivo investigation.

2

MATERIALS AND METHODS

The procedures of nanographene oxide, functionalization (covalent and noncovalent) and carboplatin loading are shown in this chapter. The characterization methods used throughout this thesis are discussed concisely.

2.1 Synthesis of nanographene oxide particles (NGO)

2.1.1 Preparation of graphite oxide materials

Graphite oxide was produced from natural graphite (99.99%, -200 mesh, Alfa Aesar) based on modified hummers method.[12, 28] Briefly, 1.0 g graphite (Gr) was ground with 50.0 g of NaCl for 10 min in order to exfoliate the graphite flakes (de-agglomeration), as well as reduce their dimensions. The ground graphite (Gnd Gr) was dissolved in warm distilled water and collected using a 450 nm porous TEFLON filter paper by suction filtration. The filtered graphite was mixed in 23 ml of H_2SO_4 (95%, VWR) overnight. Thereafter, the mixture was placed in an ice bath to ensure that the temperature remained below 10 °C. Subsequently, 3.0 g $KMnO_4$ (99%, VWR) was added gradually over 3 hours with constant stirring.

After complete addition of $KMnO_4$, the mixture was sonicated for 3 hours and continuously stirred for 30 min at 35 °C and 45 min at 50 °C, respectively. 46.0 ml distilled water was added to the mixture and kept with stirring at 98 - 105 °C for 45 min. The mixture was cooled down to room temperature (RT) and stirred with the addition of 140.0 ml distilled H_2O and 10.0 ml of 30% hydrogen peroxide H_2O_2 (30%, Sigma-aldrich). The collected samples were filtered and washed five times with HCl (5%, Sigma-aldrich) and distilled water to remove any reaction by-products.

2.1.2 Sonication of graphite oxide for size reduction

Horn - tipped ultrasonic probe (BANDELIN ultrasonic, max. power of 25 - 60%) under optimized conditions was used to crack and reduce the dimensions of exfoliated graphene oxide particles.[28, 47, 94] The concentration of GO, sonication

time and power are considered as controlled conditions for obtaining nano-scaled GO particles in water.

2.1.3 Centrifugation of NGO particles in sucrose solutions

Sucrose solutions were prepared with different viscosity to separate the sonicated GO sheets according to their dimensions.[28,95,96] Sucrose is a low cost material and environmentally friendly, since it is selected for NGO size separation. Typically, 20 - 60% sucrose solutions were prepared in distilled water, and the layers of sucrose (with increasing density) were dropped into the bottom of the centrifuge tube (335 ml each). On the top of multilayer water sucrose solutions, 335 ml NGO in water suspension was layered prior to centrifugation (BECKMAN COULTER, Allegra 64 R centrifuge) under typical centrifugation conditions (5880 g for 5 min). Three different zones along the centrifuge tube were obtained (washed sufficiently from sucrose) and separated as three sizes for NGO functionalization and carboplatin loading.

2.2 Functionalization of NGO particles

2.2.1 Covalent functionalization of NGO by PAMAM dendrimer

The PAMAM - G0 dendrimer has four amine NH_2 terminated groups.[15,28,97–100] 20 μL of a PAMAM solution in methanol (20%, wt/wt) was added to a solution of NGO (1 mg.ml^{-1}). The mixture was continuously stirred for 2 hours at RT. The PAMAM functionalized NGO was collected, washed thoroughly with distilled water and collected after centrifugation at (5880 g for 2 min) to remove unbound PAMAM and methanol. The collected material was then left to dry overnight below a temperature of 35 °C.[28] The resultant material labeled as NGO - PAMAM.

2.2.2 | Noncovalent functionalization of NGO by gelatin

20 μL of gelatin was added to a solution of NGO (1 mg.ml^{-1}), the mixture was continuously stirred for 2 hours at RT. The resultant was collected, washed thoroughly with distilled water and collected after centrifugation at 5880 g for 2 min to remove unbound gelatin. The collected material, labeled Gel_NGO, was then left to dry overnight below a temperature 35 °C.

2.3 | Carboplatin loading

2.3.1 | Preparation of CP loaded pristine NGO particles

Carboplatin stock solution (10 mg.ml^{-1}, chemical formula C$_6$H$_1$2N$_2$O$_4$Pt) was purchased from Hospira Inc. USA. In separate experiments, 20 μL of carboplatin was mixed with 1 mg.ml^{-1} NGO 100 nm, 200 nm and 300 nm with stirring for 2 hours at RT. Thereafter, the products labeled CP@NGO, collected and dried under a vacuum at RT.

2.3.2 | Preparation of CP loaded PAMAM and gelatin

20 μL of CP stock solution was added to a solution of 1 mg.ml^{-1} PAMAM. The mixture was continuously stirred for 2 hours at RT. The resultant was collected, washed thoroughly with distilled water and collected after centrifugation at 5880 g for 2 min to remove unbound PAMAM molecules.

The collected material labeled CP@PAMAM and left to dry overnight below a temperature 35 °C. The same procedure was used for CP@gelatin by using native gelatin as loading material.

2.3.3 Preparation of CP loaded nanohybrid materials

In separate experiments, 20 μL of carboplatin was mixed with 1 mg.ml^{-1} NGO-PAMAM and stirred at RT for 2 hours. Thereafter, the products labeled CP@NGO-PAMAM, were collected and dried under vacuum at RT.

The same procedure was used for the preparation of the CP@Gel_NGO nanohybrids and stored under vacuum at RT.

2.4 Cell culture

The human cervical carcinoma cell line (HeLa) obtained from American type culture collection (ATCC, Rockville, Maryland) and human neuroblastoma cell line (IMR-32) obtained from Lonza were grown in a complete cell culture medium for investigation of CP@NGO-PAMAM and CP@Gel_NGO nanohybrids respectively.[28] The cell culture medium consisting of DMEM (Dulbecco's Modified Eagle Medium) supplemented with 2 mM L-glutamine, 100 IU mL^{-1} penicillin, 100 mg.mL^{-1} streptomycin and 10% heat - inactivated fetal bovine serum (Gibco, Invitrogen).[101,102] The cell culture was maintained at 37 °C in a saturated humidity atmosphere of 95% air and 5% CO_2.

In order to test effects of NGO and NGO derivatives, a modified culture medium was prepared by mixing the nanocomposite solution with the complete culture medium, while the complete culture medium served as the control sample. Human mesenchymal stem cells, which are primary and non-malignant cells obtained from Lonza were grown in the same culture medium and introduced as healthy Cells.

2.5 Viability assay

WST - 8 (2 - (2 - methoxy - 4 nitrophenyl) - 3 (4 - nitrophenyl) - 5 (2, 4 - disulfophenyl) - 2 H - tetrazolium, monosodium salt) cell proliferation kit and Alamar blue reagent were used to evaluate the cell viability for CP@PAMAM-NGO and CP@Gel_NGO nanohybrids respectively.

HeLa, neuroblastoma cancer cells and hMSCs were cultured in DMEM supplemented with 2 mM L-glutamine, 100 IU mL^{-1} penicillin, 100 mg.mL^{-1} streptomycin and 10% heat inactivated fetal bovine serum (FBS). Cells are expanded in Petri dishes and maintained at 37 °C in a saturated humidity atmosphere containing 95% air and 5% CO_2. Thereafter the cells were plated in 96 - well plates (25x10^3 cells per well) and incubated for 24 hours.

The modified medium containing the nanocomposites was introduced separately to cells at different test concentrations and incubated for another 24 hours.
The cells cultured with the regular culture medium were tested as the control.

2.5.1 WST - 8 viability assay

A fresh media containing 10% of a WST-8 solution were added to each well and incubated for an additional 2 hours at 37 °C.

The assay is based on the cellular dehydrogenase reduction of WST-8 to an orange formazan dye which dissolves directly in a tissue culture medium, the amount of formazan produced is directly proportional to the number of living cells, the absorbance was recorded on a Versamax microplate reader (Molecular Devices, Sunnyvale, CA) at a wavelength of 450 nm with the background subtracted at 650 nm.[28, 101, 102]

2.5.2 Alamar blue assay

To determine the viability of cells exposed to NGO particles, Gel_NGO nanohybrids and CP@Gel_NGO, an Alamar Blue (AB) assay has been utilized. The active ingredient of AB dye is resazurin that is blue in color, soluble, nontoxic, virtually non-fluorescent and undergoes colorimetric change in response to cellular metabolic activity. The reduced compound is resorufin, pink in color and highly fluorescent.

The viable cells metabolize the AB dye and convert resazurin to resorufin, thereby producing an increase in the fluorescence intensity as determined by Versamax microplate reader (Molecular Devices, Sunnyvale, CA) at a wavelength of 450 nm with the background subtracted at 650 nm, the absorbance intensity is proportional to the number of living cells.
Indeed, the damage or non-viable cells have lower metabolic activity and thus generate weak absorbance than healthy cells.[103, 104]

The viability was measured as follows:
Percent viability = (experimental value/control value) x 100%.
Test media were assayed 3 times.

2.6 Statistical analysis

For the cell viability assays, three experiments were carried out and quadruplicated, the statistical values were expressed as means and the standard deviation was taken as the error. The statistical significance was assessed by one-way analysis of the variance followed by a post-hoc comparison test (Tukey). The significance was set at $p < 0.01$.

2.7 Morphology and structure characterization

In this thesis, a variety of characterization techniques have been used to under-stand the structure and properties of GO. These techniques are classified into spectroscopic and microscopic approaches. The spectroscopic approaches are used to identify the chemical structure of GO, and include Raman, FTIR and XPS. Microscopic tools (AFM and SEM) are used to map out the structure of GO at various heights and lateral dimensions.

2.7.1 Spectroscopic approaches

Raman spectroscopy, a probe of order and disorder in the carbon skeleton of sp^2 and sp^3 hybridized carbon-based materials.

Graphite material (multiple graphene sheets) has three dominant Raman features at 1580 cm^{-1} (G band), 1,350 cm^{-1} (D band) and 2,700 cm^{-1} (2D band), the G mode corresponds to planar vibrations of carbon atoms and is present in most graphite-like materials, the D mode is related to the structural defects and is present in all graphite-like carbon materials.

In GO, the G band is wider and shifted to a lower frequency region ca. 1,590 cm^{-1}, the D mode intensity increases and probably becomes higher than the G mode due to the structural disorder in the sp^3 pattern induced by oxygen containing groups on the carbon basal plane or at the edges.

On the other hand, the 2D mode reduces and becomes wider with respect to the D and G bands.[105–107]

The Raman spectra were recorded on a Thermo Scientific, DXR Smart Raman with an excitation laser wavelength of 532 nm. The samples were deposited on silicon substrate.

Fourier transform infrared spectroscopy (FTIR), an infrared spectroscopy yielding complementary information to those provided by Raman spectroscopy. The mid IR region contains the most useful vibrational frequencies of various oxygen groups. Consequently, the IR spectrum is frequently used in order to identify the presence or absence of specific functional groups in a molecule.

In the case of GO, the most characteristic peaks are the broad peak of hydroxyl group (-OH) at 3,430 cm^{-1}, the peak at 1,720 cm^{-1} corresponding to carbonyl group (C=O), 1,570 cm^{-1} representing the skeletal vibrations of sp^2 carbon atoms, 1,225 cm^{-1} and ca. 1,100 cm^{-1} referring to stretching vibrations of COOH and C-O-C, respectively.[70, 108, 109] The FTIR spectra were recorded on a Bruker IFS 113 spectrometer using the KBr disk method. The spectra of NGO samples were recorded between 4,000 and 800 cm^{-1}, each spectrum was measured by averaging 256 scans recorded at a resolution of 2 cm^{-1}.

The spectra of PAMAM, CP and CP@PAMAM thin films were recorded using a FTIR (IFS/66v/S, BRUKER Optic, GmbH, Karlsruhe, Germany) spectrometer supplied with diamond attenuated - total - reflectance - (ATR) - crystal (RESULTEC, Illerkirchberg, Germany).

X-ray photoelectron spectroscopy (XPS), known also as electron spectroscopy for chemical analysis (ESCA), a beam of X-rays in ultra-high vacuum (UHV) conditions, forcing the core electrons to be excited into unoccupied atomic/molecular orbitals above the Fermi level. Simultaneously, the kinetic energy in addition to the number of electrons that escape from the top few nanometers of the material being analyzed is measured.
The XPS provides insight into the identity of the functional groups distributed onto the surface which modulate the carbon nanomaterial's properties.
In GO, XPS further unambiguously exhibits the carbon and oxygen bonds (C1s) in their various forms; C-C (sp^2 or sp^3), C-OH, C-O-C, C=O and C=OOH.

Information provided by O1s spectra is complement with the C1s signals due to lower kinetic energy than those of C1s. XPS provides information about the identity of different kinds of metal ions like Cu, Ni, Co, Cu, Ag, Mg, Pt, etc., as well as information on the valences and the ratio of these metals.[106, 109–111]

The XPS measurements were carried out in an ultrahigh vacuum system ($<10^{-9}$ mbar) equipped with a hemispherical electron analyzer SPECS PHOIBOS 100. Photo-electrons in all XPS measurements were excited with non-monochromatic Mg Kα (1253.6 eV) radiation and analyzed with a constant pass energy of 15 eV. The X-ray source was run at a power of 300 watts.

2.7.2 Microscopic approaches

Scanning electron microscopy (SEM), a type of electron microscope which images a sample by raster scanning it with a focused beam of high-energy electrons, it is one of the most frequently used techniques in sample characterization, due to its good resolution, ease of applicability, large depth of focus and high magnification.

In a typical setup, an electron gun emits a high-energy electron beam in a high vacuum chamber, which later passes through a series of focusing and accelerating magnetic lenses, the high kinetic energy carried by the accelerated electrons, is dissipated as a variety of signals produced by electron–sample interactions when the incident electrons are decelerated in the solid sample, including, in addition to many, the secondary electrons.
The generated signals are then drawn to the secondary electron detector which is highly positively charged and guided through the Faraday cage to the collection target, finally, they are converted into 2D gray scale images.

SEM is a versatile method used to gain information on the graphene and GO domains like size, shape and nucleation density. It has also, recently, been

used to study monolayer graphene onto different surfaces.[112, 113]

SEM images were obtained using a FEI, NOVA NanoSEM 200 with an acceleration voltage of 15 kV.

Atomic Force Microscopy (AFM), a high-resolution type of scanning probe microscopy. It is a method to visualize the surface topology of materials in three-dimensional (3D) detail down to the nanometer scale.[113, 114]

AFM reveals the thickness of graphene and GO sheets, as well as the number of layers.[7] Moreover, it can show the distance between two graphene or GO layers which is essential to distinguish between them. AFM uses a laser beam detection system in order to control the piezoelectric element movements, where the laser is reflected from the back of the deflected cantilever onto a position-sensitive detector.

AFM works in three main modes: tapping mode, contact mode and non-contact mode AFM.[114] Tapping mode is frequently used in characterizing GO as it allows high resolution imaging without inducing destructive frictional forces onto the sample under investigation.
AFM images of well-defined NGO sizes and modified surfaces were acquired using Digital Instruments Veeco, NanoScope IIIa, operating in the tapping mode.
The images were analyzed using WSxM software designed by Nanotech Electronica (Madrid, Spain).[115]

3

RESULTS AND DISCUSSION

This chapter is divided into three main sections; section 3.1 explains the characterization of GO materials, as well as the optimized conditions for size controlled and reduction. Section 3.2 elucidates the covalent functionalization of NGO particles by using PAMAM as biocompatible material, the loaded and unloaded nanohybrid systems with carboplatin were investigated in vitro with HeLa cancer cells and mesenchymal stem cells, the results of this section have been published in J. Mater. Chem. B [1]. The noncovalent interaction between NGO particles and gelatin is discussed in section 3.3, the biological systems used for this study are the neuroblastoma cancer cells and mesenchymal stem cells, the result of this part has been accepted for publication in Pharm. Res. [2].

Citation:

[1] **Sami Makharza**, Giuseppe Cirillo, Alicja Bachmatiuk, Orazio Vittorio, Rafael Gregorio Mendes, Steffen Oswald, Silke Hampel and Mark H. Rümmeli. *Size-Dependent Nanographene Oxide as a Platform for Efficient Carboplatin Release.* J. Mater. Chem. B (**2013**), 1, 6107.

[2] **Sami Makharza**, Orazio Vittorio, Giuseppe Cirillo, Steffen Oswald, Maria Kavallaris, Bernd Büchner, Michael Mertig and Silke Hampel.*Graphene Oxide – Gelatin Nanohybrids as Functional Tools for Enhanced Carboplatin Activity in Neuroblastoma Cells.* Pharm. Res. December (**2014**).

3.1   Size-controlled synthesis of nanographene oxide

3.1.1   Characterization of graphene oxide materials

The GO materials were carried out from graphite by using oxidation reaction. Fig. 3.1 represents step by step the preparation reaction of GO, firstly, graphite flakes ground with NaCl salt in order to de-agglomerate graphite gallery and reduce its dimensions (lateral width and height).

Intercalation of concentrated sulfuric acid molecules (H_2SO_4) in graphite produced more expansion due to the weak interaction between graphite flakes and no change on the lateral width observed (fig. 3.2a), as well as the acidic medium is necessary for starting the oxidation reaction.

In step 1, adding $KMnO_4$ to intercalated graphite (the temperature should be below 5 °C) leads to the appearance of oxygen atoms as functional groups distributed on the basal plane of graphene layers, as well as distort the hexagonal sp^2 - sp^2 regime.

The thermal treatment in two intervals (step 2 and 3) yields more oxygen groups due to rapid kinetics.[116]

Later in step 4, H_2O_2 solution was added to terminate the oxidation process and the color changes to brown indicating a high level of oxidation (see the inset photography in fig. 3.2a). After multiple washings, as prepared graphite oxide was left in oven below 35 °C for drying.

An elemental micro-analysis (EXD (Energy-Dispersive X-ray analysis)); revealed the presence of carbon and oxygen atoms without contamination (fig. 3.2b).

The structure of graphite, ground-graphite (Gnd Gr), intercalated-graphite (IG) and GO samples (four steps) were systematically studied using Raman and

FTIR spectroscopy.

It is well known that the Raman spectrum of pristine graphite revealed three characteristic bands at 1340 cm^{-1} (D), 1570 cm^{-1} (G) and 2700 cm^{-1} (2D) as shown in fig. 3.2c, the spectra were normalized with respect to the G-band, the D-band is indicative of structural disorder, this is seen to increase relative to the G-band for the GO samples due to the increased structural disorder that occurs through oxygen groups distribution.

The intensity ratios of D- to G-bands (ID/IG) increased from ca. 0.2 for graphite to ca. 0.75 GO with addition of the oxidizing agent (KMnO$_4$). The G-band position shifts to higher frequencies from 1570 to 1598 cm^{-1} linearly with reaction steps as does the full width at half maximum (FWHM). This result indicating that a higher degree of oxidation depends on the reaction conditions. All these changes are concomitant of oxidation.[117–119]

Changes between the starting graphite and GO samples in the FTIR spectra can also be observed (fig. 3.2d). The FTIR spectrum of the pristine graphite shows weak features in the mid IR region indicating little to no oxygen groups being present as expected.[120]

The GO samples are shown to contain a variety of oxygen rich groups normalized with respect to CH$_2$ vibrational band appeared at ca. 2730 cm^{-1}. These include the hydroxyl (-OH), carbonyl (C=O) and epoxy (C-O-C) groups at 3415, 1700-1730 and 1078 cm^{-1}, respectively. The peaks from 1425 to 1225 cm^{-1} can be ascribed to COOH groups.[109] The absorption band at 1575 cm^{-1} is attributed to the sp^2-skeletal vibration of graphene sheets.[109,121]

Further chemical treatment of GO (from step 1 to step 4) brings further successive increase in the oxygen contents.[13] Throughout oxidation reaction, the dimensions of GO particles remain relatively stable for both lateral width and thickness as shown in panel (a) fig. 3.2.

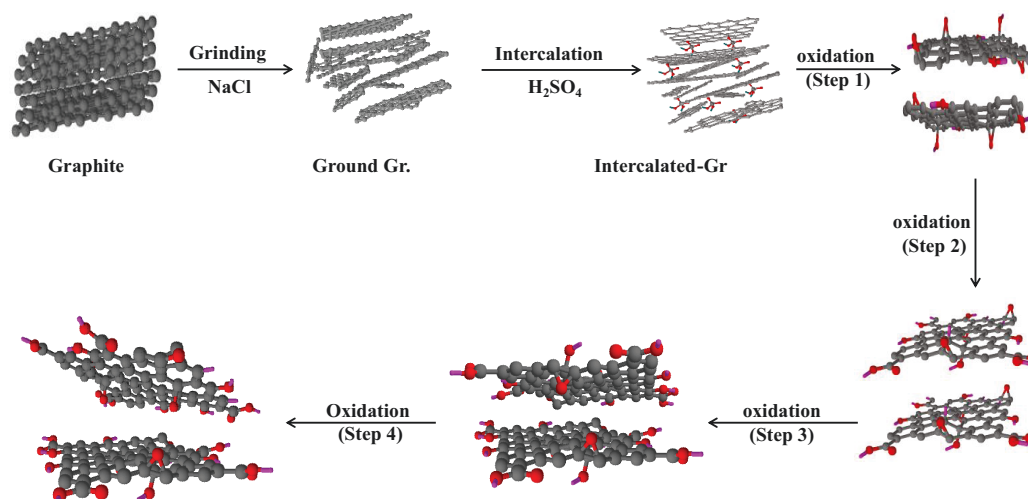SEM and AFM images of graphite and GO are presented in fig. 3.3.

Figure 3.1: Schematic representation for graphene oxide (GO) production.
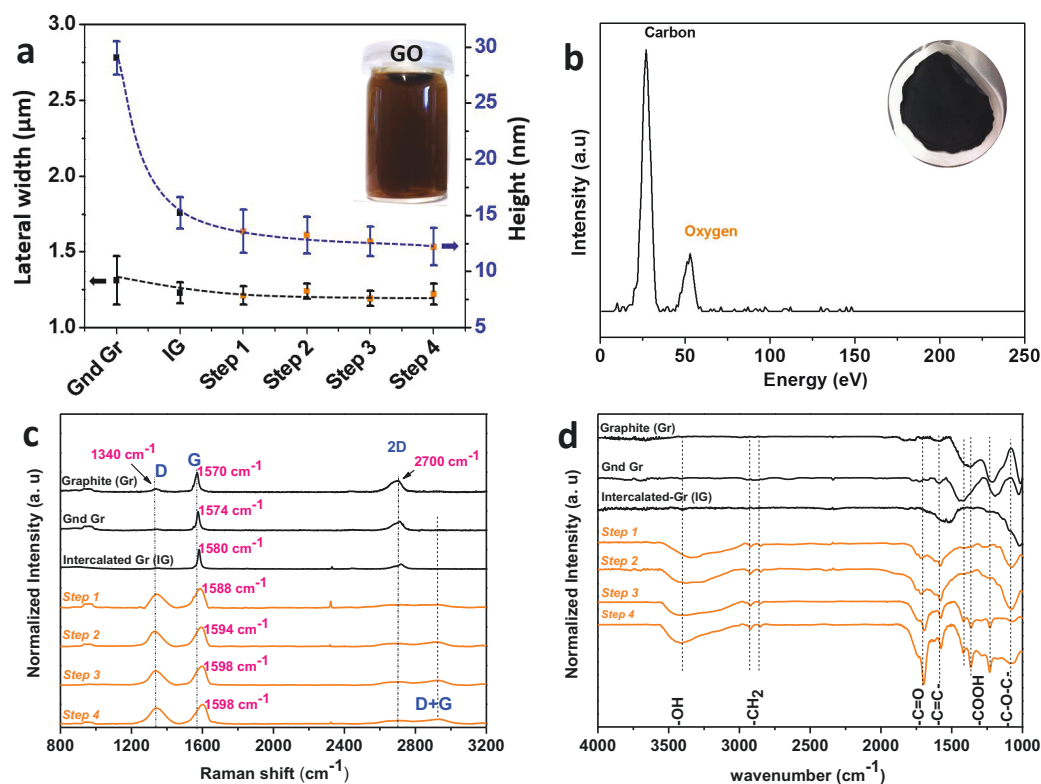
Figure 3.2: Statistical and spectroscopic analysis of graphite and graphite oxide samples. a, Lateral width (μm) and height (nm) distribution of graphite and GO samples, the inset photography is GO solution (2 mg.ml^{-1}). **b,** EDX micro-analysis of as prepared graphite oxide, the inset image is graphite oxide on filter paper. **c** and **d,** Raman and FTIR spectroscopies of graphite and GO samples respectively.
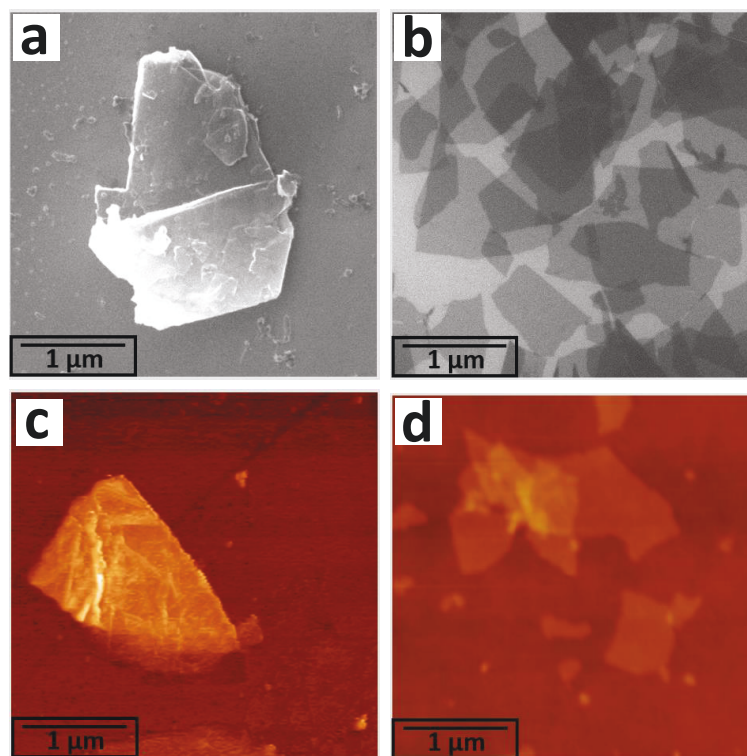
Figure 3.3: SEM and AFM images of graphite and graphite oxide. a, and **b,** SEM images of graphite and graphite oxide. **c,** and **d,** AFM images of graphite and graphite oxide respectively. The micrograph obtained through deposition on silicon substrate.

3.1.2 | Size reduction of graphene oxide particles

The size of graphene oxide particles is considered as important parameter in cell viability investigation, therefore most studies recommend to reduce their dimension.[29, 41, 89, 122] In this part, the ultra-sonication was performed in water under variable conditions; the sonication was maintained at low (15 - 17 watt) and high (26.5 - 28 watt) power for all samples. Two concentrations were selected and considered as low (0.15 mg.ml^{-1}) and high (3 mg.ml^{-1}) concentrations. The effect of power and concentration were measured at 30, 60 and 120 minutes of sonication.

As shown in fig. 3.4 panel (a) and (b), the intensity ratio (ID/IG) increased over 30 min of sonication for both power and concentration respectively, this

result is attributed to the increment of the outer surface area of GO samples. From 30 to 120 min sonication, the effect of time vanish and small change on the surface area observed indicating that the size distribution of GO particles slightly reduced.

Panel (c) and (d) demonstrated special type of sp^3 defect (C-H group) appeared at 2960 cm^{-1}, this group is sensitive to the power and concentration; at low power in panel (c), the concentration of GO is dominant, however, as seen in panel (d), high power is sufficient to increase the intensity ratio of (C-H/G) at low and high concentration, this results suggest that high power creates more C-H groups at low and high concentration.

For more understanding of size reduction, SEM and AFM are used to visualize the particles and measure their dimensions.

The statistical analysis of ca. 370 GO particles deduced from SEM and AFM images provide clear information about the size reduction at different time, power and sonication conditions. It was found that the GO particles reduced over 30 min of sonication, with respect to lateral width (fig. 3.5a) the power of sonication is crucial especially over 120 min of sonication.

However, the height distribution of GO particles is concentration dependent even at low or high power of sonication (fig. 3.5b). As a result, high power of sonication for 120 min destructs the flakes of GO to small parts, whilst at low power the flakes can be easily exfoliated due to van der Waals interaction.

The optimal conditions for size reduction of GO particles can be considered at high power and high concentration for 120 min of sonication.
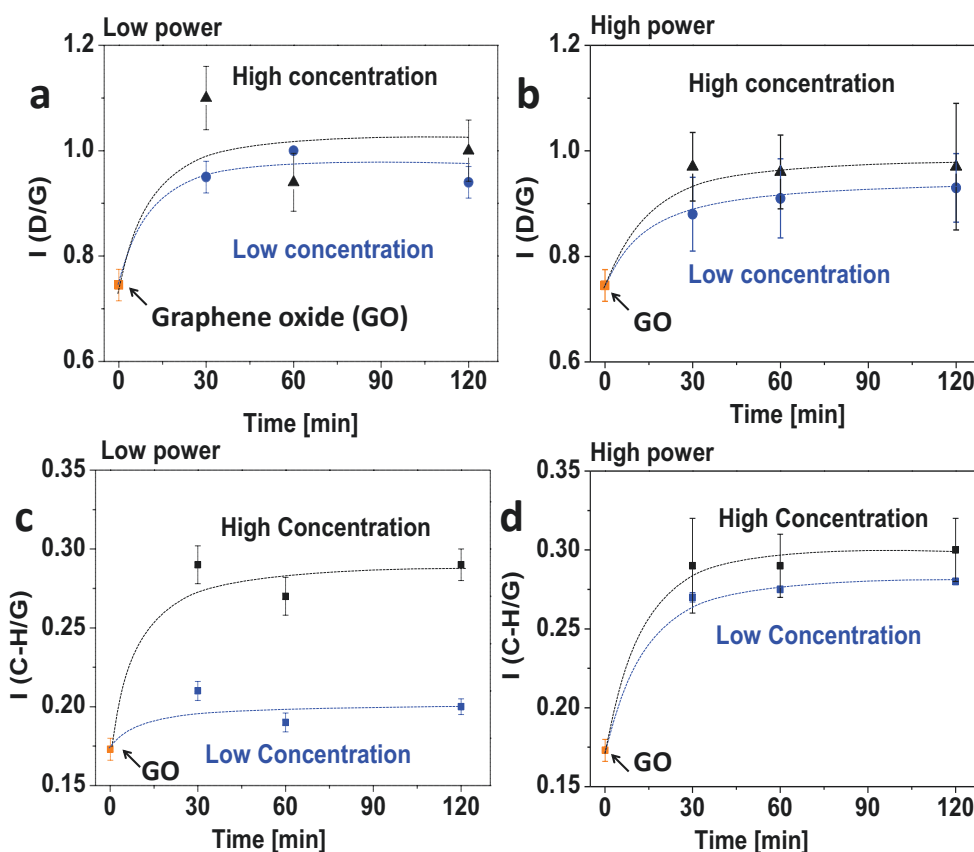
Figure 3.4: Data analysis of Raman spectroscopy at controlled sonication conditions. a, and **b,** Intensity ratio I(D/G) of graphite oxide at low and high power of sonication respectively. **c,** and **d,** Intensity ratio I(C-H/G) of GO at low and high power of sonication. The data deduced from Raman measurements.
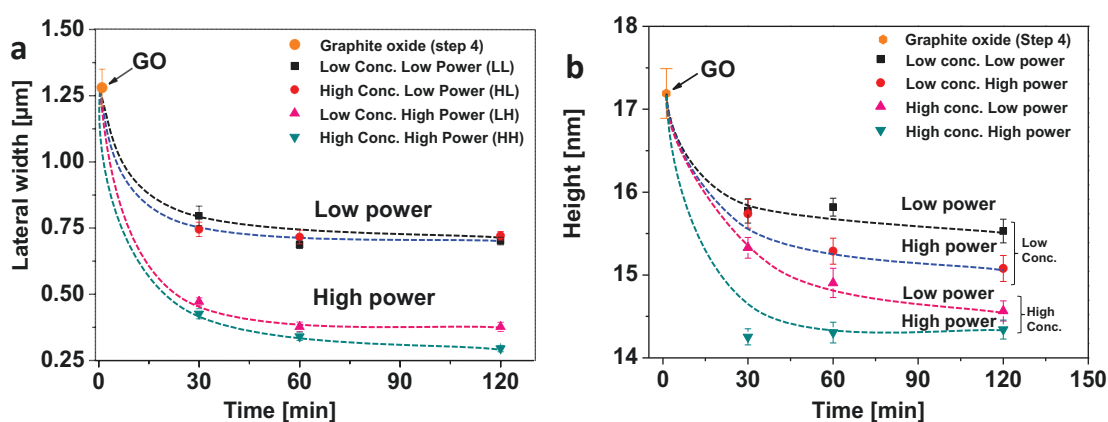

Figure 3.5: Data analysis of SEM and AFM images at controlled sonication conditions. a, Lateral and **b,** Height distribution of GO at variable sonication conditions. The data deduced from SEM and AFM images respectively.

3.1.3 Centrifugation of NGO particles in sucrose solutions

The sucrose density gradient solutions are mainly used to separate the nano - scaled particles via centrifugation.[28,96,123] The NGO particles distributed along the centrifuge tube depending on the sucrose viscosity. The small sizes of NGO remain in the upper zone, while the bigger sizes migrate to the bottom of the tube where the viscosity of sucrose is relatively high. The centrifugation speed, time and NGO concentration were optimized as controlled parameters. Along the centrifuge tube (fig. 3.6a), three zones were observed indicating that the mixture has three sizes of NGO particles.

From SEM images (fig. 3.7a - c) and statistical analysis (panel b, fig. 3.6), the three layers of NGO named L1, L2 and L3 disclose three sizes at 100 nm, 200 nm and 300 nm respectively.

The height samples (fig. 3.6c) deduced from AFM micrograph (fig. 3.7d - f) remain approximately the same for the three sizes.
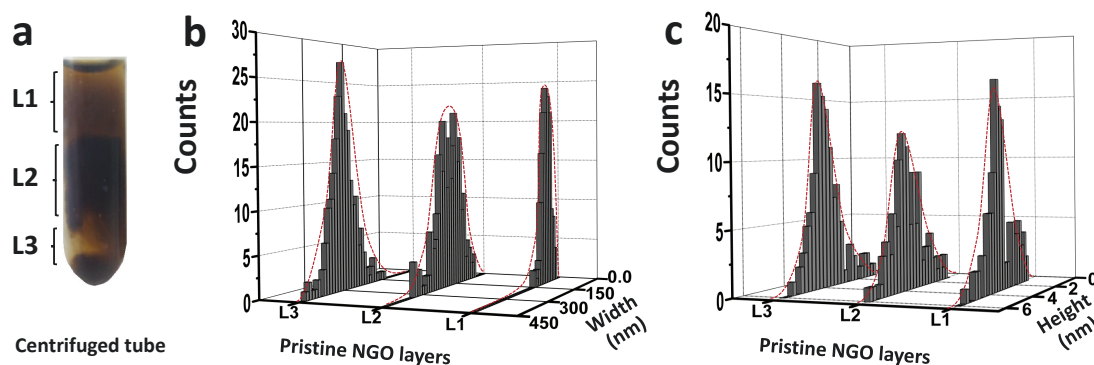

Figure 3.6: Statistical analysis of NGO particles deduced from microscopic images. a, Photograph of centrifuge tube over 5 min centrifugation at 5880 g. **b,** Histogram of the Lateral width of observed NGO sheets deduced from SEM images. **c,** Histogram of the height distribution of observed NGO sheets deduced from AFM images.
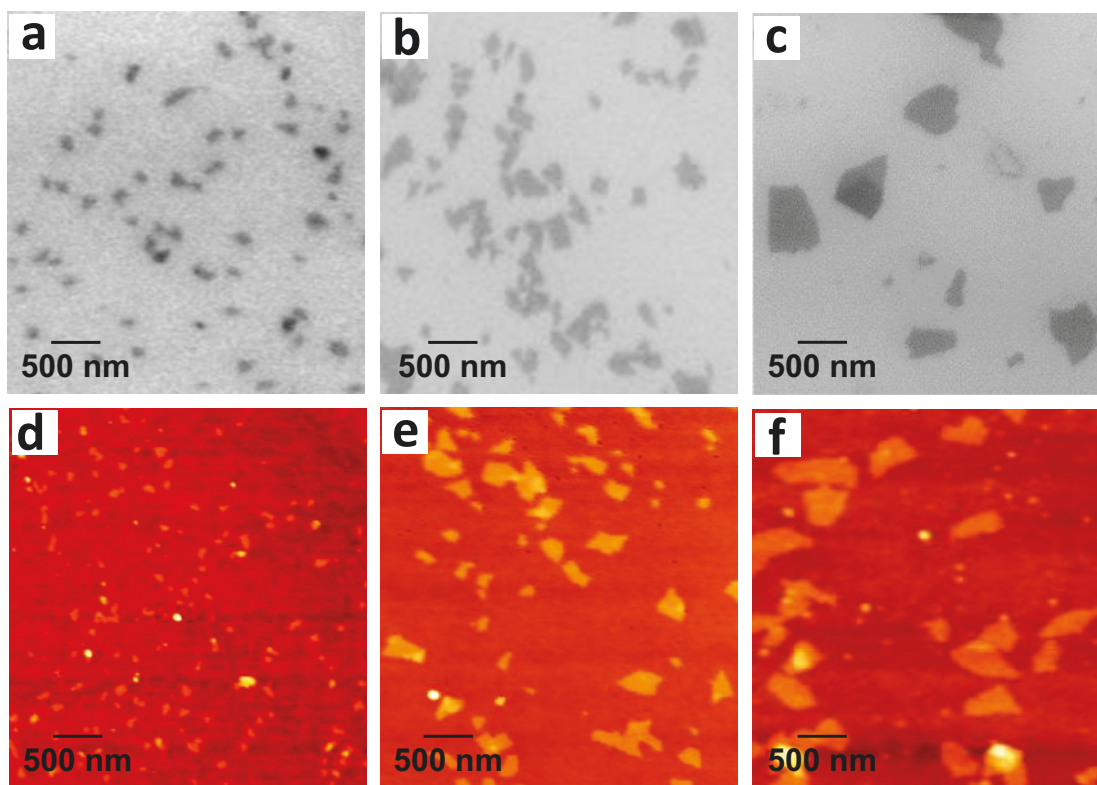
Figure 3.7: SEM and AFM images of NGO particles. a, b and **c,** SEM images of NGO 100 nm, 200 nm and 300 nm respectively. **d, e** and **f,** AFM images of NGO 100 nm, 200 nm and 300 nm respectively. (n.b.: The NGO was deposited on silicon substrates for measurement)

3.2 NGO-PAMAM/CP nanohybrids

3.2.1 Spectroscopic analysis of NGO-PAMAM

To make NGO particles truly long-term stable and dispersible in physiological media, it is important to functionalize the surface of NGO sheets by suitable bio-molecules. The functionalization of NGO particles can be performed by covalent and non-covalent approaches. It has been found that both the covalent and non-covalent functionalization reduce the oxygen-containing species and show functionalized NGO is biocompatible.

In this study, a zero generation polyamidoamide dendrimer (PAMAM-G0) is used for covalent functionalization. PAMAM-G0 consists of alkyl-diamine

core and terminates with four amine (-NH$_2$) groups,[98,99] these groups play a key role in covalent amide bond formation via a ring opening reaction.[28,109,124]

After functionalization as shown in fig. 3.8, carboplatin, anticancer therapeutic agent is loaded to obtain NGO-PAMAM/CP nanohybrids.
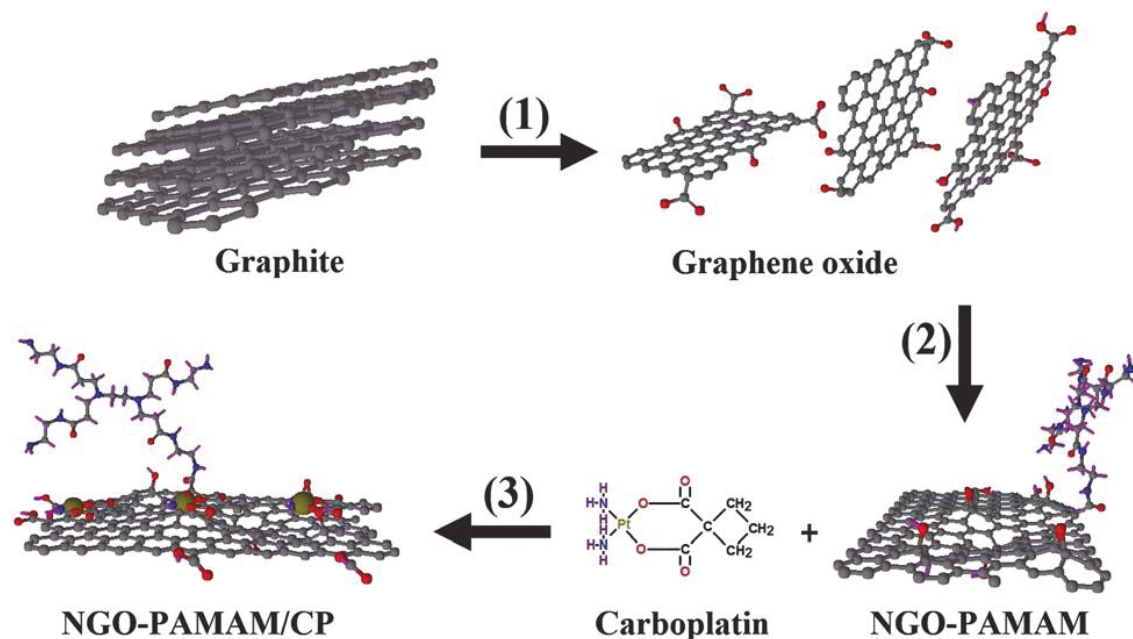
Figure 3.8: Schematic illustration of NGO-PAMAM/CP preparation. 1, Chemical oxidation exfoliation reaction. **2,** Size reduction and functionalization by PAMAM. **3,** Carboplatin loading.

1. **FTIR spectroscopy;** fig. 3.9a presents the FTIR spectra of the samples using NGO with the mean diameter of 100 nm.

The FTIR spectra of NGO functionalized with PAMAM and loaded with CP show a relative reduction in the oxygen containing groups. The absorption peaks of C=O at 1700 cm^{-1}, the OH stretching mode ranging from 1425 to 1225 cm^{-1} and the C-O-C stretching modes showed a drastic decrease after functionalization.[51]

These observations are attributed to the PAMAM which terminates with amine (-NH$_2$) groups covalently bonding with NGO epoxy groups via a ring opening reaction.

In fig. 3.9a, as compared to spectrum 1, new peaks at 1635 cm^{-1} (amide I) and 1552 cm^{-1} (amide II) can be seen in the spectra labeled 3 and 4 and arise due to the presence of PAMAM in the sample. This is further highlighted when comparing the spectra of PAMAM and CP films (fig. 3.9d), the presence of peaks at 1635 cm^{-1} (amide I) and 1552 cm^{-1} (amide II) are clearly observed in the PAMAM sample. We cannot clearly observe responses due to the C-N bond between the NGO and PAMAM, because PAMAM has the same bond in the same frequency region.[125] The absorption peaks at 1620 cm^{-1} (C=O) and 1355 cm^{-1} (C-O) were used as indications for effective loading of CP.

Similar FTIR spectra for the other NGO samples (NGO 200 nm and 300 nm) are provided in panel b and c (fig. 3.9) respectively.

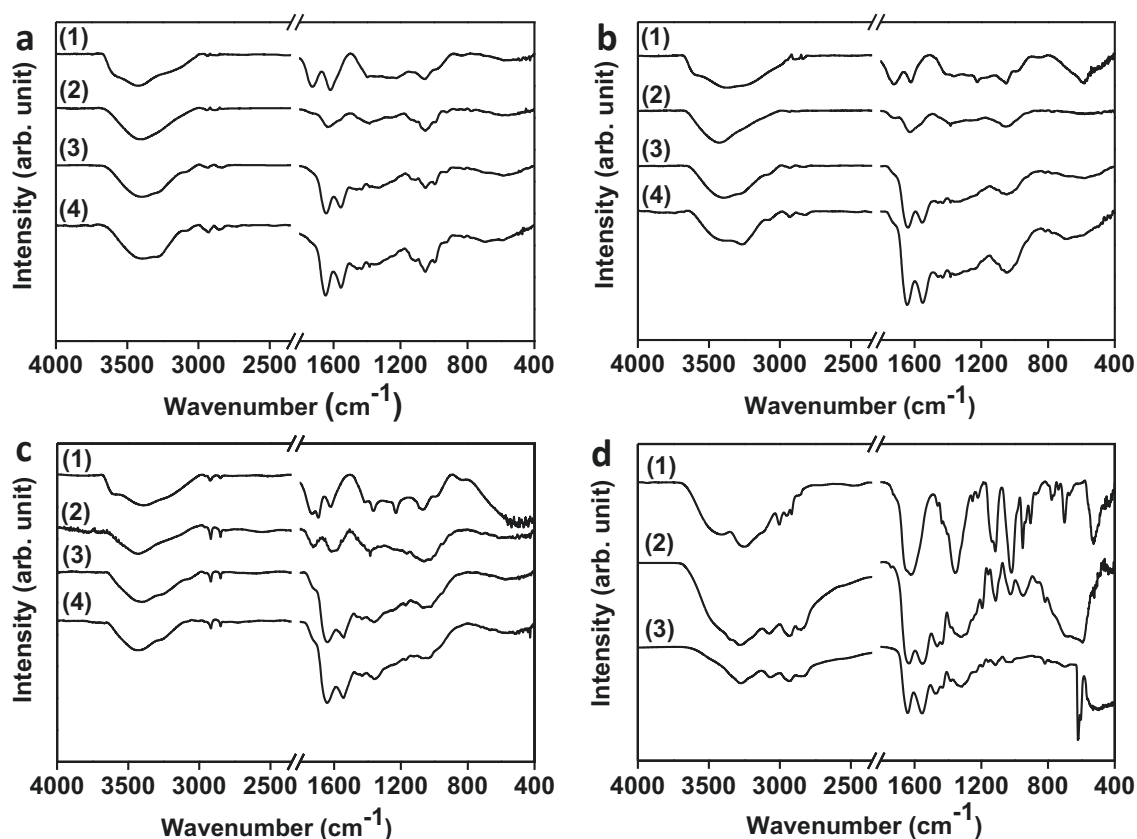**Figure 3.9: FTIR spectra of NGO particles, pure PAMAM, CP and CP@PAMAM samples. a,** FTIR spectra of pristine NGO 100 nm (1), CP@NGO (2), PAMAM-NGO (3) and CP@PAMAM-NGO (4). **b,** NGO 200 nm (1), CP@NGO (2), PAMAM-NGO (3) and CP@PAMAM-NGO (4). **c,** NGO 300 nm (1), CP@NGO (2), PAMAM-NGO (3) and CP@PAMAM-NGO (4). **d,** ATR-FTIR spectra of CP (1), PAMAM (2) and CP-PAMAM (3).

2. XPS analysis; the NGO samples were also characterized using X-ray photo-electron spectroscopy (XPS).

As shown in fig. 3.10a, the C1s spectrum of NGO 100 nm can be de-convoluted to show five components that correspond to various functional groups, the binding energies of the de-convoluted peaks centered at 284.2 eV, 285.7 eV, 286.7 eV, 287.5 eV and 288.4 eV are assigned to the graphene oxide sp^2 carbon skeleton (C-C/C=C), hydroxyl (-OH), epoxy (C-O-C), carbonyl (C=O) and carboxyl groups (COOH) respectively.[7,111]

The C1s spectra of PAMAM-NGO 100 nm, CP@NGO and CP/PAMAM-NGO exhibit the same oxygen containing functional groups as shown in fig. 3.10(b-d), however their peak intensities are reduced in comparison with pristine NGO, indicating considerable de-oxygenation due to functionalization. Moreover, the C1s spectra of PAMAM-NGO and CP/PAMAM-NGO are assigned two additional peaks for C-N and C(O)-N bonds at 286.1 eV and 287.5 eV respectively which have binding energies similar to those of C-OH and C=O respectively.[100] On the other hand, these observations are consistent with the N1s XPS spectra (fig. 3.11a), which clearly indicate the presence of nitrogen groups at 398.8 eV (N-C) and 399.7 eV (N-C(O)),[126,127] this suggests that the covalent bonding of the amine terminated PAMAM onto the NGO surface via epoxide ring opening reaction is in agreement with the FTIR data.

With regard to the O1s spectra they complement the C1s spectra in that similar trends for the oxygen based functional groups were obtained. Fig. 3.11b shows the Pt4f (7/2) and Pt4f (5/2) peaks from the CP@NGO sample confirming the immobilization of Pt (II) on the NGO surface through non-covalent interactions such as van der Waals, H-π, cation-π interactions.[128,129]

The XPS spectra of NGO 200 nm, 300 nm and their functionalization with PAMAM and CP loading show comparable trends due to their structural similarity (fig. A.1 - A.3 in appendix).
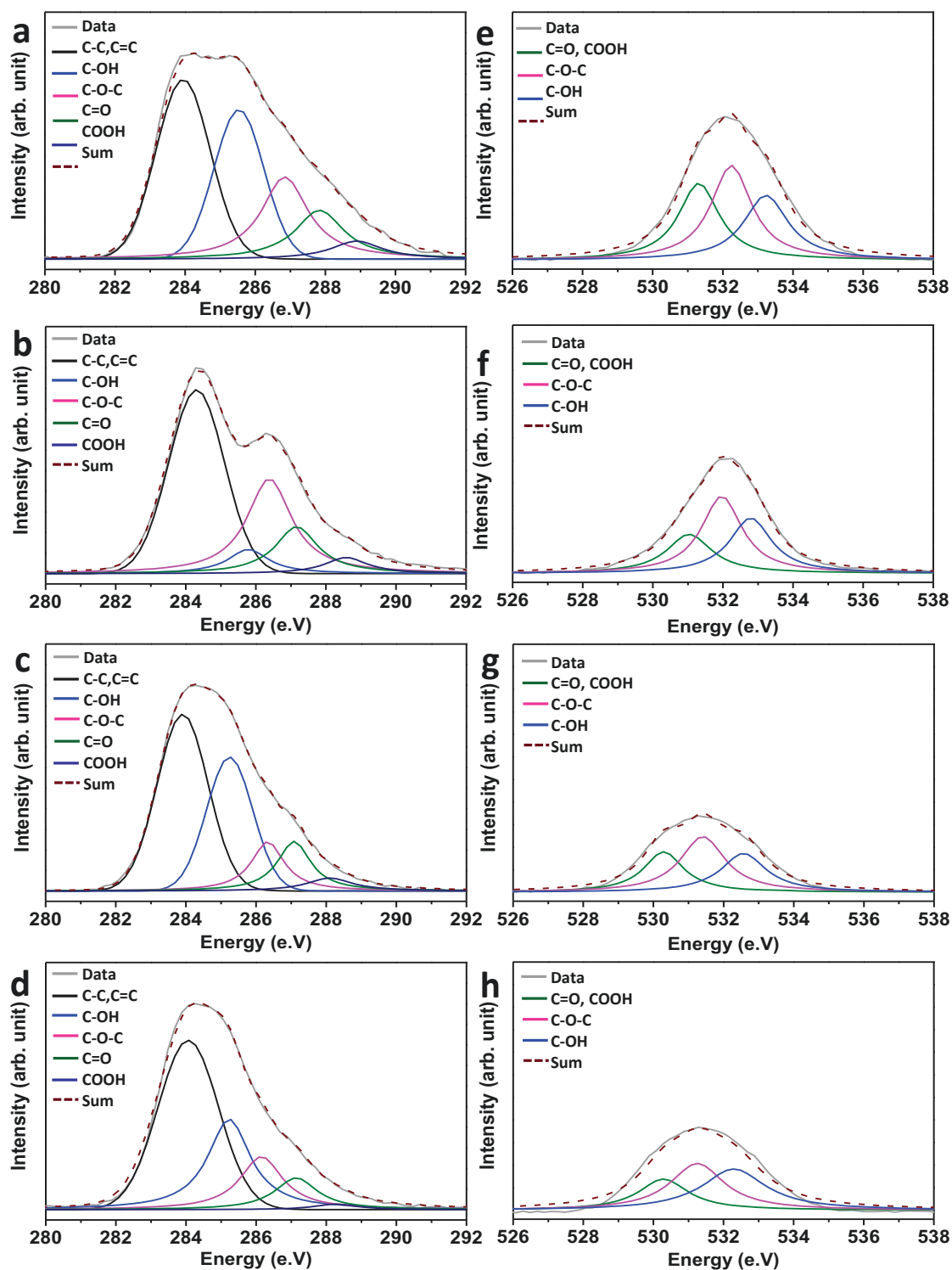
Figure 3.10: C1s and O1s XPS spectra of NGO 100 nm and PAMAM functionalized materials. a - d, C1s XPS spectra of NGO 100 nm, CP@NGO, PAMAM-NGO and CP@PAMAM-NGO respectively. **e - h,** O1s XPS spectra of NGO 100 nm, CP@NGO, PAMAM-NGO and CP@PAMAM-NGO respectively.
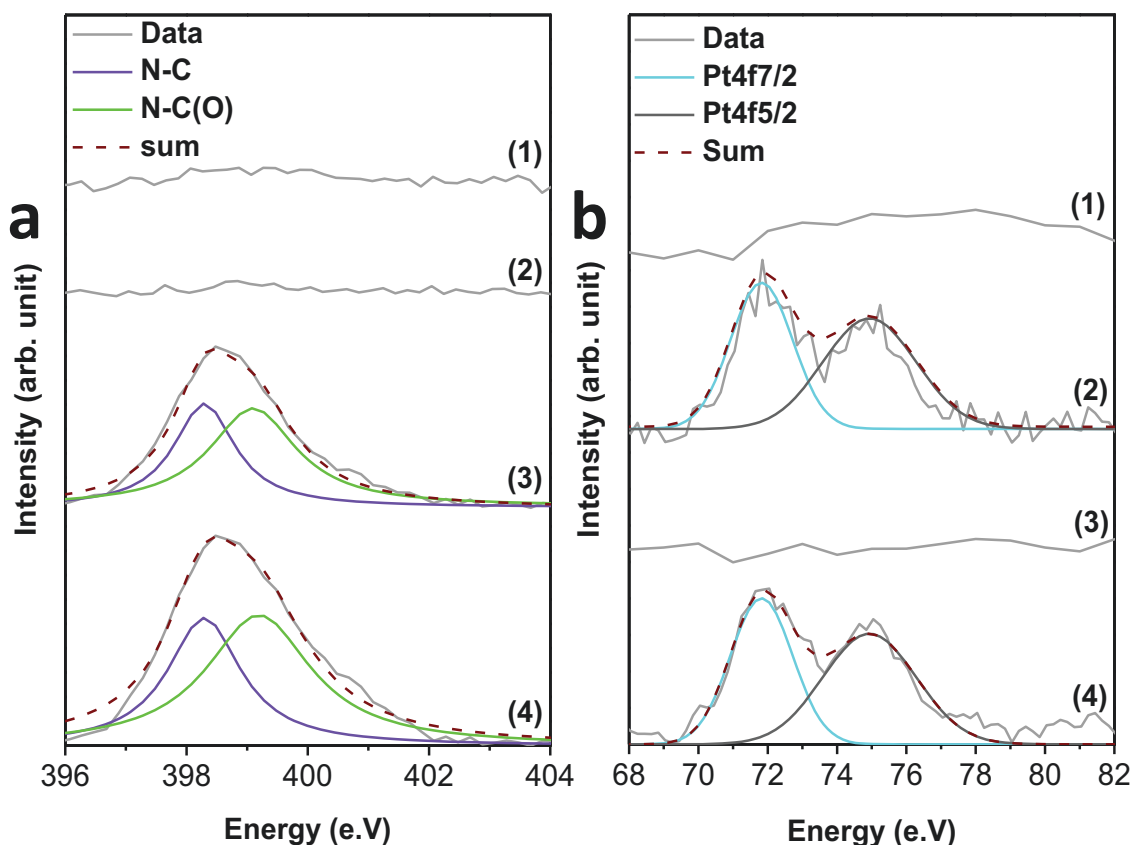
Figure 3.11: N1s and Pt4f XPS spectra of NGO 100 nm and PAMAM functionalized materials. a, N1s and **b,** Pt4f XPS spectra of pristine NGO 100 nm (1), CP@NGO (2), PAMAM-NGO (3) and CP@PAMAM-NGO (4).

3.2.2 Cell culture and anticancer activity

The efficiency of the synthesized materials as a drug delivery system for a commonly used anticancer drug (CP) was evaluated in HeLa cancer cell lines and their biocompatibility in human mesenchymal stem cells (hMSCs).

The anticancer activity of the nanocomposite was tested by means of the WST-8 assays for studying the effect on HeLa cells, its biocompatibility was assessed on hMSCs which represent a good model of non-malignant cells, the assay measures the formation of a formazan product as an index of the cellular mitochondrial dehydrogenase activity.

For the viability tests, two different concentrations of CP (10 and 20 μg.ml^{-1}) were chosen, and by considering the loading value, 50 and 100

mg.ml^{-1}composite concentrations were also tested.

First, the activity of the three components (PAMAM, CP and NGO 100 nm) on cell viability was tested (fig. 3.12). In panel (a and b), as expected, PAMAM did not show any kind of cytotoxicity on both hMSCs and HeLa cells, the cell viability values of these samples were always higher than 98%, which is an important parameter when considering further use of the composite material.

Furthermore, CP shows the typical anticancer activity on HeLa cancer cells (fig. 3.12b), which is mainly related to the formation of intra-strand DNA-platinum adducts as previously demonstrated by Zanellato and co-workers.[130] The presence of the PAMAM did not affect the anticancer activity of the CP, confirming the suitability of PAMAM for functionalizing the NGO nanoplatelets.

Significant results were obtained when pristine NGO samples were tested on HeLa cancer cells (fig. 3.12c and d), the effect on cell viability was found to be dependent on the NGO concentration (50 and 100 μg.ml^{-1})). Moreover, a strong correlation between the particles' size and the cells' viability was observed, this correlation suggests that cell death is related to the increased size of the NGO. This finding does not seem to be in agreement with literature data,[71] the discrepancy is related to different mechanisms of cell death, literature data refer to ROS-mediated phenomena occurring inside cells after NGO internalization, while in our case, cell death has to be ascribed to physical damage of the cell membrane due to an accumulation of big NGO clusters.

This phenomenon is very important in toxicological effects especially on adherent cells because it induces damage on the cellular membrane and greatly inhibits nutrient availability for cells. NGO with small particle sizes (e.g. NGO 100 nm) are well dispersed into the cell culture media, and thus they are able to easily penetrate cells by endocytosis. As a consequence, the toxicity is only related to the intracellular oxidative stress. In contrast, bigger sized NGO (e.g.

NGO 300 nm) is not well dispersed in the cell culture media, and thus bigger agglomerates can be observed. The formed NGO bundles in the media can accumulate on the cellular membrane, therefore damaging or interfering with cellular behavior.
The presence of PAMAM on the NGO surface greatly enhances the water affinity, as a result the samples are well dispersed and less toxic to the cells.

The modification of the NGO surface also leads to less toxic materials because the interaction with the cell membranes is mainly driven by the PAMAM. When compared to the pristine NGO, the PAMAM functionalization was found to increase the cell viability value up to 85% in the case of NGO 200 nm and 97% in NGO 100 nm samples. The PAMAM functionalization was ineffective in increasing the biocompatibility of NGO 300 nm, which shows strong side effects on the cells with a viability value of 25%, as the dendrimer was unable to better disperse the NGO. The potential to employ the proposed composite materials as drug delivery systems is arrived at by the evaluation of the anticancer activity of the samples after loading with CP, which strongly interacts with the NGO component by virtue of π - π interactions. As a loading protocol, a solvent evaporation method was selected, to achieve for all samples a loading efficiency of 100% and the same ratio (by weight) between drug and material (NGO or PAMAM-NGO).

The anticancer activity of CP loaded samples of NGO 300 nm was very high, but this effect is related to the NGO and it is independent of the anticancer drug. The recorded anticancer activity is practically unmodified when compared with pure NGO samples of 300 nm; NGO was, indeed, much more toxic than the pure CP and thus the effect of the drug cannot be distinguished.

In the composite materials based on NGO 200 nm and NGO 100 nm, after drug loading, very different results were obtained, the drug efficiency is greatly enhanced and there are no indications that the activity is ascribed to the carrier

itself (PAMAM-NGO). In particular they appear to be less toxic (PAMAM-NGO 200 nm) or non-toxic (PAMAM-NGO 100 nm), this finding confirms that when modified with PAMAM, NGO easily penetrates inside the cells by endocytosis,[71] and thus CP is more efficiently internalized. As a consequence, a local increase in CP intracellular concentration occurs, leading to a higher amount of dead cells. Specifically, while pure CP was able to kill 10 - 12% of cells, after its loading with NGO, the anticancer activity increases up to 39% and 46% for the 100 nm and 200 nm composites, respectively, at the same drug concentration.

These values are almost four times more effective than that of the pure drug. From the analysis of these results, the PAMAM-NGO 100 nm was found to be the most promising material to be used as an effective intracellular delivery system for anticancer therapeutics, it showed no toxicity to non-malignant cells and high killing effect on cancer cells, as a consequence of the different cell metabolism,[101,102] these results show that because of the loading onto NGO, less amount of CP can be used to achieve the same anticancer activity. The possibility to use less of the drug while maintaining the same efficacy is advantageous from both pharmaceutical and toxicological points of view.

To check the real suitability of these carriers, biocompatibility experiments were conducted on non-neoplastic cells, this provides key information on how the drug carrier is tolerated by non-cancerous cells. For this, our samples were tested on hMSCs, as shown in fig. 3.12a and according to literature data,[71] pure NGO was highly toxic to hMSCs, but its biocompatibility was greatly enhanced after functionalization with the PAMAM (cell viability: 96%), confirming the high potential application of our proposed nanocomposite system.

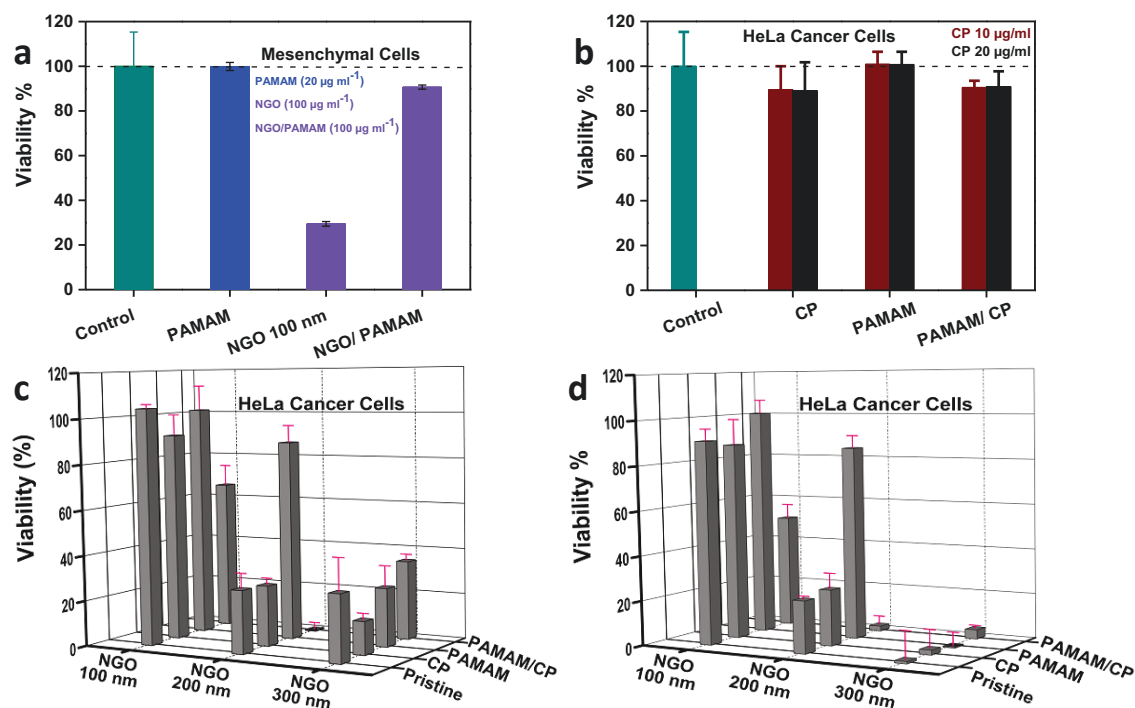**Figure 3.12: Percent viability of pure materials and functionalized NGO particles. a,** and **b,** Percent viability of mesenchymal and HeLa cells investigated by pure materials respectively. **c,** and **d,** Percent viability of mesenchymal and HeLa cells investigated by pristine NGO samples and nanohybrid systems at low (50 µg.ml^{-1}) and high (100 µg.ml^{-1}) concentrations respectively.

3.3   NGO - gelatin/CP nanohybrids

3.3.1   Characterization of Gel_NGO nanohybrids

1. UV visible spectroscopy; the estimated amount of gelatin coated NGO particles can be determined by using UV visible spectroscopy (A Shimadzu UV-vis-NIR, MPC - 3100 Model, Dual beam spectrometer with PbS photomultiplier detector). Initially, standard gelatin solutions 2.0, 1.0, 0.8, 0.6, 0.5, 0.4, 0.3, 0.2 and 0.1 mg.ml^{-1} were prepared in distilled water, followed by stirring at 40 °C for complete dissolution, 10 mg.ml^{-1} NGO solution was reacted with gelatin at different concentrations. The absorbance of gelatin solutions were recorded as shown in fig. 3.13a, (Inset figure represents the calibration curve of gelatin for binding capacity calculation). The reaction was taken place at 40 °C with stirring for 2 hours, the final product of Gel_NGO was filtrated and washed three times with distilled water in order to remove unbound gelatin. Unbound gelatin was collected and metered to exact volume for binding capacity calculation, the binding capacity (q) can be estimated by the following equation.

$$q = \left(\frac{Co - Ce}{m}\right) * V$$

Where q (mg.mg^{-1}) is the amount of gelatin bound onto NGO, Co (mg.ml^{-1}) is the initial gelatin concentration, Ce is the concentration of gelatin unbound at equilibrium (estimated from the calibration curve of gelatin standard solution presented in fig. 3.13a, V is the total volume of mixture (10 ml) and m is the mass of NGO (10 mg). As shown in fig. 3.13b, the maximum capacity of gelatin to NGO is 4:1 wt.wt^{-1} ratio, indicating that no more gelatin molecules will absorb by NGO particles.

A slight change appeared at different NGO sizes, NGO 100 nm consumed more gelatin molecules than NGO 200 nm and NGO 300 nm (table 3.1), the

result indicates that NGO 100 nm with more edges can have more efficiency to bind with gelatin molecules. The percent efficiency of gelatin coated NGO can be estimated by using the following equation.[51,131]

$$\% \text{ efficiency} = \left(\frac{C_o - C_e}{C_o}\right) * 100\%$$

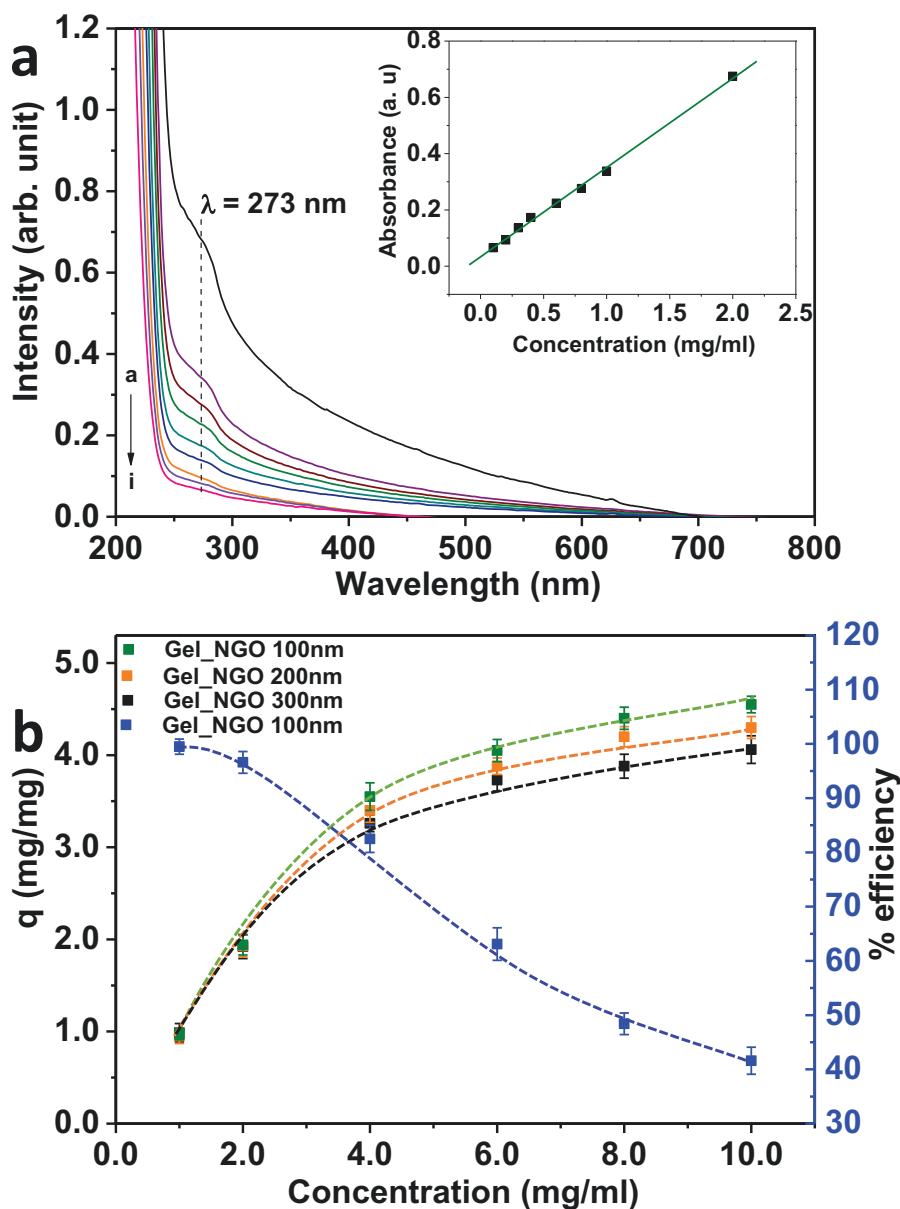**Figure 3.13: Binding capacity of gelatin coated NGO particles. a,** UV-vis absorption spectra of gelatin solutions at different concentrations, (a -i): 2.0, 1.0, 0.8, 0.6, 0.5, 0.4, 0.3, 0.2 and 0.1 mg.ml^{-1} respectively, (inset: calibration curve of gelatin). **b,** Binding capacity of gelatin coated NGO particles at different sizes, blue curve represents the percent efficiency of Gel_NGO 100 nm.

Table 3.1: Binding capacity of gelatin coated NGO and percent efficiency

Gel_NGO ratio wt/wt	Gel_NGO 100 nm Ce (mg/mg)	q (mg/mg)			Gel_NGO 100 nm % efficiency
		Gel_NGO 300 nm	Gel_NGO 200 nm	Gel_NGO 100 nm	
1:1	0.013	0.98	0.95	0.97	98.7
2:1	0.078	1.92	1.93	1.94	96.1
4:1	0.72	3.26	3.4	3.55	81.5
6:1	2.27	3.73	3.88	4.05	62.2
8:1	4.12	3.88	4.2	4.4	48.5
10:1	5.94	4.06	4.3	4.55	40.6

2. Raman spectroscopy; Raman spectra (fig. 3.14) provide the vibrational regimes of graphite, pristine NGO and Gel_NGO nanohybrid materials.[118,132,133] The characteristic bands of graphite at 1360 cm^{-1}, 1578 cm^{-1} and 2705 cm^{-1} which correspond to D-, G- and 2D-band respectively.

The sp^2 carbon skeletal disorder induced D-band due to oxygen rich groups; this band presumed as a key to emphasize the oxidation through the increment of band width and integrated intensity. The G-band of graphite, sp^2 (C-C) bond appeared at 1578 cm^{-1} is an interesting band concerning its position and full width at half maximum (FWHM).

NGO 100 nm revealed a significant change during oxidation in FWHM and intensity ratio I (D/G) to 0.9 as a result of oxygen incorporation.[105] The 2D-band at 2705 cm^{-1} denoted the second order of D-band and the number of graphene layers, the functional groups on graphene basal plan or edges reduced this band due to high structural disorder and exfoliation. The Gel_NGO at different sizes show no considerable change in comparison with pristine NGO, however the Raman shift in the G-band position by ca. 25 cm^{-1} could be considered as indication for functionalization (fig. 3.14(c - e)).
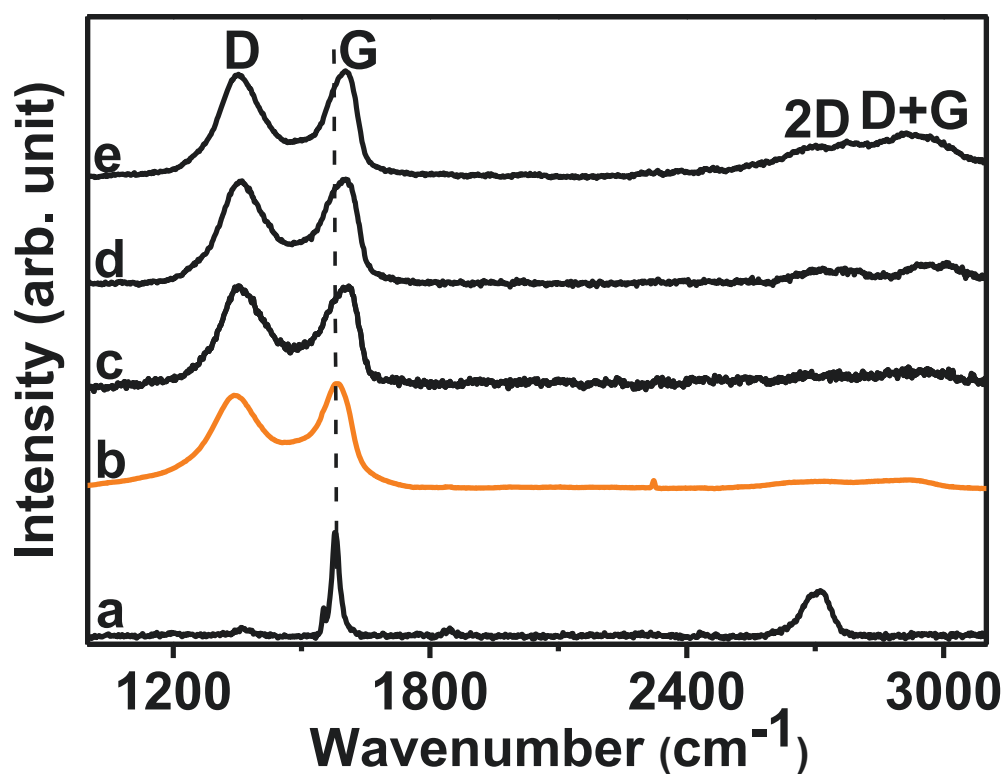
Figure 3.14: Raman spectra of gelatin functionalized NGO particles. a, Graphite. **b,** Pristine NGO 100 nm. **c - e,** Gel_NGO 100 nm, 200 nm and 300 nm respectively.

3. X-ray photoelectron spectroscopy; the chemical state of pristine NGO and Gel_NGO samples at all sizes were characterized using high resolution X-ray photoelectron spectroscopy (XPS).

The C1s, O1s and N1s exhibit different components, indicating that these elements have different chemical environments,[28] the peaks were fitted with Gaussian-Lorenzian mixed function, as shown in fig. 3.15a. The C1s peaks appeared at 284.3 eV, 285.6 eV, 286.7 eV, 287.3 eV and 288.5 eV are ascribed to sp^2 hybrids (C-C / C=C), hydroxyl (-OH), epoxy (C-O-C), carbonyl (C=O) and carboxyl (COOH) groups respectively.

The C1s spectra of CP@NGO 100 nm, Gel_NGO 100 nm and CP@Gel_NGO 100 nm revealed at first glance the same oxygen groups as shown in fig. 3.15(b - d), however NGO coated gelatin nanohybrid generates two prominent peaks for C-N and C(O)-N bonds at 286.4 eV and 287.2 eV respectively, which have binding energies closed to those of C-OH and C=O.[124,134] These finding are consistent with the N1s XPS spectra (fig. 3.16a).

As shown in fig. 3.15(e - h), the O1s XPS spectra of pristine NGO and functionalized samples were fitted to three main peaks around 531.2 eV, 532.07 eV and 533.01 eV, these peaks assigned to carboxyl, epoxide and hydroxyl groups respectively and provide information complement with the information obtained from C1s spectra. The C1s and O1s peak intensities of pristine NGO reduced drastically after coating by gelatin, which attribute to deoxygenation.

Fig. 3.16b shows the Pt4f (7/2) and Pt4f (5/2) peaks originated from the immobilization of Platinum in the samples containing carboplatin molecules, confirming the noncovalent interactions such as van der Waals, π - π, H - bonding, and cationic - π interactions with NGO particles.[129,135]

The XPS spectra of NGO 200 nm, 100 nm and functionalized materials exhibit analogous trends due to their structural similarity (see in appendix fig. A.4 - A.7).
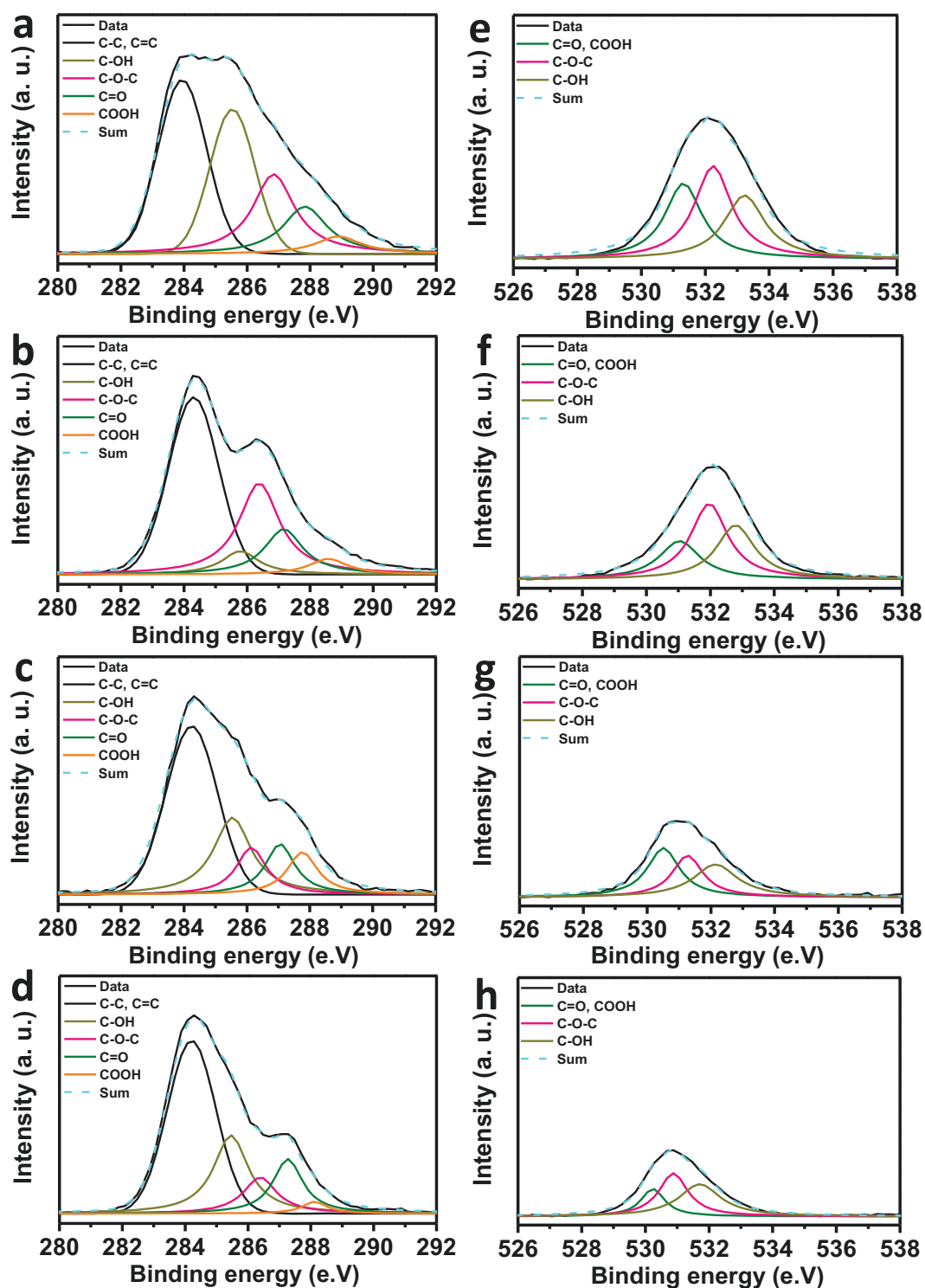
Figure 3.15: C1s and O1s XPS spectra of NGO 100 nm and gelatin functionalized materials. a - d, C1s XPS spectra of NGO 100 nm, CP@NGO, Gel_NGO and CP@Gel_NGO respectively. **e - h,** O1s XPS spectra of NGO 100 nm, CP@NGO, Gel_NGO and CP@Gel_NGO respectively. All XPS data normalized at C - C peak position.
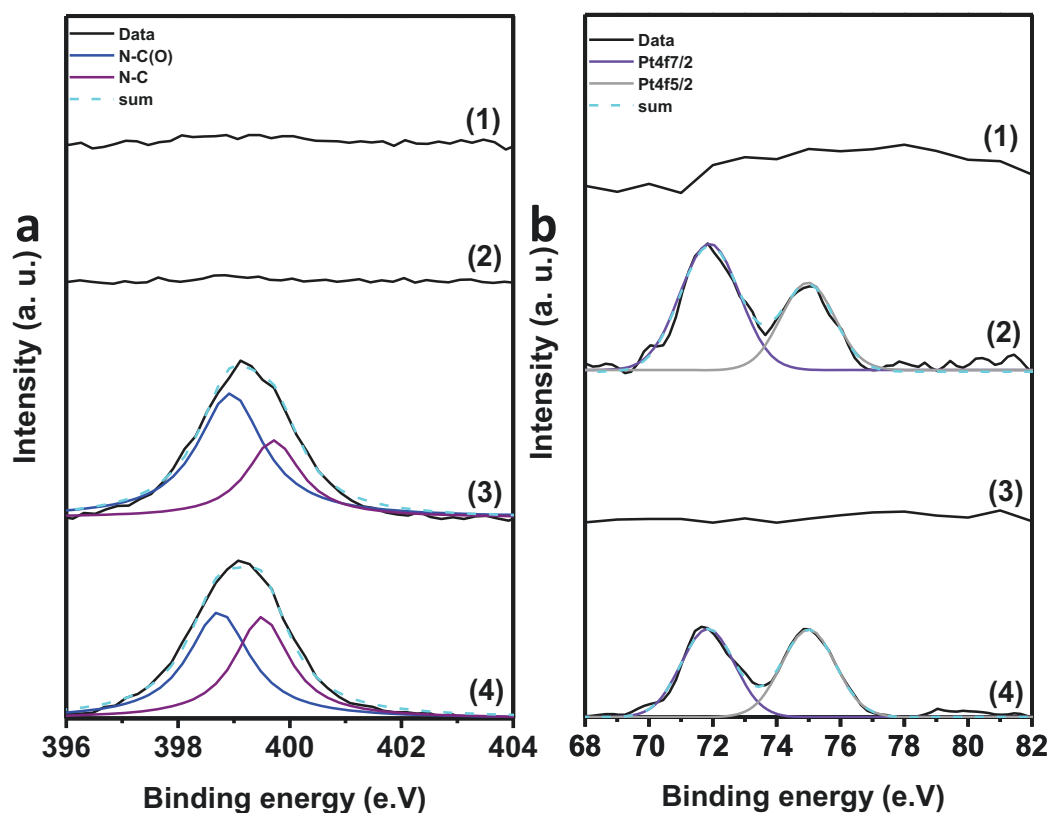
Figure 3.16: N1s and Pt4f XPS spectra of NGO 100 nm and gelatin functionalized materials. a, N1s and **b,** Pt4f XPS spectra of pristine NGO 100 nm (1), CP@NGO (2), Gel_NGO (3) and CP@Gel_NGO (4) respectively.

4. Atomic force microscopy; fig. 3.17(a - c) shows AFM images of the three different sizes of NGO, the thickness of selected particle is shown below each image. The statistical analysis of about 250 particles of the three samples confirmed the thickness of pristine NGO particles as appeared in fig. 3.17g, the thickness for all samples is approximately 3.4 nm and the number of NGO sheets is ca. 6 (assuming an interlayer distance of 0.7 nm).[136]

After gelatin functionalization, the thickness of NGO flakes increased up to approximately 12 nm (panel h), indicating that gelatin shielded NGO particles via noncovalent interaction (fig. 3.17(d-f)).

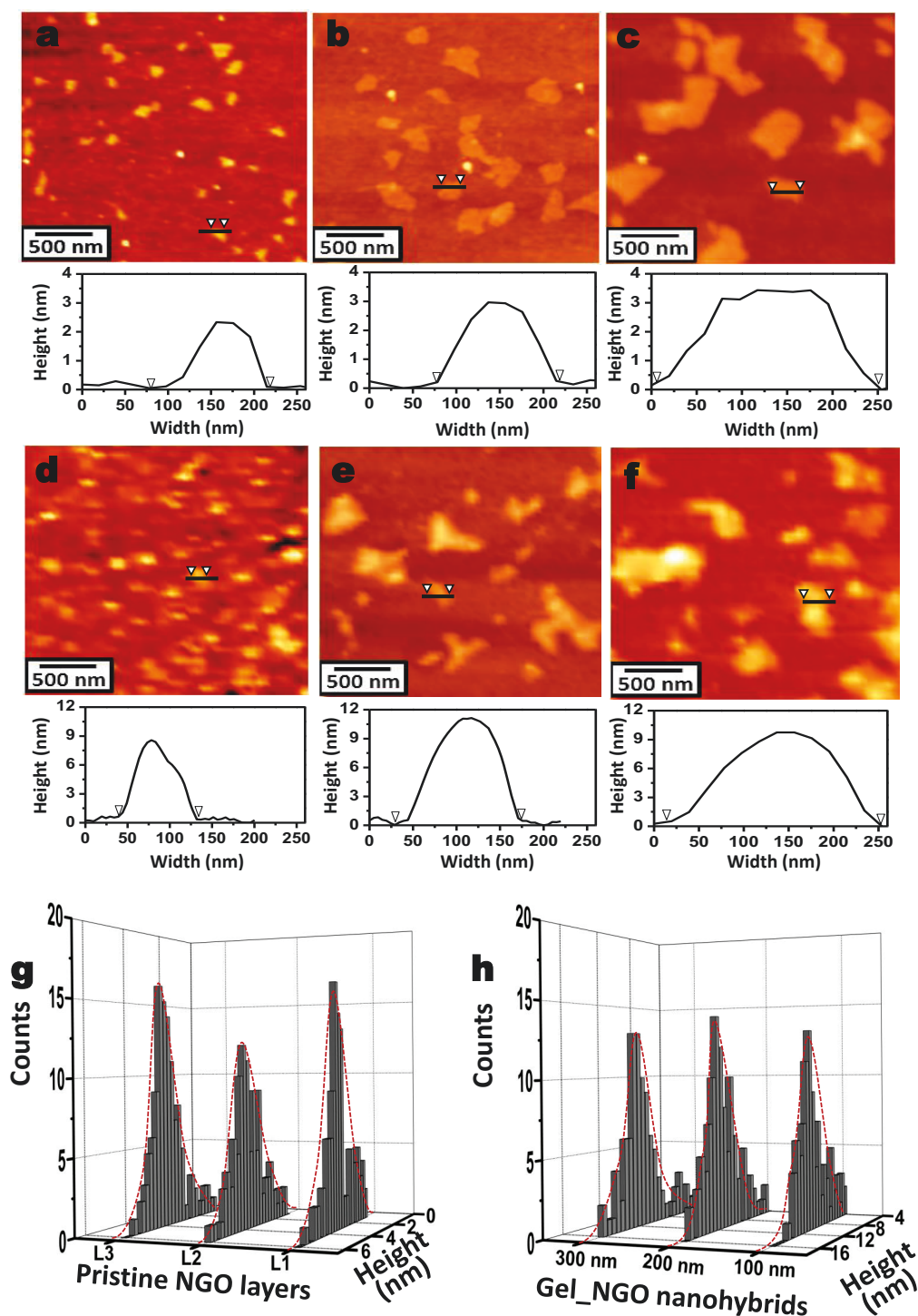**Figure 3.17: AFM images and statistical data of NGO particles. a - c,** AFM images of pristine NGO 100 nm, 200 nm and 300 nm respectively. **d - f**, Gel_NGO 100 nm, 200 nm and 300 nm nanohybrids (n.b.: samples were deposited on silicon substrates for measurements. **g,** and **h,** Histograms of the observed NGO particles at different sizes and Gel_NGO nanohybrids respectively. The data deduced from AFM images.

3.3.2 Cell culture and anticancer activity

IMR-32 human neuroblastoma cells were used as a model for evaluating the efficiency of the proposed nanohybrids to act as carriers for carboplatin which is used for the treatment of various cancer. Here, we explore the strategy of noncovalent modification via loading onto a hybrids nanocarrier, with the aim to enhance the anticancer efficiency of the drug. All the samples were tested at 5 µg.ml^{-1} CP equivalent concentration, corresponding to a nanohybrid concentration of 25µg.ml^{-1}. Any drug carrier and biomaterials proposed for use in biomedicine need to strictly address the biocompatibility issues.[71,137] The absence of any trace of toxic effect on non-malignant cells is the ideal behavior for biomaterials, and in this work we used hMSCs as an effective in vitro model for healthy cells. These cells were selected by virtue of their metabolic pathways conferring them high susceptibility to foreign compounds and biomaterials.[137,138]

In our previous work,[28] the activity of NGO on hMSCs at a concentration of 100 µg.ml^{-1} was analyzed. The results show a very high toxicity of the pristine NGO, and even at the concentration tested here 25 µg.ml^{-1}, the cell viability value lower of ca. 30% is recorded, highlighting the need to functionalize the NGO surface before any kind of biological application (fig. 3.18a). The suitability of the proposed strategy of functionalizing NGO with gelatin was proven when considering the recorded biocompatibility of the Gel_NGO samples, which were found to have no effect on the cell viability.

Interestingly, gelatin as shown in fig. 3.19, is able to reduce the toxicity of all sized NGO because of the formation of a protein shell around the nanoparticles, allowing an easier NGO dispersion and preventing any kind of damage on the cell surface. As expected, gelatin alone did not affect the cell viability, while it was found to reduce the activity of the platinum drug. The CP efficiency is
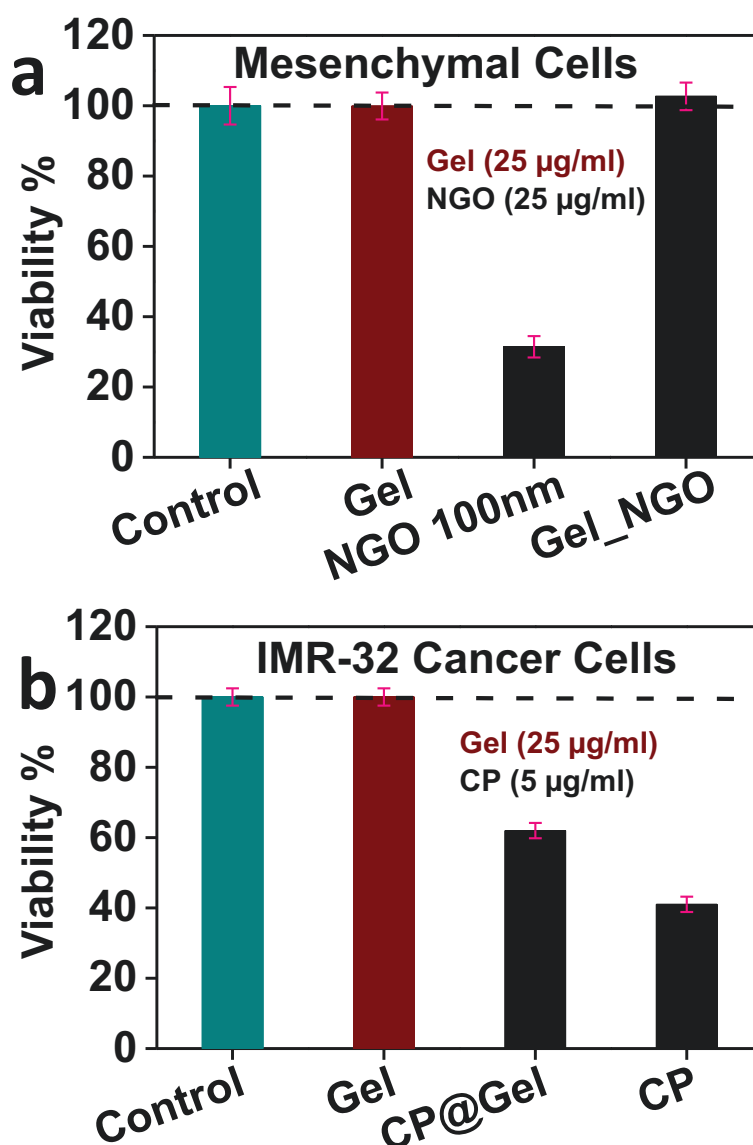
Figure 3.18: Viability percent of pure samples prior NGO functionalization. a, Mesenchymal stem cells. **b,** IMR-32 cancer cells after 24 h of incubation.

reduced by almost 50%, since it moves from 41 to 62% for CP and CP@Gel, respectively (fig. 3.18b), this behavior can be ascribed to the high molecular weight of protein, which prevents CP entering cells.

When considering the activity of the CP loaded Gel_NGO samples, the strong dependency between the efficiency and the size of the carriers is clearly evident. Gel_NGO 300 nm and Gel_NGO 200 nm were found to not significantly modify the drug activity, as assessed by the recorded cell viability close to that
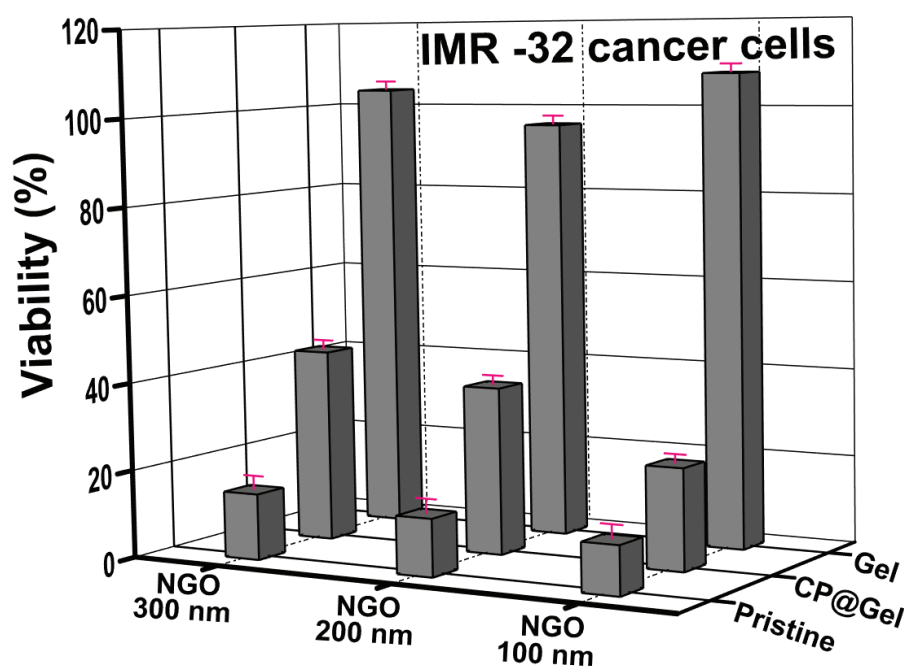
Figure 3.19: Viability percent of NGO particles and functionalized materials.

of the free form of the drug. Gel_NGO 100 nm denotes a completely different behavior, since in this case the activity of the CP is almost doubled, with a cell viability of 41 and 23%, for CP and CP@Gel_NGO 100 respectively.

The size dependency of the carrier efficiency is strictly related to their ability to enter cells, and this is in agreement with data in literature showing that lower sized NGO are able to strongly interact with the cell environment with a more efficient delivery of the hosted drug. This denotes the ability of the carrier to increase the local concentration of the drug inside the cells, thus resulting in enhanced activity. This is of tremendous importance when thinking of potential clinical applications, since it is possible to dramatically reduce the drug doses, with the advantages of reducing systemic side effects. Gel_NGO 100 nm and CP have a synergistic activity, offering potential enhancement of drug desired properties, such as increased water solubility, cellular uptake and targeted delivery and thus the development of a combination therapeutic protocol involving the use of the proposed nanohybrid carrier can be hypothesized.

4

CONCLUSION

This thesis demonstrates the synthesis of Nanographene oxide with well-defined sizes from natural graphite by using oxidation exfoliation reaction. The exceptional chemical structure of graphene oxide due to the presence of oxygen containing groups offers covalent and noncovalent functionalization, which overtures to exciting prospects in biological applications.

In this work, NGO particles have been functionalized by PAMAM and gelatin via covalent and noncovalent interactions respectively, yielding NGO-PAMAM and Gel_NGO nanohybrids with high dispersibility and stability in physiological media, as well as reducing cytotoxicity toward HeLa and Neuroblastoma cells. The comparative toxicities of three sizes of pristine NGO are different, the results highlight the potential of low dimensional (ca. 100 nm) NGO as functional tool for enhancing carboplatin activity in cancer cell lines. The size of NGO is considered as a crucial key in how they interact with cells and other biological systems. The investigated nanohybrid materials, particularly with low NGO sizes, exhibit no obvious toxicity to in vitro cell culture models, The results suggest that functionalization of NGO by using biocompatible substances will reduce the oxidative stress which is one of mechanisms considered in cytotoxic effects of NGO particles. In vitro studies revealed that such nanohybrid materials could offer a platform for targeted carboplatin delivery, raise the cellular uptake and controlled drug release in biological system.

Owing to its small size, large specific surface area, various oxygen groups, low cost, and mostly no cytotoxicity to human stem cells, the NGO-PAMAM and Gel_NGO could be considered as exciting nanohybrids to have broad biological applications.

The lower sized NGO 100 nm coated gelatin exhibits excellent stability and biocompatibility in cell culture media according to their potency to interact with cellular membrane. A synergistic activity between CP and carrier was recorded, as suggested by the enhanced efficiency in CP in killing cancer cells after loading onto the Gel_NGO. Interestingly, the cell viability was not affected by Gel_NGO, confirming that the recorded anticancer activity is related to an increased local concentration of the drug inside the cells, thus resulting in enhanced activity. Further investigation should be done to this regard, but the data reported have evidenced a very promising starting point for further research by chemists, nanotechnologists, biologists and oncologists.

Bibliography

[1] A. Hirsch. The Era of Carbon Allotropes. *Nature materials*, 9(11):868–871, November 2010.

[2] H. W. Krotto, J. R. Heath, S. C. O'Brien, R. F. Curl, and R. E. Smalley. C60: Buckminsterfullerene. *Nature*, 318(14):162 – 163, 1985.

[3] S. Iijima. Helical Microtubules of Graphitic Carbon. *Nature*, 354:56–58, 1991.

[4] K. S. Novoselov, D. Jiang, F. Schedin, T. J. Booth, V. V. Khotkevich, S. V. Morozov, and A. K. Geim. Two-Dimensional Atomic Crystals. *Proceedings of the National Academy of Sciences of the United States of America*, 102(30):10451–3, July 2005.

[5] I. Lyuksyutov, A. G. Naumovets, and V. Pokshishevsky. *Two-Dimensional Crystals*. Academic Press, INC, London, 1992.

[6] A. K. Geim and K. S. Novoselov. The Rise of Graphene. *Nature materials*, 6(3):183–191, March 2007.

[7] S. Stankovich, D. A. Dikin, R. D. Piner, K. A. Kohlhaas, A. Kleinhammes, Y. Jia, Y. Wu, S. T. Nguyen, and R. S. Ruoff. Synthesis of Graphene-Based Nanosheets via Chemical Reduction of Exfoliated Graphite Oxide. *Carbon*, 45(7):1558–1565, June 2007.

[8] C. Berger, Z. Song, X. Li, X. Wu, N. Brown, C. Naud, D. Mayou, T. Li, J. Hass, A. N. Marchenkov, E. H. Conrad, P. N. First, and W. A. de Heer. Electronic Confinement and Coherence in Patterned Epitaxial Graphene. *Science*, 312(5777):1191–6, May 2006.

[9] K. S. Kim, Y. Zhao, H. Jang, S. Y. Lee, J. M. Kim, K. S. Kim, J.-H. Ahn, P. Kim, J.-Y. Choi, and B. H. Hong. Large-Scale Pattern Growth of Graphene Films for Stretchable Transparent Electrodes. *Nature*, 457(7230):706–710, February 2009.

[10] K. S. Novoselov, A. K. Geim, S. V. Morozov, D. Jiang, Y. Zhang, S. V. Dubonos, I. V. Grigorieva, and A. A. Firsov. Electric Field Effect in Atomically Thin Carbon Films. *Science*, 306(5696):666–669, October 2004.

[11] D. Li, M. B. Müller, S. Gilje, R. B. Kaner, and G. G. Wallace. Processable Aqueous Dispersions of Graphene Nanosheets. *Nature nanotechnology*, 3(2):101–105, February 2008.

[12] D. C. Marcano, D. V. Kosynkin, J. M. Berlin, A. Sinitskii, Z. Sun, A. Slesarev, L. B. Alemany, W. Lu, and J. M. Tour. Improved Synthesis of Graphene Oxide. *ACS nano*, 4(8):4806–4814, August 2010.

[13] D. R. Dreyer, S. Park, C. W. Bielawski, and R. S. Ruoff. The Chemistry of Graphene Oxide. *Chemical Society reviews*, 39(1):228–240, January 2010.

[14] K. P. Loh, Q. Bao, P. K. Ang, and J. Yang. The Chemistry of Graphene. *Journal of Materials Chemistry*, 20(12):2277–2289, 2010.

[15] S. Makharza, G. Cirillo, A. Bachmatiuk, I. Ibrahim, N. Ioannides, B. Trzebicka, S. Hampel, and M. H. Rümmeli. Graphene Oxide-Based Drug Delivery Vehicles: Functionalization, Characterization, and Cytotoxicity Evaluation. *Journal of Nanoparticle Research*, 15(12):2099–2124, November 2013.

[16] J.-A. Yan and M. Y. Chou. Oxidation Functional Groups on Graphene: Structural and Electronic Properties. *Physical Review B*, 82(12):125403, September 2010.

[17] D. W. Boukhvalov and M. I. Katsnelson. Modeling of Graphite Oxide. *Journal of the American Chemical Society*, 130(32):10697–701, August 2008.

[18] H. A. Becerril, J. Mao, Z. Liu, R. M. Stoltenberg, Z. Bao, and Y. Chen. Evaluation of Solution-Processed Reduced Graphene Oxide Films as Transparent Conductors. *ACS nano*, 2(3):463–470, 2008.

[19] I. Jung, M. Pelton, R. Piner, D. A. Dikin, S. Stankovich, S. Watcharotone, M. Hausner, and R. S. Ruoff. Simple Approach for High-Contrast Optical Imaging and Characterization of Graphene-Based Sheets. *Nano Letters*, 7(12):3569–3575, 2007.

[20] S. Park and R. S. Ruoff. Chemical Methods for the Production of Graphenes. *Nature nanotechnology*, 4(4):217–24, April 2009.

[21] B. C. Brodie. On the Atomic Weight of Graphite. *Philosophical Transactions of the Royal Society of London*, 149(12):249–259, January 1859.

[22] L. Staudenmaier. Verfahren zur darstellung der graphitsäure. *Berichte der deutschen chemischen Gesellschaft*, 31(2):1481–1487, 1898.

[23] W. S. Hummers and R. E. Offeman. Preparation of Graphitic Oxide. *Journal of American Chemical Society*, 80(6):1339–1339, 1958.

[24] M. Hirata, T. Gotou, S. Horiuchi, M. Fujiwara, and M. Ohba. Thin-Film Particles of Graphite Oxide 1:High-Yield Synthesis and Flexibility of the Particles. *Carbon*, 42(14):2929–2937, January 2004.

[25] N. I. Kovtyukhova, P. J. Ollivier, B. R. Martin, T. E. Mallouk, S. A. Chizhik, E. V. Buzaneva, and A. D. Gorchinskiy. Layer-by-Layer Assembly of Ultrathin Composite Films from Micron-Sized Graphite Oxide Sheets and Polycations. *Chemistry of Materials*, 11(3):771–778, March 1999.

[26] H. He, T. Riedl, A. Lerf, and J. Klinowski. Solid-State NMR Studies of the Structure of Graphite Oxide. *Journal of Physical Chemistry*, 3654(96):19954–19958, 1996.

[27] P. A. Marques, G. Gonçalves, S. Cruz, N. Almeida, M. K. Singh, J. Grácio, and A. A. Sousa. Functionalized Graphene Nanocomposites. In Abbass Hashim, editor, *Advances in Nanocomposite Technology*, page 374. InTech, 2011.

[28] S. Makharza, G. Cirillo, A. Bachmatiuk, O. Vittorio, R. G. Mendes, S. Oswald, S. Hampel, and M. H. Rümmeli. Size-Dependent Nanographene Oxide as a Platform for Efficient Carboplatin Release. *Journal of Materials Chemistry B*, 1(44):6107–6114, 2013.

[29] X. Sun, Z. Liu, K. Welsher, J. T. Robinson, A. Goodwin, S. Zaric, and H. Dai. Nano-Graphene Oxide for Cellular Imaging and Drug Delivery. *Nano research*, 1(3):203–212, January 2008.

[30] P. Tarakeshwar, H. S. Choi, and K. S. Kim. Olefinic vs. Aromatic pi-H Interaction: A Theoretical Investigation of the Nature of Interaction of First-Row Hydrides with Ethene and Benzene. *Journal of the American Chemical Society*, 123(14):3323–31, April 2001.

[31] E. C. Lee, D. Kim, P. Jurecka, P. Tarakeshwar, P. Hobza, and K. S. Kim. Understanding of Assembly Phenomena by Aromatic-Aromatic Interactions: Benzene Dimer and the Substituted Systems. *Journal of physical chemistry. A*, 111(18):3446–3457, May 2007.

[32] S. Grimme. On the Importance of Electron Correlation Effects for the p-p Interactions in Cyclophanes. *Chemistry - A European Journal*, 10(14):3423–3429, July 2004.

[33] Z. Liu, J. T. Robinson, X. Sun, and H. Dai. Pegylated nanographene oxide for delivery of water-insoluble cancer drugs. *Journal of the American Chemical Society*, 130(33):10876–10877, 2008.

[34] R. J. Knox, F. Friedlos, D. A. Lydall, and J. J. Roberts. Mechanism of cytotoxicity of anticancer platinum drugs: Evidence that cis-diamminedichloroplatinum(ii) and cis-diammine-(1,1-cyclobutanedicarboxylato)platinum(ii) differ only in the kinetics of their interaction with dna. *Cancer Research*, 46(4 Part 2):1972–1979, 1986.

[35] K. C. Micetich, D. Barnes, and L. C. Erickson. A comparative study of the cytotoxicity and dna-damaging effects of cis-(diammino)(1,1-cyclobutanedicarboxylato)-platinum(ii) and cis-diamminedichloroplatinum(ii) on l1210 cells. *Cancer Research*, 45(9):4043–4047, 1985.

[36] A. Brüning and I. Mylonas. New emerging drugs targeting the genomic integrity and replication machinery in ovarian cancer. *Archives of Gynecology and Obstetrics*, 283(5):1087–1096, 2011.

[37] H. Chen, M. B. Müller, K. J. Gilmore, G. G. Wallace, and D. Li. Mechanically Strong, Electrically Conductive, and Biocompatible Graphene Paper. *Advanced Materials*, 20(18):3557–3561, July 2008.

[38] S. Agarwal, X. Zhou, F. Ye, Q. He, G. C. K. Chen, J. Soo, F. Boey, H. Zhang, and P. Chen. Interfacing Live Cells with Nanocarbon Substrates. *Langmuir : the ACS journal of surfaces and colloids*, 26(4):2244–2247, February 2010.

[39] K. Wang, J. Ruan, H. Song, J. Zhang, Y. Wo, S. Guo, and D. Cui. Biocompatibility of Graphene Oxide. *Nanoscale Research Letters*, 6(1):8, August 2010.

[40] X. Zhang, W. Hu, J. Li, L. Tao, and Y. Wei. A Comparative Study of Cellular Uptake and Cytotoxicity of Multi-Walled Carbon Nanotubes, Graphene Oxide, and Nanodiamond. *Toxicology Research*, 1(1):62–68, 2012.

[41] Y. Chang, S.-T. Yang, J.-H. Liu, E. Dong, Y. Wang, A. Cao, Y. Liu, and H. Wang. In Vitro Toxicity Evaluation of Graphene Oxide on A549 Cells. *Toxicology letters*, 200(3):201–10, March 2011.

[42] S. Park, N. Mohanty, J. W. Suk, A. Nagaraja, J. An, R. D. Piner, W. Cai, D. R. Dreyer, V. Berry, and R. S. Ruoff. Biocompatible, Robust Free-Standing Paper Composed of a TWEEN/Graphene Composite. *Advanced materials*, 22(15):1736–1740, April 2010.

[43] W. Hu, C. Peng, W. Luo, M. Lv, X. Li, D. Li, Q. Huang, and C. Fan. Graphene-Based Antibacterial Paper. *ACS nano*, 4(7):4317–4323, July 2010.

[44] K. Yang, H. Gong, X. Shi, J. Wan, Y. Zhang, and Z. Liu. In Vivo Biodistribution and Toxicology of Functionalized Nano-Graphene Oxide in Mice after Oral and Intraperitoneal Administration. *Biomaterials*, 34(11):2787–95, April 2013.

[45] K. Yang, J. Wan, S. Zhang, Y. Zhang, S.-T. Lee, and Z. Liu. In vivo pharmacokinetics, long-term biodistribution, and toxicology of pegylated graphene in mice. *ACS Nano*, 5(1):516–522, 2011.

[46] S. Zhang, K. Yang, L. Feng, and Z. Liu. In Vitro and In Vivo Behaviors of Dextran Functionalized Graphene. *Carbon*, 49(12):4040–4049, October 2011.

[47] K.-H. Liao, Y.-S. Lin, C. W. Macosko, and C. L. Haynes. Cytotoxicity of Graphene Oxide and Graphene in Human Erythrocytes and Skin Fibroblasts. *ACS applied materials & interfaces*, 3(7):2607–2615, July 2011.

[48] M. C. Duch, G. R. S. Budinger, Y. T. Liang, S. Soberanes, D. Urich, S. E. Chiarella, L. A. Campochiaro, A. Gonzalez, N. S. Chandel, M. C. Hersam, and G. M. Mutlu. Minimizing oxidation and stable nanoscale dispersion improves the biocompatibility of graphene in the lung. *Nano Letters*, 11(12):5201–5207, 2011.

[49] X. C. Qin, Z. Y. Guo, Z. M. Liu, W. Zhang, M. M. Wan, and B. W. Yang. Folic Acid-Conjugated Graphene Oxide for Cancer Targeted Chemo-Photothermal Therapy. *Journal of Photochemistry and Photobiology B: Biology*, 120(5):156–162, December 2012.

[50] K. Liu, J.-J. Zhang, F.-F. Cheng, T.-T. Zheng, C. Wang, and J.-J. Zhu. Green and Facile Synthesis of Highly Biocompatible Graphene Nanosheets and Its Application for Cellular Imaging and Drug Delivery. *Journal of Materials Chemistry*, 21(32):12034–40, 2011.

[51] J. An, Y. Gou, C. Yang, F. Hu, and C. Wang. Synthesis of a Biocompatible Gelatin Functionalized Graphene Nanosheets and its Application for Drug Delivery. *Materials Science and Engineering: C*, 33(5):2827–2837, March 2013.

[52] L. Zhang, J. Xia, Q. Zhao, L. Liu, and Z. Zhang. Functional Graphene Oxide as a Nanocarrier for Controlled Loading and Targeted Delivery of Mixed Anticancer Drugs. *Small*, 6(4):537–544, March 2010.

[53] W. Hu, C. Peng, M. Lv, X. Li, Y. Zhang, N. Chen, C. Fan, and Q. Huang. Protein Corona-Mediated Mitigation of Cytotoxicity of Graphene Oxide. *ACS nano*, 5(5):3693–3700, May 2011.

[54] W. Zhang, Z. Guo, D. Huang, Z. Liu, X. Guo, and H. Zhong. Synergistic Effect of Chemo-Photothermal Therapy Using PEGylated Graphene Oxide. *Biomaterials*, 32(33):8555–8561, November 2011.

[55] K. Yang, Y. Li, X. Tan, R. Peng, and Z. Liu. Behavior and Toxicity of Graphene and Its Functionalized Derivatives in Biological Systems. *Small (Weinheim an der Bergstrasse, Germany)*, 9(9-10):1492–503, May 2013.

[56] K. Yang, S. Zhang, G. Zhang, X. Sun, S.-T. Lee, and Z. Liu. Graphene in Mice: Ultrahigh In Vivo Tumor Uptake and Efficient Photothermal Therapy. *Nano letters*, 10(9):3318–3323, September 2010.

[57] E. L. K. Chng and M. Pumera. The Toxicity of Graphene Oxides: Dependence on the Oxidative Methods Used. *Chemistry - A European Journal*, 19(25):8227–35, June 2013.

[58] N. Shinohara, K. Matsumoto, S. Endoh, J. Maru, and J. Nakanishi. In Vitro and In Vivo Genotoxicity Tests on Fullerene C60 Nanoparticles. *Toxicology letters*, 191(2-3):289–296, December 2009.

[59] A. Casey, E. Herzog, F. M. Lyng, H. J. Byrne, G. Chambers, and M. Davoren. Single Walled Carbon Nanotubes Induce Indirect Cytotoxicity by Medium Depletion in A549 Lung Cells. *Toxicology letters*, 179(2):78–84, June 2008.

[60] A. M. Schrand, L. Dai, J. J. Schlager, S. M. Hussain, and E. Osawa. Differential Biocompatibility of Carbon Nanotubes and Nanodiamonds. *Diamond and Related Materials*, 16(12):2118–2123, December 2007.

[61] H. Yang, C. Liu, D. Yang, H. Zhang, and Z. Xi. Comparative Study of Cytotoxicity, Oxidative Stress and Genotoxicity Induced by Four Typical Nanomaterials: The Role of Particle Size, Shape and Composition. *Journal of applied toxicology*, 29(1):69–78, January 2009.

[62] Z. Liu, W. Cai, L. He, N. Nakayama, K. Chen, X. Sun, X. Chen, and H. Dai. In Vivo Biodistribution and Highly Efficient Tumour Targeting of Carbon Nanotubes in Mice. *Nature nanotechnology*, 2(1):47–52, January 2007.

[63] J. M. Wörle-Knirsch, K. Pulskamp, and H. F. Krug. Oops They Did it Again! Carbon Nanotubes Hoax Scientists in Viability Assays. *Nano letters*, 6(6):1261–8, June 2006.

[64] G. von Maltzahn, J.-H. Park, A. Agrawal, N. K. Bandaru, S. K. Das, M. J. Sailor, and S. N. Bhatia. Computationally Guided Photothermal Tumor Therapy Using Long-Circulating Gold Nanorod Antennas. *Cancer research*, 69(9):3892–900, May 2009.

[65] H. W. Krotto, J. R. Heath, S. C. O'Brien, R. F. Curl, and R. E. Smalley. C60: Buckminsterfullerene. *Nature*, 318(14):162 – 163, 1985.

[66] S. Bosi, L. Feruglio, T. Da Ros, G. Spalluto, B. Gregoretti, M. Terdoslavich, G. Decorti, S. Passamonti, S. Moro, and M. Prato. Hemolytic Effects of Water-Soluble Fullerene Derivatives. *Journal of medicinal chemistry*, 47(27):6711–6715, December 2004.

[67] B. Han and M N. Karim. Cytotoxicity of Aggregated Fullerene C60 Particles on CHO and MDCK Cells. *Scanning*, 30(2):213–220, 2008.

[68] K. P. Loh, Q. Bao, G. Eda, and M. Chhowalla. Graphene Oxide as a Chemically Tunable Platform for Optical Applications. *Nature chemistry*, 2(12):1015–1024, December 2010.

[69] L. Dong, K. L. Joseph, C. M. Witkowski, and M. M. Craig. Cytotoxicity of Single-Walled Carbon Nanotubes Suspended in Various Surfactants. *Nanotechnology*, 19(25):255702–255706, June 2008.

[70] X. Yang, Y. Wang, X. Huang, Y. Ma, Y. Huang, R. Yang, H. Duan, and Y. Chen. Multi-Functionalized Graphene Oxide Based Anticancer Drug-Carrier with Dual-Targeting Function and pH-Sensitivity. *Journal of Materials Chemistry*, 21:3448–3454, 2011.

[71] H. Yue, W. Wei, Z. Yue, B. Wang, N. Luo, Y. Gao, D. Ma, G. Ma, and Z. Su. The Role of The Lateral Dimension of Graphene Oxide in The Regulation of Cellular Responses. *Biomaterials*, 33(16):4013–21, June 2012.

[72] C. Cheng, S. Nie, S. Li, H. Peng, H. Yang, L. Ma, S. Sun, and C. Zhao. Biopolymer Functionalized Reduced Graphene Oxide with Enhanced Biocompatibility via Mussel Inspired Coatings/Anchors. *Journal of Materials Chemistry B*, 1(3):265–275, 2013.

[73] H. Bao, Y. Pan, Y. Ping, N. G. Sahoo, T. Wu, L. Li, J. Li, and L. H. Gan. Chitosan-functionalized graphene oxide as a nanocarrier for drug and gene delivery. *Small*, 7(11):1569–1578, 2011.

[74] P. Cherukuri, S. M. Bachilo, S. H. Litovsky, and R. B. Weisman. Near-Infrared Fluorescence Microscopy of Single-Walled Carbon Nanotubes in Phagocytic Cells. *Journal of the American Chemical Society*, 126(48):15638–39, December 2004.

[75] N. W. Shi Kam, T. C. Jessop, P. A Wender, and H. Dai. Nanotube Molecular Transporters: Internalization of Carbon Nanotube-Protein Conjugates into Mammalian Cells. *Journal of the American Chemical Society*, 126(22):6850–6851, June 2004.

[76] G. Jia, H. Wang, L. Yan, X. Wang, R. Pei, T. Yan, Y. Zhao, and X. Guo. Cytotoxicity of Carbon Nanomaterials: Single-Wall Nanotube, Multi-Wall Nanotube, and Fullerene. *Environmental science & technology*, 39(5):1378–1383, March 2005.

[77] F. Tian, D. Cui, H. Schwarz, G. G. Estrada, and H. Kobayashi. Cytotoxicity of Single-Wall Carbon Nanotubes on Human Fibroblasts. *Toxicology in vitro*, 20(7):1202–1212, October 2006.

[78] U. C. Nygaard, J. S. Hansen, M. Samuelsen, T. Alberg, C. D. Marioara, and M. Løvik. Single-walled and multi-walled carbon nanotubes promote allergic immune responses in mice. *Toxicological Sciences*, 109(1):113–123, 2009.

[79] M. Kakran, N. G. Sahoo, H. Bao, Y. Pan, and L. Li. Functionalized graphene oxide as nanocarrier for loading and delivery of ellagic acid. *Current Medicinal Chemistry*, 18(29):4503–4512, 2011.

[80] M. Arlt, D. Haase, S. Hampel, S. Oswald, A. Bachmatiuk, R. Klingeler, R. Schulze, M. Ritschel, A. Leonhardt, S. Fuessel, B. Büchner, K. Kraemer, and M. P. Wirth. Delivery of Carboplatin by Carbon-Based Nanocontainers Mediates Increased Cancer Cell Death. *Nanotechnology*, 21(33):335101–335109, August 2010.

[81] X. Zhang, L. Meng, Q. Lu, Z. Fei, and P. J. Dyson. Targeted Delivery and Controlled Release of Doxorubicin to Cancer Cells Using Modified Single Wall Carbon Nanotubes. *Biomaterials*, 30(30):6041–6047, October 2009.

[82] Z. Liu, A. C. Fan, K. Rakhra, S. Sherlock, A. Goodwin, X. Chen, Q. Yang, D. W. Felsher, and H. Dai. Supramolecular Stacking of Doxorubicin on Carbon Nanotubes for In Vivo Cancer Therapy. *Angewandte Chemie International ed.*, 48(41):7668–72, January 2009.

[83] C. Tripisciano, K. Kraemer, A. Taylor, and E. Borowiak-Palen. Single-Wall Carbon Nanotubes Based Anticancer Drug Delivery System. *Chemical Physics Letters*, 478(4-6):200–205, August 2009.

[84] J. Shi, H. Zhang, L. Wang, L. Li, H. Wang, Z. Wang, Z. Li, C. Chen, L. Hou, C. Zhang, and Z. Zhang. PEI-Derivatized Fullerene Drug Delivery Using Folate as a Homing Device Targeting to Tumor. *Biomaterials*, 34(1):251–261, January 2013.

[85] C. M. Sayes, A. M. Gobin, K. D. Ausman, J. Mendez, J. L. West, and V. L. Colvin. Nano-C60 Cytotoxicity is Due to Lipid Peroxidation. *Biomaterials*, 26(36):7587–7595, December 2005.

[86] C. M. Sayes, J. D. Fortner, W. Guo, D. Lyon, A. M. Boyd, K. D. Ausman, Y. J. Tao, B. Sitharaman, L. J. Wilson, J. B. Hughes, J. L. West, and V. L. Colvin. The differential cytotoxicity of water-soluble fullerenes. *Nano Letters*, 4(10):1881–1887, 2004.

[87] E. M. Horwitz, M. Andreef, and F. Frassoni. Mesenchymal Stromal Cells. *Current Opinion in Hematology*, 13(6):419–425, November 2006.

[88] Y. Talukdar, J. T. Rashkow, G. Lalwani, S. Kanakia, and B. Sitharaman. The Effects of Graphene Nanostructures on Mesenchymal Stem Cells. *Biomaterials*, 35:4863–4877, March 2014.

[89] O. Akhavan, E. Ghaderi, and A. Akhavan. Size-dependent genotoxicity of graphene nanoplatelets in human stem cells. *Biomaterials*, 33(32):8017 – 8025, 2012.

[90] S. Goenka, V. Sant, and S. Sant. Graphene-Based Nanomaterials for Drug Delivery and Tissue Engineering. *Journal of Controlled Release*, 173:75–88, January 2014.

[91] O. Akhavan, E. Ghaderi, H. Emamy, and F. Akhavan. Genotoxicity of Graphene Nanoribbons in Human Mesenchymal Stem Cells. *Carbon*, 54:419–431, April 2013.

[92] J. Panno. *Cancer : The Role of Genes , Lifestyle , and Environment.* 2 edition, 2010.

[93] H.-B. Park, H.-G. Nam, H.-G. Oh, J.-H. Kim, C.-M. Kim, K.-S. Song, and K.-H. Jhee. Effect of Graphene on Growth of Neuroblastoma Cells. *Journal of microbiology and biotechnology*, 23(2):274–277, February 2013.

[94] D. Ghosh, S. Chandra, A. Chakraborty, S. K. Ghosh, and P. Pramanik. A Novel Graphene Oxide-Para Amino Benzoic Acid Nanosheet as Effective Drug Delivery

System to Treat Drug Resistant Bacteria. *International Journal of Pharmaceutical Sciences and Drug Research*, 2(2):127–133, 2010.

[95] K. N. J. Burger, R. W. H. M. Staffhorst, H. C. de Vijlder, M. J. Velinova, P. H. Bomans, P. M. Frederik, and B. de Kruijff. Nanocapsules: Lipid-Coated Aggregates of Cisplatin with High Cytotoxicity. *Nature medicine*, 8(1):81–84, January 2002.

[96] X. Sun, D. Luo, J. Liu, and D. G. Evans. Monodisperse chemically modified graphene obtained by density gradient ultracentrifugal rate separation. *ACS nano*, 4(6):3381–9, June 2010.

[97] S. Sadekar and H. Ghandehari. Transepithelial Transport and Toxicity of PAMAM Dendrimers: Implications for Oral Drug Delivery. *Advanced drug delivery reviews*, 64(6):571–88, May 2012.

[98] D. A. Tomalia and J. M. J. Frechet. Discovery of Dendrimers and Dendritic Polymers: A Brief Historical Perspective. *Journal of Polymer Science Part A: Polymer Chemistry*, 40(16):2719–2728, August 2002.

[99] S. H. Medina and M. E. H. El-Sayed. Dendrimers as Carriers for Delivery of Chemotherapeutic Agents. *Chemical reviews*, 109(7):3141–3157, July 2009.

[100] J. M. Kim, J. Kim, and J. Kim. Covalent Decoration of Graphene Oxide with Dendrimer-Encapsulated Nanoparticles for Universal Attachment of Multiple Nanoparticles on Chemically Converted Graphene. *Chemical communications*, 48(74):9233–9235, September 2012.

[101] G. Cirillo, O. Vittorio, S. Hampel, F. Iemma, P. Parchi, M. Cecchini, F. Puoci, and N. Picci. Quercetin Nanocomposite as Novel Anticancer Therapeutic: Improved Efficiency and Reduced Toxicity. *European journal of pharmaceutical sciences*, 49(3):359–365, April 2013.

[102] G. Cirillo, O. Vittorio, S. Hampel, U. G. Spizzirri, N. Picci, and F. Iemma. Incorporation of Carbon Nanotubes into a Gelatin-Catechin Conjugate: Innovative Approach for the Preparation of Anticancer Materials. *International journal of pharmaceutics*, 446(1-2):176–182, March 2013.

[103] S. K. Vashist, D. Zheng, G. Pastorin, K. Al-Rubeaan, J. H.T. Luong, and F.-S. Sheu. Delivery of Drugs and Biomolecules Using Carbon Nanotubes. *Carbon*, 49(13):4077–4097, November 2011.

[104] H. Haniu, N. Saito, Y. Matsuda, T. Tsukahara, K. Maruyama, Y. Usui, K. Aoki, S. Takanashi, S. Kobayashi, H. Nomura, M. Okamoto, M. Shimizu, and H. Kato. Culture Medium Type Affects Endocytosis of Multi-walled Carbon Nanotubes in BEAS-2B Cells and Subsequent Biological Response. *Toxicology in vitro*, 27(6):1679–1685, September 2013.

[105] K. N. Kudin, B. Ozbas, H. C. Schniepp, R. K. Prud'homme, I. A. Aksay, and R. Car. Raman Spectra of Graphite Oxide and Functionalized Graphene Sheets. *Nano letters*, 8(1):36–41, January 2008.

[106] D. Yang, A. Velamakanni, G. Bozoklu, S. Park, M. Stoller, R. D. Piner, S. Stankovich, I. Jung, D. A. Field, C. A. Ventrice, and R. S. Ruoff. Chemical Analysis of Graphene Oxide Films After Heat and Chemical Treatments by X-ray Photoelectron and Micro-Raman Spectroscopy. *Carbon*, 47(1):145–152, January 2009.

[107] N. R. Wilson, P. A. Pandey, R. Beanland, R. J. Young, I. A. Kinloch, L. Gong, Z. H. Liu, K. Suenaga, J. P. Rourke, S. J. York, and J. Sloan. Graphene Oxide: Structural Analysis and Application as a Highly Transparent Support for Electron Microscopy. *ACS nano*, 3(9):2547–56, September 2009.

[108] Y. Xu, Z. Liu, X. Zhang, Y. Wang, J. Tian, Y. Huang, Y. Ma, X. Zhang, and Y. Chen. A Graphene Hybrid Material Covalently Functionalized with Porphyrin: Synthesis and Optical Limiting Property. *Advanced Materials*, 21(12):1275–1279, March 2009.

[109] M. Acik, G. Lee, C. Mattevi, A. Pirkle, R. M. Wallace, M. Chhowalla, K. Cho, and Y. Chabal. The Role of Oxygen during Thermal Reduction of Graphene Oxide Studied by Infrared Absorption Spectroscopy. *The Journal of Physical Chemistry C*, 115(40):19761–19781, October 2011.

[110] C. Altavilla and E. Ciliberto, editors. *Inorganic Nanoparticles: Synthesis, Applications, and Perspectives.* CRC Press, Taylor & Francis Group, 2010.

[111] A. Ganguly, S. Sharma, P. Papakonstantinou, and J. Hamilton. Probing the Thermal Deoxygenation of Graphene Oxide Using High-Resolution In Situ X-ray-Based Spectroscopies. *The Journal of Physical Chemistry C*, 115(34):17009–019, September 2011.

[112] K. Takahashi, K. Yamada, H. Kato, H. Hibino, and Y. Homma. In Situ Scanning Electron Microscopy of Graphene Growth on Polycrystalline Ni Substrate. *Surface Science*, 606(7-8):728–732, April 2012.

[113] J. I. Paredes, S. Villar-Rodil, P. Solís-Fernández, A. Martínez-Alonso, and J. M. D. Tascón. Atomic Force and Scanning Tunneling Microscopy Imaging of Graphene Nanosheets Derived from Graphite Oxide. *Langmuir : the ACS journal of surfaces and colloids*, 25(10):5957–68, May 2009.

[114] G. Haugstad. *Atomic Force Microscopy: Understanding Basic Modes and Advanced Applications.* John Wiley & Sons, Inc., New Jersey, 2012.

[115] I. Horcas, R. Fernández, J. M. Gómez-Rodríguez, J. Colchero, J. Gómez-Herrero, and A. M. Baro. WSXM: A Software for Scanning Probe Microscopy and A Tool for Nanotechnology. *Review of scientific instruments*, 78(1):013705–08, January 2007.

[116] A. Ganguly, S. Sharma, P. Papakonstantinou, and J. Hamilton. Probing the thermal deoxygenation of graphene oxide using high-resolution in situ x-ray-based spectroscopies. *The Journal of Physical Chemistry C*, 115(34):17009–17019, 2011.

[117] L. M. Malard, M. A. Pimenta, G. Dresselhaus, and M. S. Dresselhaus. Raman Spectroscopy in Graphene. *Physics Reports*, 473(5-6):51–87, April 2009.

[118] A. Das, B. Chakraborty, and A. K. Sood. Raman Spectroscopy of Graphene on Different Substrates and Influence of Defects. *Bulletin of Materials Science*, 31(3):579–584, 2008.

[119] C. Reich, S.and Thomsen. Raman Spectroscopy of Graphite. *Philosophical transactions. Series A, Mathematical, physical, and engineering sciences*, 362(1824):2271–88, November 2004.

[120] Z. Tang, L. Zhang, C. Zeng, T. Lin, and B. Guo. General Route to Graphene with Liquid-Like Behavior by Non-covalent Modification. *Soft Matter*, 8(35):9214–9220, 2012.

[121] S. Mao, H. Pu, and J. Chen. Graphene Oxide and its Reduction: Modeling and Experimental Progress. *RSC Advances*, 2(7):2643–2662, 2012.

[122] K. Yang, J. Wan, S. Zhang, B. Tian, Y. Zhang, and Z. Liu. The Influence of Surface Chemistry and Size of Nanoscale Graphene Oxide on Photothermal Therapy of Cancer Using Ultra-Low Laser Power. *Biomaterials*, 33(7):2206–14, March 2012.

[123] V. Singh, D. Joung, L. Zhai, S. Das, S. I. Khondaker, and S. Seal. Graphene Based Materials: Past, Present and Future. *Progress in Materials Science*, 56(8):1178–1271, October 2011.

[124] H. Yang, C. Shan, F. Li, D. Han, Q. Zhang, and L. Niu. Covalent Functionalization of Polydisperse Chemically-Converted Graphene Sheets with Amine-Terminated Ionic Liquid. *Chemical communications*, (26):3880–2, July 2009.

[125] M. Najlah, S. Freeman, D. Attwood, and A. D'Emanuele. Synthesis, Characterization and Stability of Dendrimer Prodrugs. *International journal of pharmaceutics*, 308(1-2):175–182, February 2006.

[126] L. Minati, G. Speranza, I. Bernagozzi, S. Torrengo, A. Chiasera, and M. Ferrari. Luminescent Short Thiol-Functionalized Multi-wall Carbon Nanotubes. *Diamond and Related Materials*, 20(7):1046–1049, July 2011.

[127] J. Zhu, Y. Li, Y. Chen, J. Wang, B. Zhang, J. Zhang, and W. J. Blau. Graphene Oxide Covalently Functionalized with Zinc Phthalocyanine for Broadband Optical Limiting. *Carbon*, 49(6):1900–1905, May 2011.

[128] I. G. Casella and E. Desimoni. Xps, sem and electrochemical characterization of a platinum-based glassy carbon modified electrode. electrocatalytic oxidation of ethanol in acidic medium. *Electroanalysis*, 8(5):447–453, 1996.

[129] J. C. Ma and D. A. Dougherty. The Cation-π Interaction. *Chemical reviews*, 97(5):1303–1324, December 2012.

[130] I. Zanellato, I. Bonarrigo, E. Gabano, M. Ravera, N. Margiotta, P.-G. Betta, and D. Osella. Metallo-Drugs In The Treatment of Malignant Pleural Mesothelioma. *Inorganica Chimica Acta*, 393:64–74, December 2012.

[131] S.-T. Yang, S. Chen, Y. Chang, A. Cao, Y. Liu, and H. Wang. Removal of Methylene Blue from Aqueous Solution by Graphene Oxide. *Journal of colloid and interface science*, 359(1):24–29, July 2011.

[132] M. A. Pimenta, G. Dresselhaus, M. S. Dresselhaus, L. G. Cançado, A. Jorio, and R. Saito. Studying Disorder in Graphite-Based Systems by Raman Spectroscopy. *Physical chemistry chemical physics*, 9(11):1276–1291, March 2007.

[133] L.G. Cançado, K. Takai, T. Enoki, M. Endo, Y.A. Kim, H. Mizusaki, N.L. Speziali, A. Jorio, and M.A. Pimenta. Measuring The Degree of Stacking Order in Graphite by Raman Spectroscopy. *Carbon*, 46(2):272–275, February 2008.

[134] V. Georgakilas, M. Otyepka, A. B. Bourlinos, V. Chandra, N. Kim, K. C. Kemp, P. Hobza, R. Zboril, and K. S. Kim. Functionalization of Graphene: Covalent and Non-Covalent Approaches, Derivatives and Applications. *Chemical reviews*, 112(11):6156–6214, November 2012.

[135] T. S. Sreeprasad, S. M. Maliyekkal, K. P. Lisha, and T. Pradeep. Reduced Graphene Oxide-Metal/Metal Oxide Composites: Facile Synthesis and Application in Water Purification. *Journal of hazardous materials*, 186(1):921–931, February 2011.

[136] H. C. Schniepp, J.-L. Li, M. J. McAllister, H. Sai, M. Herrera-Alonso, D. H. Adamson, R. K. Prud'homme, R. Car, D. A. Saville, and I. A. Aksay. Functionalized single graphene sheets derived from splitting graphite oxide. *The Journal of Physical Chemistry B*, 110(17):8535–8539, 2006.

[137] U. G. Spizzirri, S. Hampel, G. Cirillo, F. P. Nicoletta, A. Hassan, O. Vittorio, N. Picci, and F. Iemma. Spherical Gelatin/CNTs Hybrid Microgels as Electro-Responsive Drug Delivery Systems. *International journal of pharmaceutics*, 448(1):115–122, May 2013.

[138] O. Vittorio, G. Cirillo, F. Iemma, G. D. Turi, E. Jacchetti, M. Curcio, S. Barbuti, N. Funel, O. I. Parisi, F. Puoci, and N. Picci. Dextran-Catechin Conjugate: A Potential Treatment Against the Pancreatic Ductal Adenocarcinoma. *Pharmaceutical Research*, 29(9):2601–2614, 2012.
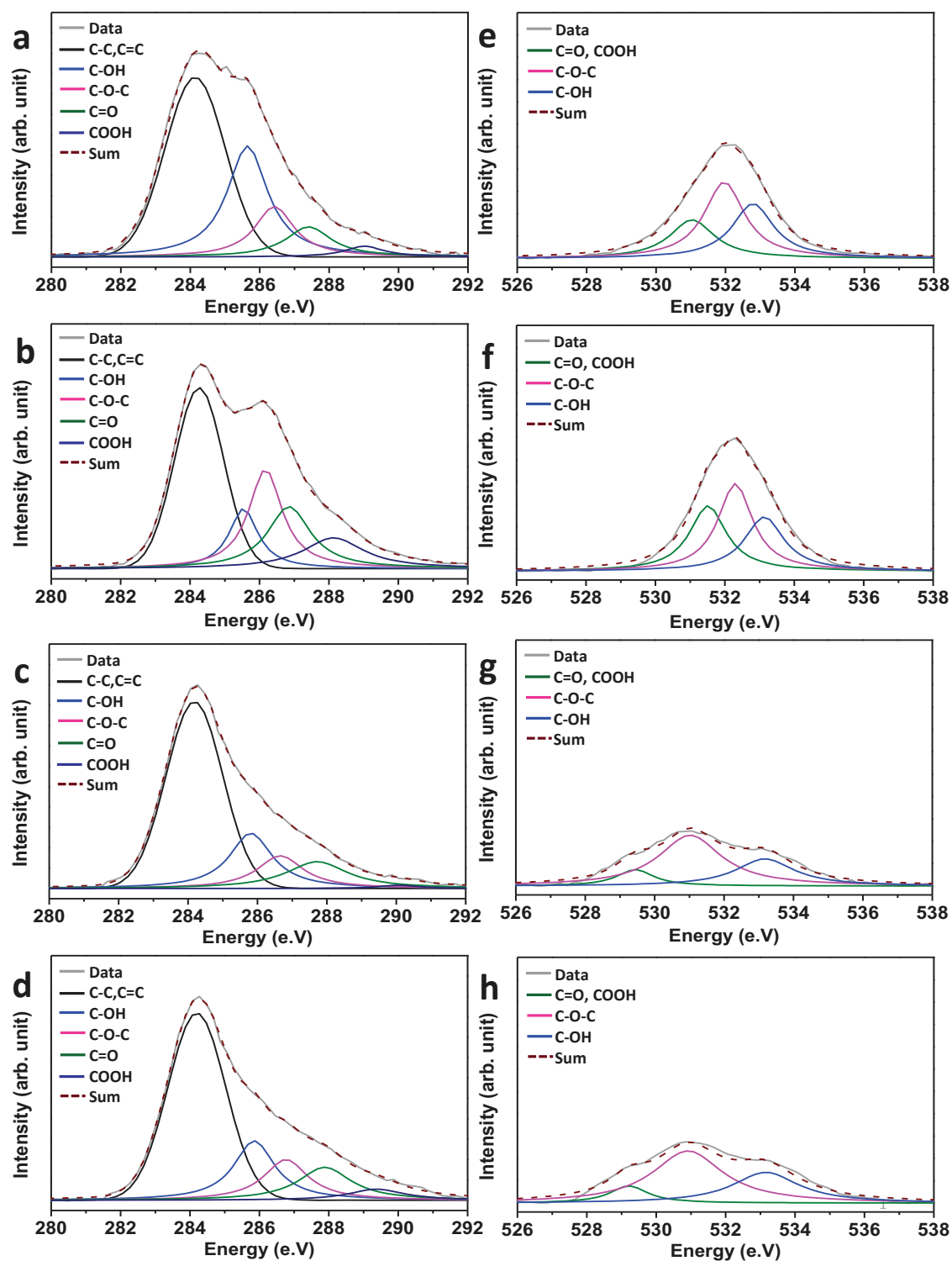
A

APPENDIX

Contents:

Figure A.1: C1s and O1s XPS spectra of NGO 200 nm and PAMAM functionalized materials. a - d, C1s XPS spectra of NGO 200 nm, CP@NGO, PAMAM-NGO and CP@PAMAM-NGO respectively. **e - h,** O1s XPS spectra of NGO 200 nm, CP@NGO, PAMAM-NGO and CP@PAMAM-NGO respectively.
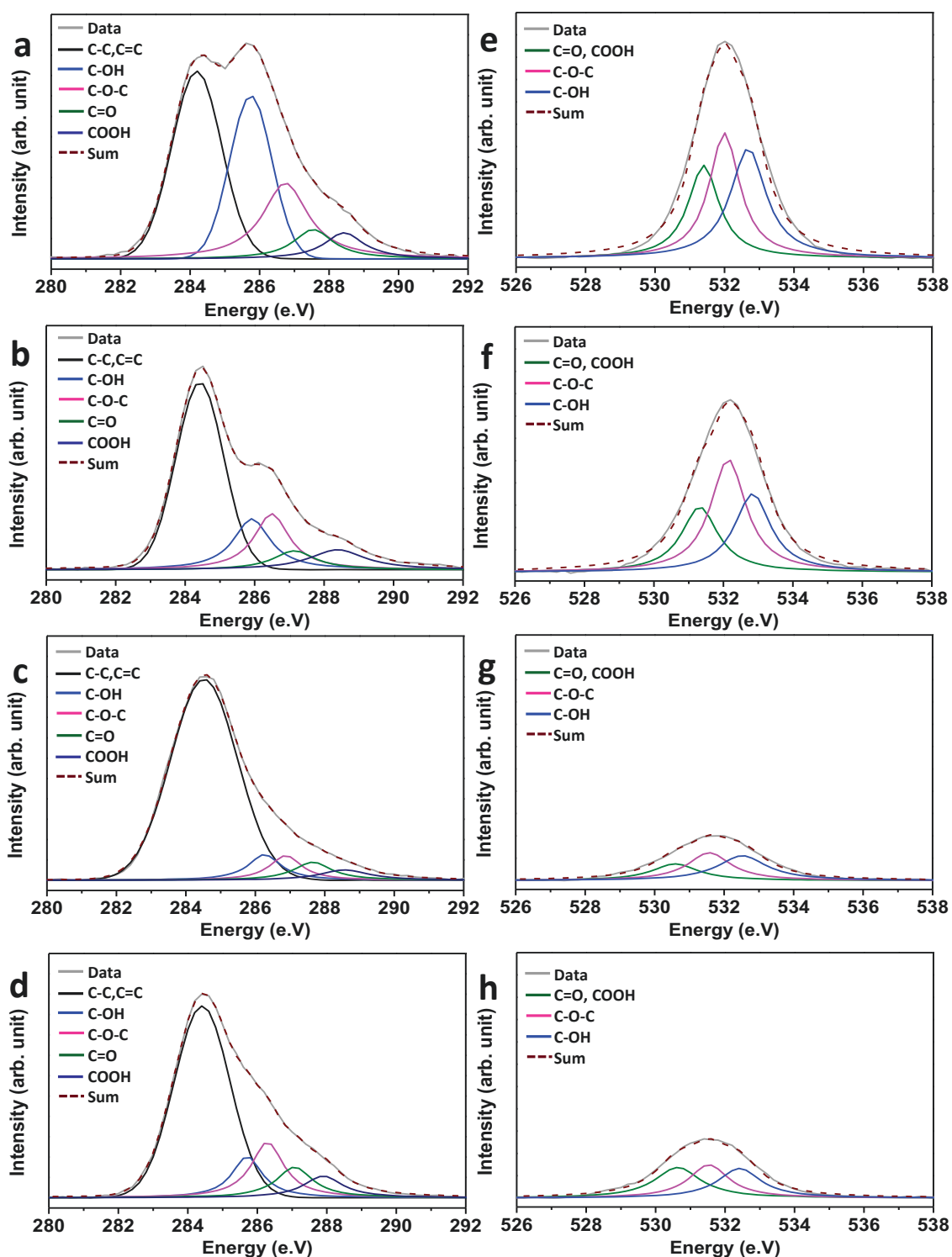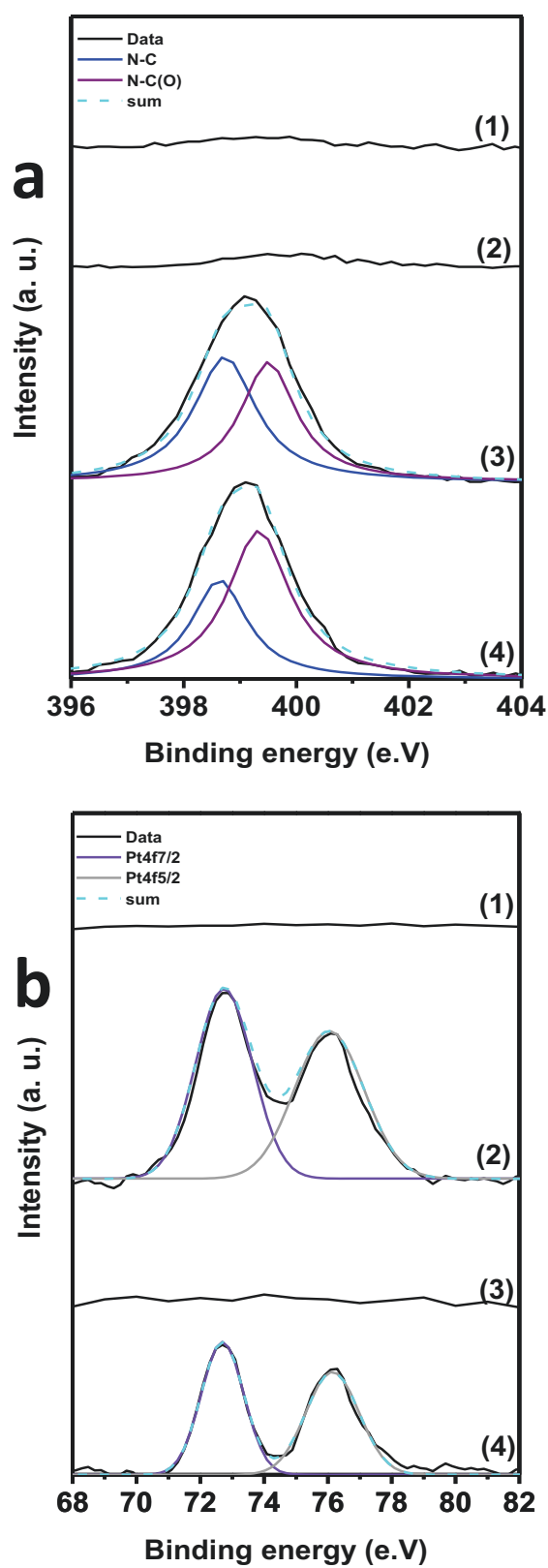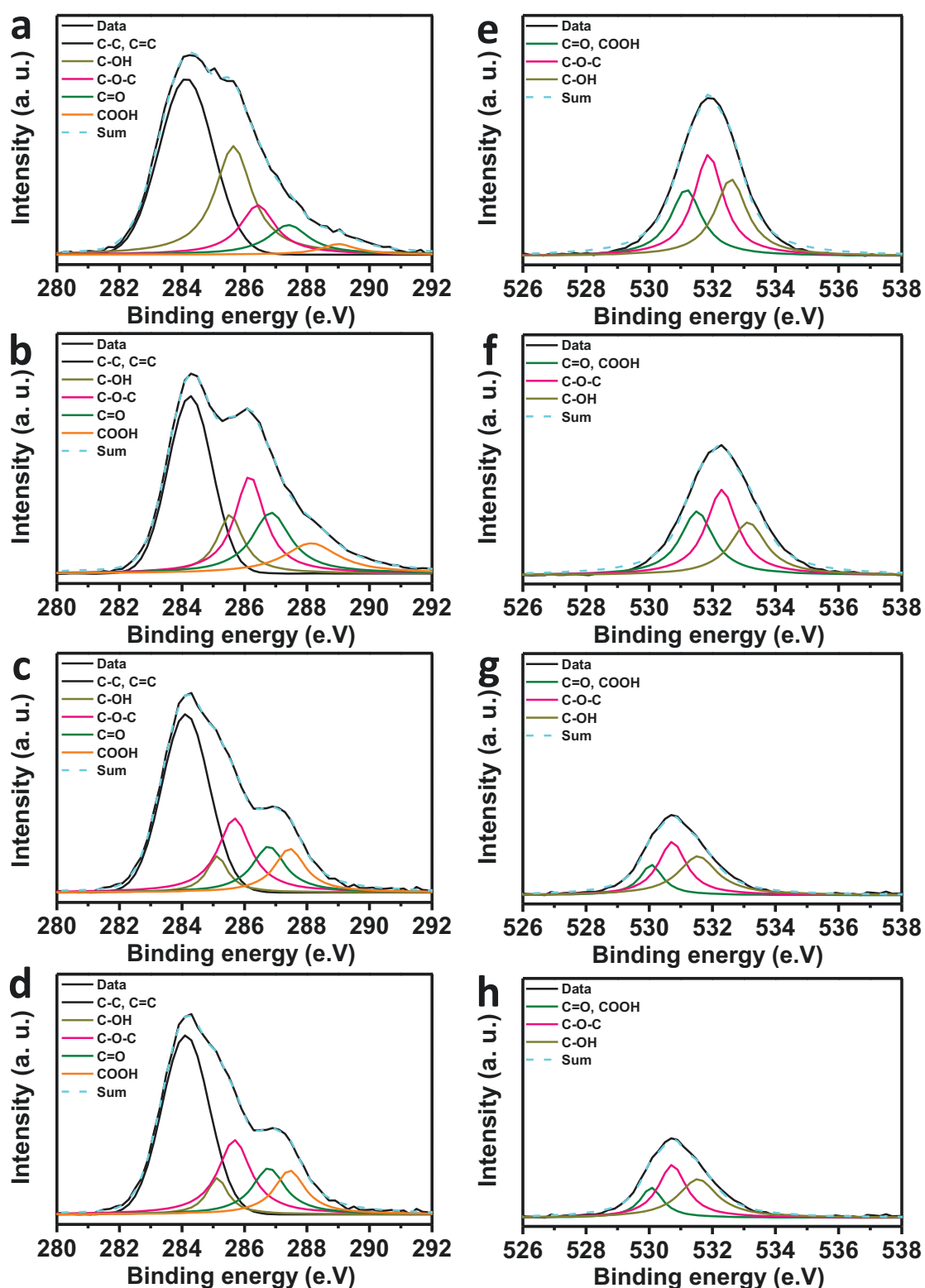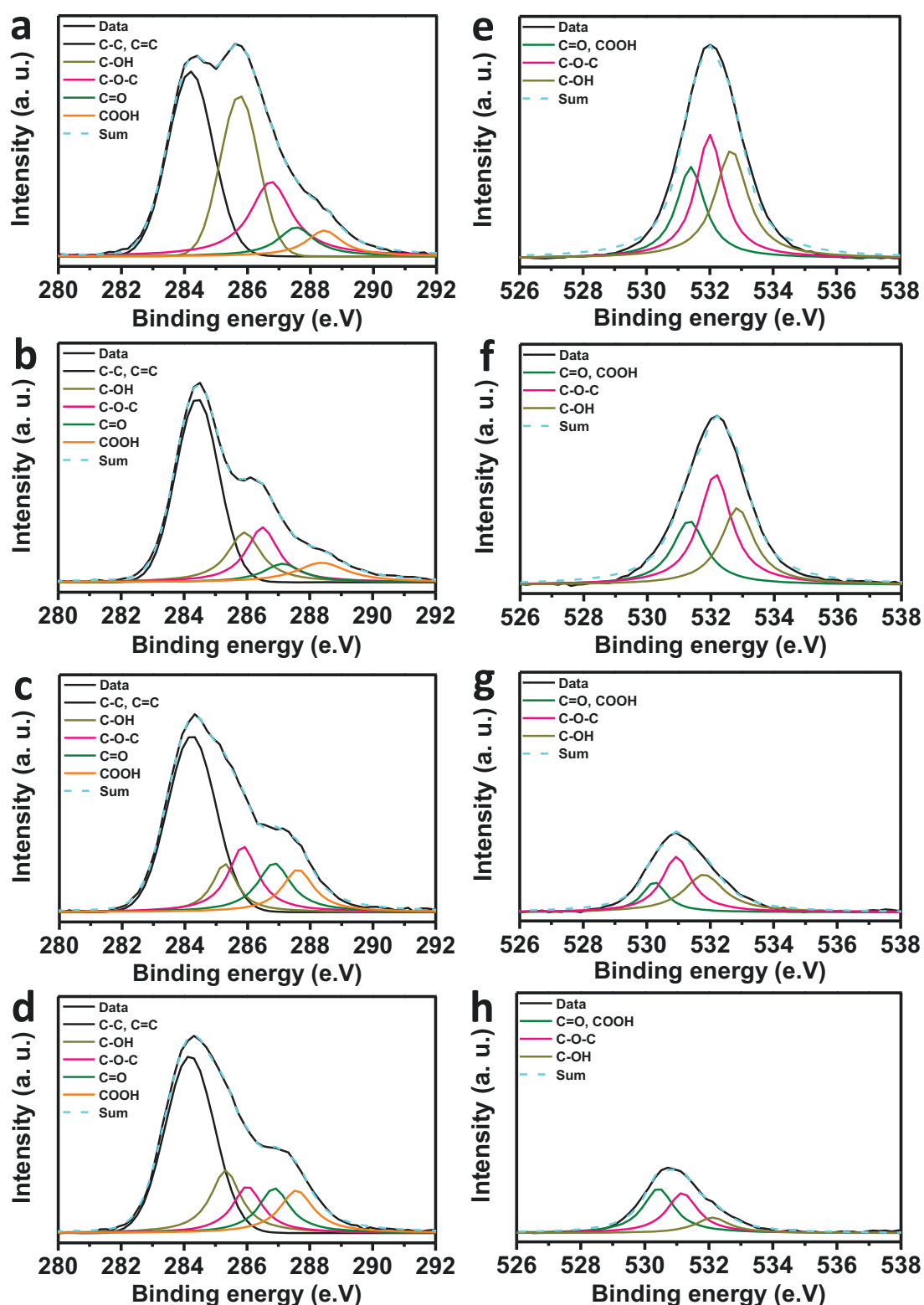
Figure A.2: C1s and O1s XPS spectra of NGO 300 nm and PAMAM functionalized materials. a - d, C1s XPS spectra of NGO 300 nm, CP@NGO, PAMAM-NGO and CP@PAMAM-NGO respectively. **e - h,** O1s XPS spectra of NGO 300 nm, CP@NGO, PAMAM-NGO and CP@PAMAM-NGO respectively.

Figure A.3: N1s and Pt4f XPS spectra of NGO 300 nm and PAMAM functionalized materials. a, N1s and **b,** Pt4f XPS spectra of pristine NGO 300 nm (1), CP@NGO (2), PAMAM-NGO (3) and CP@PAMAM-NGO (4).

Figure A.4: C1s and O1s XPS spectra of NGO 200 nm and gelatin functionalized materials. a - d, C1s XPS spectra of NGO 200 nm, CP@NGO, Gel_NGO and CP@Gel_NGO respectively. **e - h,** O1s XPS spectra of NGO 200 nm, CP@NGO, Gel_NGO and CP@Gel_NGO respectively. All XPS data normalized at C - C peak position.
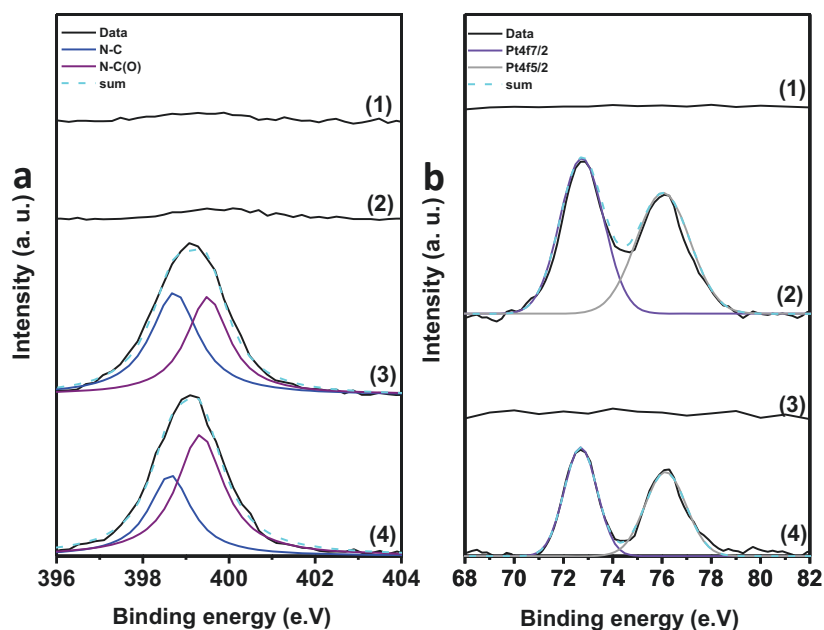
Figure A.5: C1s and O1s XPS spectra of NGO 300 nm and gelatin functionalized materials. a - d, C1s XPS spectra of NGO 300 nm, CP@NGO, Gel_NGO and CP@Gel_NGO respectively. **e - h,** O1s XPS spectra of NGO 300 nm, CP@NGO, Gel_NGO and CP@Gel_NGO respectively. All XPS data normalized at C - C peak position.
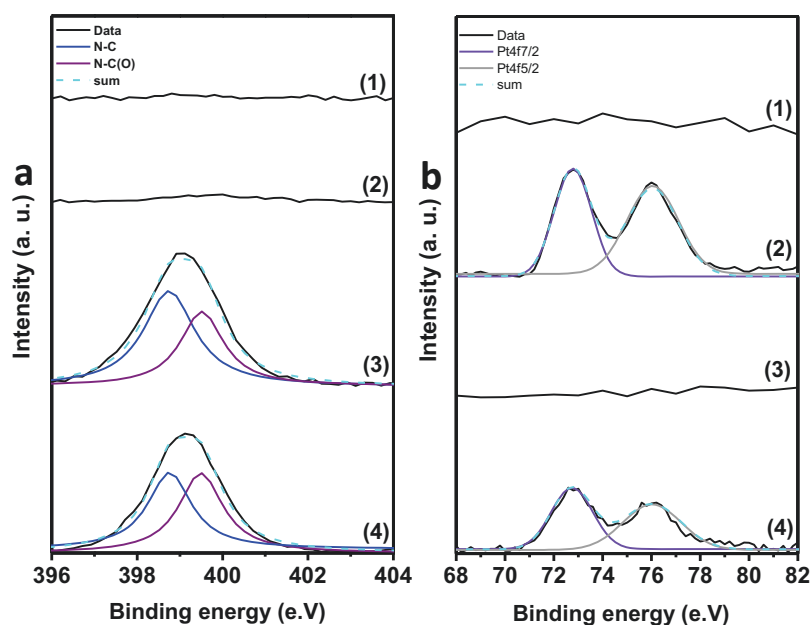
Figure A.6: N1s and Pt4f XPS spectra of NGO 200 nm and gelatin functionalized materials. a, N1s and **b,** Pt4f XPS spectra of pristine NGO 200 nm (1), CP@NGO (2), Gel_NGO (3) and CP@Gel_NGO (4) respectively.

Figure A.7: N1s and Pt4f XPS spectra of NGO 300 nm and gelatin functionalized materials. a, N1s and **b,** Pt4f XPS spectra of pristine NGO 300 nm (1), CP@NGO (2), Gel_NGO (3) and CP@Gel_NGO (4) respectively.

Curriculum Vitae

SAMI A MAKHARZA

Leibniz Institute for Solid State and Materials Research.

IFW Dresden e.V., Helmholtzstraße 20

D-01069 Dresden

IFF: Institute for Solid State Research

Tel. +49 (0)351 4656-228

Fax. +49 (0)351 4659-313

Email: s.a.m.makharza@ifw-dresden.de

makharza.sami@gmail.com

Homepage: http://www.ifw-dresden.de/institutes/iff/nanoscale-chemistry/

PERSONAL INFORMATION:

Place, Date of Birth: Al-Thahria, October 07, 1978

Gender: Male/Married

Nationality: Palestinian

WORK EXPERIENCE:

PhD Student from 2010 till now (DAAD scholarship) - Leibniz Institute for Solid State and Materials Research. TU Dresden.

Research Scientist from 5/2007 to 3/2010 - Nanotechnology Research Laboratory Materials Engineering Department - Faculty of Engineering - Al-Quds University, Abu Dies, Jerusalem - Palestine.

Teaching Assistant from 11/2002 to 2/2006 Al-Quds University, Faculty of Science and Technology, Department of Chemistry, Palestine. Manufacturer of Detergents and cosmetics from 01/2001 to 01/2003 Brothers Company for Detergents, Jerusalem-Alsawahra, Palestine.

EDUCATION:

Master Degree, 2005, in Applied Industrial Technology, Deanship of Graduate Studies, Al-Quds University, Jerusalem, Palestine.

Bachelor Degree, 2001, in Chemistry, and minor Chemical Technology, Al-Quds University, Jerusalem, Palestine.

General Secondary School, 1997, Al-Thahria schools, Southern Hebron, Palestine.

ERKLÄRUNG